A Study of the Regulation Mechanisms of Platelet Activation

A DISSERTATION SUBMITTED TO THE FACULTY OF THE GRADUATE SCHOOL OF THE UNIVERSITY OF MINNESOTA
BY

Solaire Finkenstaedt-Quinn

IN PARTIAL FULFILLMENT OF THE REQUIREMENTS
FOR THE DEGREE OF
DOCTOR OF PHILOSOPHY

Christy Haynes, Advisor

January, 2016

Acknowledgements

I would like to acknowledge and thank my thesis advisor, Christy Haynes, for her continual support throughout my graduate career. Her dedication to both the research and cultivating a learning environment make her a wonderful advisor and one that I am honored to have worked with.

I would also like to thank the members of the Haynes research lab, both past and current. The community that they have created and fostered makes a hard, long road both educational and enjoyable. Specifically, I want to thank Katie Hurley who was always available for a needed hug and to Joe Buchman for always being able to make me chuckle. I would also like to thank Shencheng Ge for mentoring me when I started working with platelets and Sarah Gruba for being my platelet co-conspirator.

Lastly, I would like to thank Diana Freeman and Ellorie Liljequist for performing the rabbit blood draws, without which I could not have done any of the experiments.

This thesis is dedicated to my parents who have supported and encouraged me throughout my life and will never stop believing in me.

I would also like to dedicate it to my best friend Kira Spencer who has always been at my side despite the many miles that have often separated us.

Abstract

Platelets play an important role in maintaining hemostasis in the body. As they circulate through the blood stream, platelets receive signals from other cells that call them to sites of vascular damage. When platelets reach a damaged area, they go through the processes of activation and aggregation. During activation, platelets begin to change shape and release their granular contents via exocytosis. During exocytosis, a series of small molecules and proteins are released that serve to propagate the platelet activation signal and initiate wound healing. Overall, this work explores the different aspects of platelet activation using microscopy and single cell methods.

Chapter One reviews the different components of the cytoskeleton and the current advances in microscopy that are being applied to study it. While light microscopy is a useful technique for studying cellular dynamics, super-resolution imaging allows for more in depth exploration of the many regulatory roles that the cytoskeleton plays in cells. Chapter Two focuses on work performed to investigate the toxicity of mesoporous silica nanoparticles on platelets. In Chapters Three and Four, the role that the cytoskeleton and plasma membrane play in the shape change dynamics of platelet activation is detailed, with a focus on using microscopy to visualize these changes. Chapter Five analyzes platelet activation to characterize fusion pore dynamics during exocytosis.

Lastly, Chapter Six provides an overview of three different chemical education projects I have worked on. The first two projects involved the development and implementation of outreach events at a local community center to teach students about the scientific process and the chemistry behind climate change. The third project is in progress and aims to develop labs for use in the high school chemistry classroom that combine literature with general chemistry concepts to promote student engagement and interdisciplinary focus.

Table of Contents

Acknowledgements ..... **i**

Abstract ..... **iii**

List of Tables ..... **vii**

List of Figures ..... **viii**

List of Abbreviations and Symbols ..... **x**

Chapter 1

Super-Resolution Imaging for Monitoring Cytoskeleton Dynamics **1**

1.1 Introduction **2**

1.1.1 Cytoskeletal Elements 2

1.1.2 Microscopy 5

1.1.3 Fixed versus Live Cell Imaging 6

1.2 Fluorescence Imaging **8**

1.2.1 Nearing the Resolution Limit 8

1.2.2 Super-Resolution Fluorescence Imaging 11

1.3 Conclusion **19**

Chapter 2

On-chip Evaluation of Platelet Adhesion and Aggregation upon Exposure to Mesoporous Silica Nanoparticles **21**

2.1 Introduction **22**

2.2 Methods and Experimental Setup **24**

2.2.1 Fabrication of Microfluidic Platforms 24

2.2.2 Endothelial Cell Culture 24

2.2.3 Platelet Isolation 25

2.2.4 Mesoporous Silica Nanoparticle Synthesis 26

2.2.5 Mesoporous Silica Nanoparticle Characterization 26

2.2.6 On-chip Adhesion and Aggregation Assays 27

2.2.7 Viability Assay 28

2.2.8 Fixed-cell Fluorescence Imaging for Platelet Aggregation Assessment 28

2.3 Results and Discussion **30**

2.3.1 Nanoparticle Synthesis/Characterization 30

2.3.2 FMS@PEG/TMS and Platelet Viability 30

2.3.3 FMS@PEG/TMS and Platelet Adhesion and Aggregation 32

2.3 Conclusion **39**

Chapter 3

Cytoskeleton Dynamics in Drug-treated Platelets 40
3.1 Introduction 41
3.2 Materials and Methods 43
3.2.3 Drug Treatment 44
3.2.4 Image Analysis 45
3.3 Results and Discussion 45
3.3.1 Microtubule results 46
3.3.2 Actin results 50
3.4 Conclusions 54

Chapter 4

Cholesterol Membrane Content Plays a Minor Role in Platelet Aggregation 56
4.1. Introduction 57
4.2 Methods 58
4.2.1 Platelet Isolation and Membrane Manipulation 58
4.2.2 Cholesterol Content Determination 59
4.2.3 Aggregation Assay 60
4.3.5 Data Analysis 61
4.3 Results and Discussion 61
4.3.1 Cholesterol Content 61
4.3.2 Aggregation 62
4.3.3 Shape Change Analysis 64
4.4 Conclusion 66

Chapter 5

Variations in Fusion Pore Formation in Cholesterol-Treated Platelets 67
5.1 Introduction 68
5.2 Materials and Methods 72
5.2.1 Cell Manipulation and Amperometry 72
5.2.2 Peak Categorization 72
5.2.3 Non-Traditional Events 73
5.3 Results and Discussion 75
5.3.1 Categorization of Foot Events 75
5.3.2 Pre-Spike Foot Events 77
5.3.3 Post-Spike Foot Events 81
5.3.4 Non-Traditional Events 82
5.4 Conclusion 85

Chapter 6

Engaging Chemistry – Learning by doing 87
6.1 Introduction 88
6.2 Activities for Middle School Students to Sleuth a Chemistry "Whodunit" and Investigate the Scientific Method 89
6.2.1 Background 89
6.2.2 Methods 89
6.2.3 Results and Discussion 93
6.2.4 Conclusion 95
6.3 Developing a Conceptual Understanding of Climate Change 96
6.3.1 Background 96
6.3.2 Methods 100
6.3.3 Results and Discussion: 103
6.3.4 Conclusion 112
6.4 Increasing chemical understanding using literature to stimulate student interest 113
6.4.1 Methods 113
6.4.2 Preliminary Results 114
6.5 Conclusion 116

References 117

Curriculum Vita 134

List of Tables

Chapter 4

Table 4.1 Platelet aggregation characteristics 63

Chapter 5

Table 5.1 Non-traditional events were characterized by their 10/90 slope and area. 74

Chapter 6

Table 6.1 Overview of the evidence kit contents and available assays for the three mystery activities 92
Table 6.2 Comparison of correct student responses to pre- and post-activity assessments 94
Table 6.3 Overview of outreach programs demonstrations and activities 102
Table 6.4 'Little Kids' percentage correct of the assessment questions 104
Table 6.5 Assessment questions for the 'Big Kids' 107
Table 6.6 'Big Kids' percentage correct of the assessment questions 107
Table 6.7 Assessment questions for the STEM kids 110
Table 6.8 STEM students percentage correct of the assessment questions 111
Table 6.9 Circle all that apply assessment questions for the STEM students 111
Table 6.10 Short answer assessment questions administered to the STEM kids 111

List of Figures

Chapter 1

Figure 1.1 Schematic representations of the three main categories of cytoskeletal filaments 4
Figure 1.2 High resolution fluorescence microscopy techniques 13
Figure 1.3 Comparisons of fluorescence microscopy techniques 14
Figure 1.4 Dual-objective microscope setup for improved resolution STORM imaging 18

Chapter 2

Figure 2.1 On-chip platelet adhesion/aggregation assay platform schematic ... 29
Figure 2.2 RITC-MS@PEG/TMS nanoparticle characterization 31
Figure 2.3 Percent viability of platelets by trypan blue assay 31
Figure 2.4 Adhesion of non-activated and ADP-activated platelets onto endothelial cells 35
Figure 2.5 Representative images from fixed-cell fluorescence imaging 35
Figure 2.6 Aggregation of non-activated and ADP-activated platelets 37
Figure 2.7 Aggregation assay by fixed-cell fluorescence imaging 38
Figure 2.8 Aggregation of more than 4 platelets 38

Chapter 3

Figure 3.1 Timeline of microtubule ring shrinkage dynamics during activation . 48
Figure 3.2 Microtubule ring – progressions 49
Figure 3.3 Timeline of actin matrix shrinkage dynamics during activation 52
Figure 3.4 Actin matrix – progressions 53
Figure 3.5 Additional structures revealed by actin labeling 53

Chapter 4

Figure 4.1 Average cholesterol content of control and MβCD-treated platelets 62
Figure 4.2 Schematic platelet aggregation curve 63
Figure 4.3 Circumference change of the platelet membrane upon activation ... 65

Chapter 5

Figure 5.1 Various proposed modes of exocytosis..... 71
Figure 5.2 Classes of peaks 76
Figure 5.3 Pre-spike foot events..... 79
Figure 5.4 Pre-spike foot events with ramp-like character 79
Figure 5.5 Pre-spike foot events with plateau-like character..... 80
Figure 5.6 Percent of event area and time for pre-spike feet 80
Figure 5.7 Post-spike foot events 81
Figure 5.8 Non-traditional events 83
Figure 5.9 Area and duration of non-traditional events 84
Figure 5.10 Kiss-and-run events 84

Chapter 6

Figure 6.1 Students participating in the ‘Whodunit’ activity 94
Figure 6.2 Overview of the various chemical processes directing climate change 99
Figure 6.3 Students participating in the ‘Climate Change’ activity..... 99
Figure 6.4 Changes in student understanding for the three groups tested 104
Figure 6.5 ‘Little Kids’ understanding of the time scale of climate change 104
Figure 6.6 Breakdown of the multiple choice questions by fossil fuel or light-matter interactions 111
Figure 6.7 *Fahrenheit 451* soda can calorimetry lab 116

List of Abbreviations and Symbols

ACD: acid-citrate-dextrose
ADP: adenosine diphosphate
AFM: atomic force microscopy
APTES: 3-aminopropyltriethoxy silane
CFMA: carbon-fiber microelectrode amperometry
CMFDA: 5-chloromethylfluorescein diacetate
DMEM: Dulbecco's Modified Eagle Medium
DMSO: dimethyl sulfoxide
EDTA: ethylenediaminetetraacetic acid
FBS: fetal bovine serum
FCS: fluorescence correlation spectroscopy
FMS: fluorescent mesoporous silica
FMS@PEG/TMS: fluorescent MS nanoparticles co-modified with PEG and trimethylsilane
FRAP: fluorescence recovery after photobleaching
GFP: green fluorescent protein
I_{RMS}: root mean square of the current function
MβCD: methyl-beta-cyclodextrin
MS: mesoporous silica
NTE: non-traditional event
OCS: open canalicular system
PALM: photoactivated localization microscopy
PDMS: polydimethylsiloxane
PEG: polyethylene glycol
PEI: polyethylimine
PPP: platelet poor plasma
PRP: platelet rich plasma
PSF: point spread function
RITC: rhodamine B isothiocyanate
SiR: silicon-rhodamine
SEM: standard error of the mean
SNARE: soluble NSF attachment protein receptor
STED: stimulated emission depletion
STEM: science, technology, engineering, and mathematics
STORM: stochastic optical reconstruction microscopy
TEOS: tetraethylorthosilicate
TIRF: total internal reflection fluorescence
TMS: chlorotrimethyl silane
QD: quantum dot

Chapter 1

Super-Resolution Imaging for Monitoring Cytoskeleton Dynamics

1.1 Introduction

The mammalian cell cytoskeleton is composed of three main filament types: actin, microtubules, and intermediate filaments (Figure 1.1). While there are variations between cell types in the structures that these cytoskeletal elements form, the basic components are the same.[1-4] The cytoskeleton is key to controlling the mechanical properties, cargo transportation, and shape of cells.[1,5,-7] Through the cytoskeleton, cells control their stiffness, shape, and can receive cues about the external environment surrounding them.[8,9] Often, cells respond to environmental cues through cytoskeletal rearrangement.[10] Due to their importance in controlling many cellular processes and their small size, it is optimal to study the cytoskeleton of fixed or living cells using super-resolution microscopy techniques.

1.1.1 Cytoskeletal Elements

The role of actin is multiplex in cells, and its presence is almost ubiquitous in eukaryotic cells. The basic structure of actin is a series of monomers that form filaments about 7 nm in diameter with a helical shape with a plus and minus end, giving them polarity.[6] Despite this simplicity, this building block is used to create a huge variety of structures, ranging from filaments that criss-cross cells to sheets and extensions at the edges of cells.[1] Actin serves to provide structure, is involved in endocytosis and exocytosis, transport within cells, cell division, and cellular movement.[7] In endocytosis, actin is involved in the formation and then internalization of endosomes. Both organelles and vesicles have been shown to travel along actin networks. In conjunction with myosin, actin governs cell division by forming a contractile ring that splits a cell into two daughter cells. The assembly and disassembly of actin filaments creates the crawling motion that cells use to move.[5,6] Its diversity in cellular function and the importance of the many roles it plays make actin an important structure to study towards achieving fundamental insights into cell biology and facilitating medical advances.

Microtubules serve primarily in intracellular trafficking, organelle positioning, and cellular polarization.[8] Microtubules are made up of α- and β-tubulin subunits that link to form hollow tubes 25 nm in diameter.[11] Like actin, microtubules are polar and together are key to conferring polarity in cells. In most cells, microtubules grow out from centrosomes toward the cell membrane in such a way that results in a higher concentration at the 'front' of the cell so as to direct cellular motility, for example in directing axonal growth.[8,10,12] Microtubules are also important in the process of cell division as they modulate separation of the replicated chromosomes.[5] In platelets, microtubules serve to stabilize the discoid resting shape and, as in other cells, stabilize the filopodia structure in spread platelets.[13]

Like actin and microtubules, intermediate filaments are present in many types of cells. Unlike the other two elements however, they are very diverse in composition with high variability in their exact components but retaining the same basic structure. Each intermediate filament is structured as a rod with variable head and tail domains. The rod itself is about 8 – 12 nm in diameter and is composed of a series of two parallel, α-helix chains which, like the head and tail domains, are diverse in makeup.[3,4] The variability of the structure is due to the diversity of cellular and tissue environments in which they reside.[3,9] Despite this diversity, the main function of intermediate filaments appears to be consistent, managing cellular stress, primarily through mechanical means.[9] There are a few main types of intermediate filaments with differences in amino acid sequence and filament structure. Key intermediate filament types are keratin which modulates mechanical tensions, desmin which is important in mechanical stress resilience, and vimentin which plays a role in mechanotransduction. In addition, intermediate filaments are important in conditions of osmotic stress and in the central nervous system during trauma responses.[9] Intermediate filaments form a complex network that are the basis of the viscoelastic properties of cells.[4]

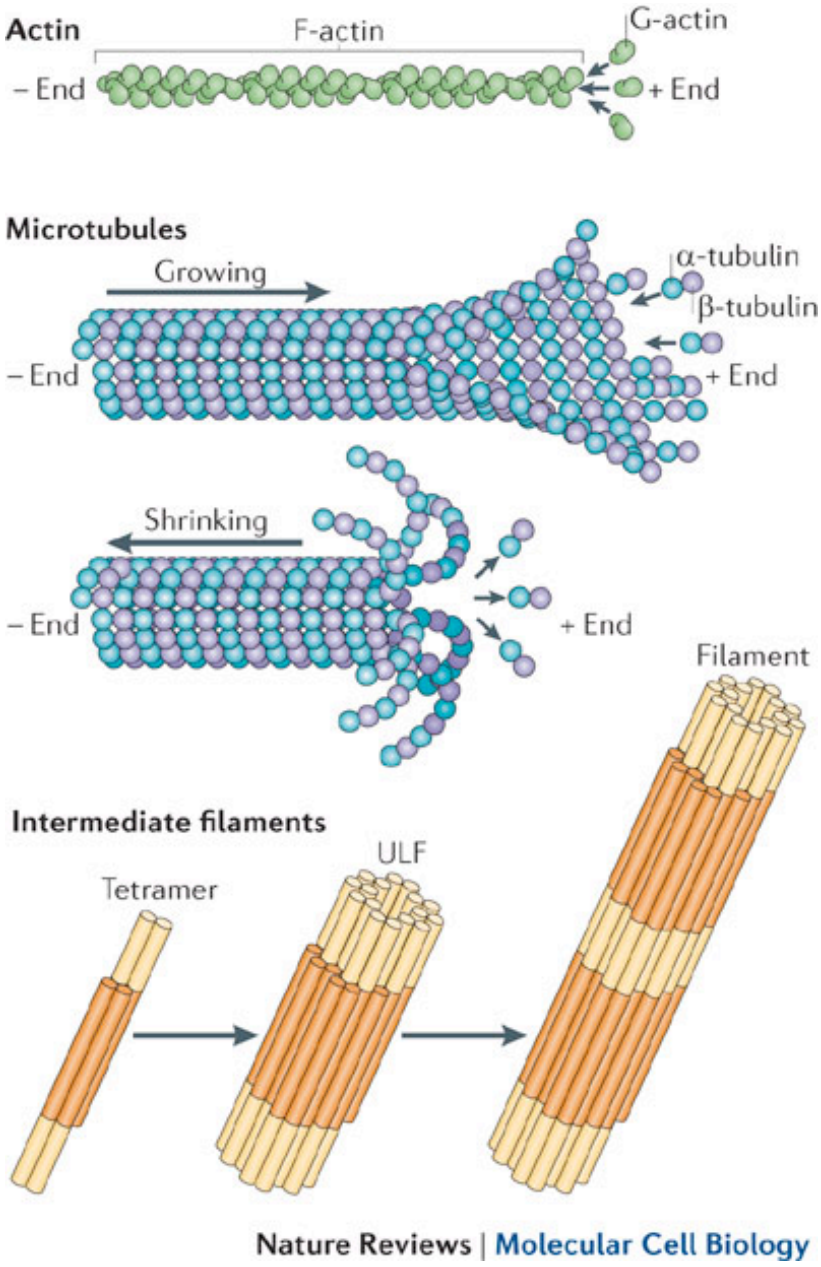

Figure 1.1 Schematic representation of the three main categories of cytoskeletal filaments.[14]

1.1.2 Microscopy

Microscopy is ideal for studying cytoskeletal dynamics and structure due to their macromolecular nature. Microscopy has provided scientists with important insights on biological processes and structure since 1665 when Hooke used it to visualize the first cell.[15] Imaging has since then been applied in biological studies to bulk samples, tissues, individual cells, and individual proteins. Light microscopy encompasses many different imaging techniques, including bright field, dark field, and fluorescence microscopy. This review will focus on super-resolution fluorescence microscopy techniques, which utilize fluorescent probes attached to targets as a mode to selectively achieve sub-diffraction-limited images of specific features.

While traditional light-based microscopy techniques are useful, the resolution required for imaging certain processes cannot always be achieved if the limit of diffraction for light is reached. The traditional Abbe spatial resolution of light is determined by $\Delta r = \lambda/(2n \sin \alpha)$; where r is the resolution, λ the wavelength of light used, *n* the aperture angle, and α the refractive index.[16] This limitation can be overcome through electron microscopy and super-resolution fluorescence imaging techniques. In electron microscopy, a sample is bombarded with a beam of electrons as opposed to light, and the diffraction of the beam is used to generate an image, completely avoiding the visible light diffraction limit with the much shorter electron wavelength. Each microscopy method can provide important answers to different questions. For example, the high resolution of electron microscopy makes it ideal for imaging small structural details, whereas using fluorescence microscopy one can easily identify different cellular components and tag species of interest. One major drawback to electron microscopy is the difficulty of sample preparation as it is both time-consuming and prone to altering biological structure.[15] In the past two decades, advances in the area of super-resolution fluorescence microscopy have been revolutionizing

the imaging of cellular structures.[17-19] These super-resolution fluorescence microscopy techniques allow us to image structures far below the spatial resolution traditionally allowed by visible light, down into the tens of nanometers.[16]

1.1.3 Fixed versus Live Cell Imaging

As with electron microscopy, sample preparation is a major consideration in fluorescence imaging. In addition, fluorescence imaging can be performed on both live and fixed cells, adding another consideration when preparing samples. Traditionally, the investigation of cellular structures and protein localization via imaging has been performed on fixed cells, where the target is labeled using an antibody tagged with a fluorophore, either small molecules or quantum dots (QDs). With the advent of fusion proteins, which encode for fluorescent proteins directly attached to the target, there has been a shift towards more live-cell imaging.[20,21] It is important to consider how the perturbations that can be caused by either the probe or methods used to prepare the cells for either fixed or live cell imaging may lead to imaging artifacts. This is particularly important to consider for super-resolution fluorescence imaging, as some of the techniques do not have time resolution on par with the biological processes of interest.

Fixed cell imaging generally has four stages of sample preparation: (1) fixation of the cell to preserve the structure of interest, (2) permeabilization so that the probe can enter the cell and bind to the structure of interest, (3) blocking nonspecific binding, and (4) introduction of the probe. Organic solvents, such as methanol, ethanol, and acetone perform stages (1) and (2) in one step. Another common method of immunofluorescence sample preparation includes fixation with an aldehyde followed by permeabilization by a saponin or detergent. Both modes of fixation/permeabilization can result in a number of problems. During fixation, the sites for probe binding can be blocked or protein structure altered. Fixation can also result in membrane or organelle disruption. A common problem

with permeabilization is the loss of proteins via extraction or relocalization.[22] In particular, the side effect of protein extraction and redistribution is dependent upon protein size and cell type, making it difficult to predict changes.[23] When imaging the cytoskeleton, extraction of the smaller components can be advantageous as it is generally desirable to image only the filaments rather than the monomers and dimers. However, the protocol should certainly take the protein of interest into consideration.[24,25] The common labeling method used with fixed cells (used in Chapters 2 and 3) is use of an immunofluorophore conjugate, wherein antibody labels are used to mark the protein, or organelle, of interest. One major benefit of immunofluorescence is the ease of labeling multiple proteins with different probes so that colocalization of various elements can be studied. In addition, as cells are fixed prior to labeling, there are no concerns about the probe altering the function of the target or cellular processes.

Live cell imaging allows for a more dynamic study of cells, which is fairly important for studying the cytoskeleton. However, live cell imaging can be difficult to perform, with problems generally arising either from the difficulty in delivering the probe to the location of interest or disruptions caused by either the delivery method or the probe itself to the cell or the target that it is marking. Fusion proteins require cells that can be readily transfected and contain the cellular machinery to then translate the encoding gene into a protein. The large size of fusion proteins can lead to disruption in target's function.[26] There is, however, a large variety of fluorescent proteins to choose from, allowing researchers to select for fluorescence character, size, and stability relative to the surrounding environment amongst others.[27] While small molecules and QDs can circumvent some of these issues, such as size and tunability of fluorescent character, they are more likely to be toxic to the cell and both targeting and internalization can be difficult. Probe internalization can be achieved through a variety of methods, not limited to electroporation, use of pore-forming small molecules, and microinjection.[28,29] Commonly used targeting moieties for the cytoskeleton are β-

tubulin subunits to label microtubules, phalloidin to label actin, and various antibodies to label intermediate filaments.[30-33]

1.2 Fluorescence Imaging

Fluorescence imaging is an important technique due to its ability to selectively identify specific characteristics of a sample. It is particularly useful in the study of the cytoskeleton as it can be used to study both the dynamics of the cytoskeleton and its association with various proteins by labeling both components and imaging for colocalization. Optimal probes for fluorescence microscopy should have the following characteristics: (1) the probe should have specific association and a large binding constant with the protein of interest, (2) it should be nontoxic and not alter the natural cellular processes, (3) it should have a quantum yield greater than 0.3 when bound to the target, (4) it should have an excitation close to or above 500 nm to minimize autofluorescence from the cell, and (5) it should have no or minimal photobleaching.[34] While much of the initial work to elucidate the structure and function of the cytoskeleton in cells was done using epifluorescence, recently there has been a push towards using higher resolution fluorescence techniques.[35-37]

1.2.1 Nearing the Resolution Limit

A few different fluorescence imaging techniques have been developed to get resolution closer to the Abbe diffraction limit. Two of these methods, confocal microscopy and total internal reflection fluorescence (TIRF) microscopy, function by reducing the volume of the sample that is illuminated.[11,35] This effectively reduces the level of background fluorescence, resulting in a clearer, higher signal-to-noise image.

Confocal microscopy functions by adding a pinhole to the microscope setup between the sample and the camera. The pinhole only allows passage of light from the focal plane of interest, thereby reducing out-of-focus light (Figures 1.2A and 1.3A).[35] Using confocal microscopy, z-section imaging of samples can be

performed; z-slices between 0.6 – 1 μm in thickness are commonly obtained.[11] One benefit of confocal imaging is that it is not restricted by a penetration depth of light into cells or tissues and can be used to image a thick sample by combining many cross-sectional z-slices. One potential disadvantage of confocal fluorescence microscopy is that it is often performed using a laser to illuminate the sample and is more likely to result in sample damage or photobleaching of the fluorophore than epifluorescence.[35]

The thin z-slicing obtained by confocal works nicely for imaging neurons as it is on the scale of the dendrite and axonal extension thicknesses.[38] Confocal microscopy is often used for fluorescence recovery after photobleaching (FRAP) experiments to monitor diffusion of labeled targets.[39,40] Through the use of FRAP and photoactivatable proteins, Hotulainen, et al. were able to monitor and quantify the treadmilling of actin subunits in dendritic spines.[39,40] By disrupting actin, the synaptic activity at dendrite ends is disrupted.[40] By disrupting cofilin, an actin disassembly protein, both the number and formation of protruding spines decreased.[40]

TIRF takes advantage of the optical phenomenon known as total internal reflection (TIR). When light traveling with a high angle of incidence reaches the boundary between two media with different refractive indices, typically a solid-liquid interface, TIR may occur. When the TIR critical angle is reached, nearly all the light will reflect back into the first medium. This reflectance generates a decaying evanescent field in the overlaying medium with a penetration depth on the order of 100 – 200 nm when using visible light (Figures 1.2B and 1.3B).[11,29,41] The evanescent wave has a small excitation distance that can be used for high resolution imaging of fluorophores close to the media interface.[29,41-43]

TIRF microscopy has many benefits over other optical sectioning techniques. The thickness of the optical sections derived from TIRF are about one fifth of that

which can be obtained using confocal imaging.[43] One large difference between confocal and TIRF microscopy is that in the former, the entire sample is illuminated but only one section is observed. In TIRF, only the portion of the sample in the evanescent wave is illuminated, which serves to reduce damage and photobleaching. This also means however, that only events taking place in, at, or near the plasma membrane can be observed and quantified at high resolution. By decreasing the angle of incidence, the penetration depth can be increased in what is termed 'near-TIRF' imaging.[11] Due to its ability to monitor events at the cell surface, TIRF is often used to monitor surface membrane dynamics and kinetics, the cytoskeleton near the plasma membrane, fusion of proteins to the surface membrane, and secretion events.

TIRF has been applied to study the cytoskeletal-membrane dynamics of both B-cells and T-cells upon immune response. The cytoskeleton appears to be important in both the resting state and the initial stages of immune response, directing the movement and grouping of immunoreceptors.[44] TIRF has also been used to monitor how molecular motors travel along both actin and microtubule cytoskeleton tracks.[45] Zong, et al. demonstrated through TIRF imaging that during endocytosis in insulin-secreting cells, clathrin-coated pits are stationary at locations where microtubules are attached to the plasma membrane, whereas clathrin-coated vesicles move along microtubule filaments.[46] The importance of microtubules to maintaining filopodia structure has also been investigated.[11] Interestingly, through TIRF imaging it is known that the growing ends of the microtubules making up the mitotic spindle do not come close to the cell membrane.[11]

In part, because the exciting evanescent wave is localized to within a few hundred nanometers of the plasma membrane, the uses of TIRF for cytoskeletal imaging are limited. Further studies of cytoskeleton dynamics and structure within cells require techniques with sub-diffraction limit spatial resolution imaging.

Ideally, these techniques can also be used to develop three-dimensional images as is possible with diffraction-limited confocal microscopy.

1.2.2 Super-Resolution Fluorescence Imaging

Despite the improved spatial resolution of confocal and TIRF microscopy compared to epifluorescence, they can not reveal cytoskeletal structures smaller than the Abbe diffraction limit allows. The cytoskeletal elements often form a very intricate network, making it hard to resolve individual elements. Using super-resolution fluorescence imaging, some of the unanswered questions regarding the cytoskeleton can be probed. Due to its nature, there are a few obstacles to applying super-resolution imaging to biological samples. The two main problems that arise are reducing background fluorescence and finding fluorescent probes with high quantum yield, slow photobleaching, and low cellular toxicity. As so few photons are collected in super-resolution imaging, any background fluorescence can be highly detrimental and easily override the signal of interest. To help reduce this, most stochastic optical reconstruction microscopy (STORM) and photoactivated localization microscopy (PALM) setups are similar to that of a TIRF microscope, thus reducing out-of-focus fluorescence.[47] The pool of fluorophores available for super-resolution imaging has also been expanding, with work being performed to either create new probes or modify existing probes initially used for epifluorescence imaging.[48-50]

STORM and PALM work though a series of activation and bleaching steps (Figures 1.2C and 1.3B). During each imaging cycle, a small subset of probes are activated, imaged, and then photobleached. PALM was developed by Betzig, et al. and uses a pattern of activating fluorescent proteins and then photobleaching most them so as to localize individual fluorophores with high resolution.[17] STORM functions by utilizing fluorescent dye molecules that can be switched between fluorescent and dark states dependent upon the presence of an activator and wavelength of light used.[18] By taking many images of the same

area while switching the fluorophores on and off, a sub-diffraction limit resolution image can be constructed. In both STORM and PALM, the centroid of the fluorophores can be mathematically determined after detection by modeling the fluorescent area as a point spread function (PSF) and fitting it to a Gaussian. By combining each fit image a super-resolution image can be generated.[17,18,51] Work has been progressing to make STORM and PALM imaging systems that can provide high resolution in all three dimensions. The currently used methods exploit PSF calculations, harnessing astigmatism in the microscope setup, and dual-objective systems.[52-57]

Stimulated emission depletion (STED) fluorescence microscopy functions by using two lasers, one to initially excite the sample and a second laser to deplete the excited state of the outer ring of fluorophores in an illuminated area, resulting in a smaller fluorescent area and thereby creating a narrower PSF to give high resolution images (Figures 1.2D and 1.3A).[19] Using this technique a resolution below 10 nm can be achieved.[58]

While STORM and PALM can reach a theoretical resolution of ~25 nm and STED a resolution of 10 nm, achieving this high resolution can be difficult in both live and fixed cell samples.[17,18,52,58] To collect enough photons to resolve a structure, samples need to be imaged on the time scale of seconds, a timescale slower than many live-cell processes. In addition, the effectiveness of the labeling of the fluorescent probes plays a large role in the resolution that can be obtained. Low labeling efficiency, blinking, or clustering of the probes can all result in imaging artifacts.[59,60] As with all imaging schemes, the effects of the probe on the cell and structure of interest as well as the cell preparation methods also need to be considered.

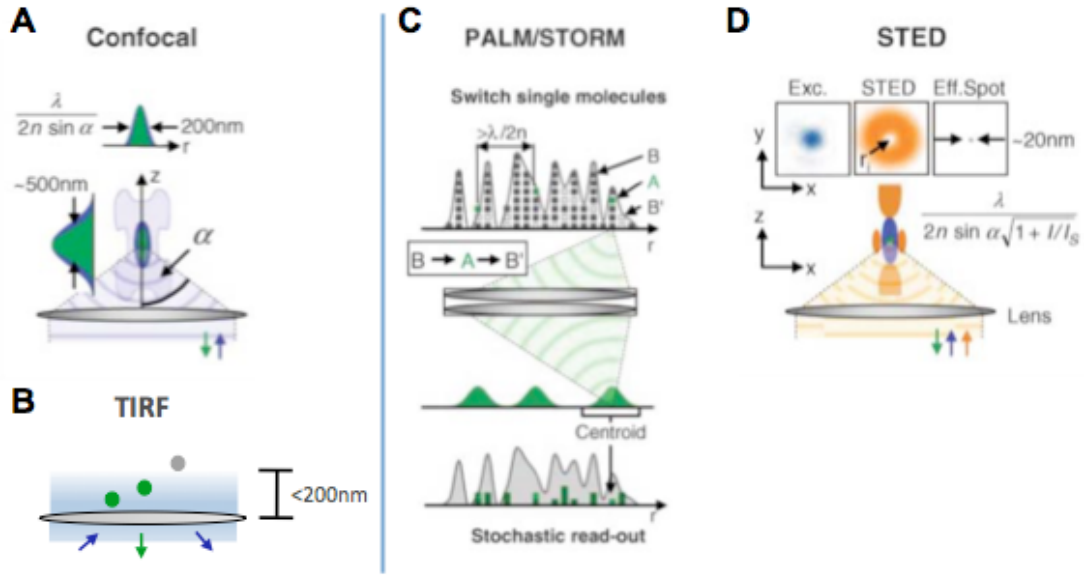

Figure 1.2 High resolution fluorescence microscopy techniques. A) Confocal microscopy, where the green represents the excited region of the sample. B) TIRF microscopy, where the green represents the excited fluorophores within the evanescent field whereas the gray represents a non-excited molecule located above the field. C) PALM/STORM microscopy. The stochastic nature of PALM and STORM turn on and off the fluorophores, allowing for the localization of the centroid. D) STED microscopy. The stimulated depletion of the outer ring of excited fluorophores allows for high resolution imaging. Modified from Hell Science 2007.[16]

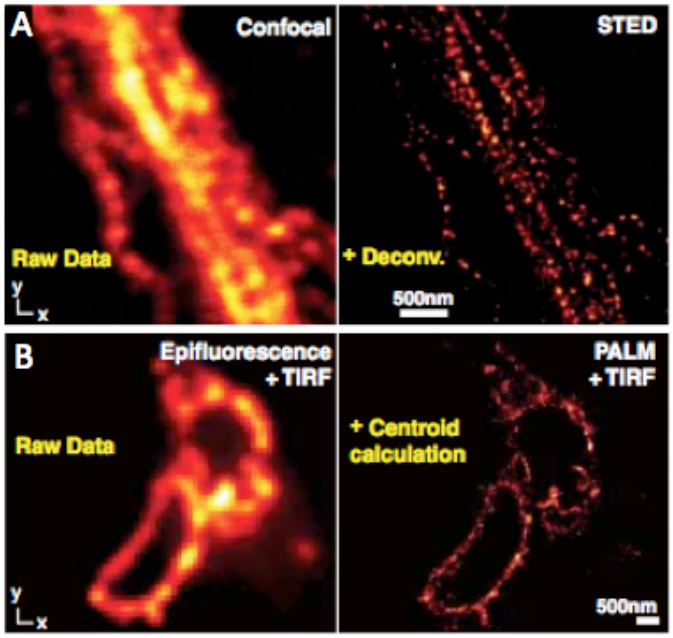

Figure 1.3 Comparisons of fluorescence microscopy techniques. A) Comparison of confocal and STED imaged neurofilaments. B) Comparison of TIRF and PALM imaged transmembrane proteins. Modified from Hell Science 2007.[16]

Probes

Due to the long acquisition times and specific wavelengths required for super-resolution fluorescence imaging, the number of probes that can be used is limited but a number of strategies have been used to broaden the available scope.[59,61,62] Multiple groups have modified fluorescent proteins for cytoskeleton imaging.[59,61,62] Izeddin, et al. designed a probe for PALM by combining an actin-binding peptide with a fluorescent protein. The resulting probe had a low affinity binding for actin to decrease imaging time.[59] Using their probe, they investigated the long-term dynamics of the actin making up the dendritic spine in neurons in both fixed and live cells. In fixed cells, they obtained approximately 25 nm spatial resolution and in live cells Izeddin, et al. were able to attain 65 nm spatial resolution with a corresponding 50 s temporal resolution for up to 30 min.[59] Additionally, by labeling the plasma membrane through a GFP-quantum dot construct and imaging it with single particle tracking, the authors were able to obtain colocalization data about the actin-membrane interactions.[59] Gunewardene, et al. developed a photoactivatable fluorescent protein which functions in the far-red region.[61] Using this fluorescent protein, they were able to perform simultaneous three-color live cell imaging using PALM to study the colocalization of both raft- and non-raft- associated membrane proteins with the actin cytoskeleton.[61] Another group used the method of genetic code expansion to create proteins that could be easily tagged by fluorescent probes and imaged actin filaments in COS-7 cells using STORM.[62]

Development of small molecule probes is also ongoing.[63,60] By using a Ti:Sapphire oscillator for STED microscopy, Liu, et al. found that DyLight 650 is an effective fluorescent dye for STED imaging. Using this setup, they were able to resolve microtubules, intermediate filaments, and actin filaments in fixed cells.[63] Lukinavičius, et al. designed probes specifically for actin and microtubule investigations using silicon-rhodamine (SiR) derivatives linked to small molecules which bind selectively to the cytoskeletal elements. These probes exhibited

minimal cytotoxicity and fluoresce in the far-red region with 10-fold and 100-fold increased intensity when bound to microtubules and actin, respectively.[60]

To enable colocalization imaging, Nanguneri, et al. investigated the use of rhodamine and bodipy fluorescent dyes that can be quenched by tryptophan as effective probes for dual-color STORM imaging.[64] The use of tryptophan-quenched synthetic dyes means that specific imaging buffers, which can interfere with fluorescent proteins, are not necessary. Thus, cells can be labeled with both synthetic dyes and fluorescent proteins to perform co-localization imaging experiments.[64]

Structure

Using these labeling strategies, there have been many studies applying super-resolution fluorescence imaging to reveal details about cytoskeletal structure. Frost, et al. used PALM to track individual actin molecules as they traveled along actin filaments in dendritic spines.[65] Using this method, they were able to identify areas of actin polymerization located throughout the spine.[65] PALM allowed Scarselli, et al. to determine that the clustering of the G protein-coupled receptor β2-adrenergic receptor is directed by actin.[66]

The Zhuang group has applied STORM to investigating the actin structure in cells.[56,67,68] Initial studies optimized the use of a dual-objective setup to facilitate greater photon collection efficiency, serving to increase spatial resolution (Figure 1.4). Using this setup, they achieved ~9 nm spatial resolution in the *x, y* direction and ~19 nm spatial resolution in the *z* direction. By applying this technique to cells stained with an actin-labeling fluorophore conjugate, they were able to image individual actin filaments and detect two actin layers in the protruding edges of cells.[56] They further applied this technique to investigate the structure of actin and spectrin in neurons. Imaging showed that the actin formed long filaments down the neuronal dendritic shaft. In axons, however, the actin formed

circumferential rings periodically spaced along the entire shaft.[67] Through colocalization experiments they found that βII spectin alternated in occurrence down the axonal shaft and that expression levels of βII spectrin were found to determine the presence of the periodic lattice structure.[68] Lukinavičious, et al. used STED to image the periodic actin structure previously identified via STORM by Xu, et al. in live cells.[60,68] In addition, they obtained the first live cell images showing the ninefold symmetry of the microtubule-based centriole.

Van den Dries, et al. used dual-color STORM to clarify the structure of podosomes in dendritic cells, adhesion structures that specialize in sensing the extracellular matrix.[69] Due to the super-resolution capabilities of STORM, they were able to disprove the previously hypothesized 'closed' ring structure of podosomes. In addition, they found that actin podosome cores were connected to nearby cores with actin filaments, a fact that had been previously unknown.[69]

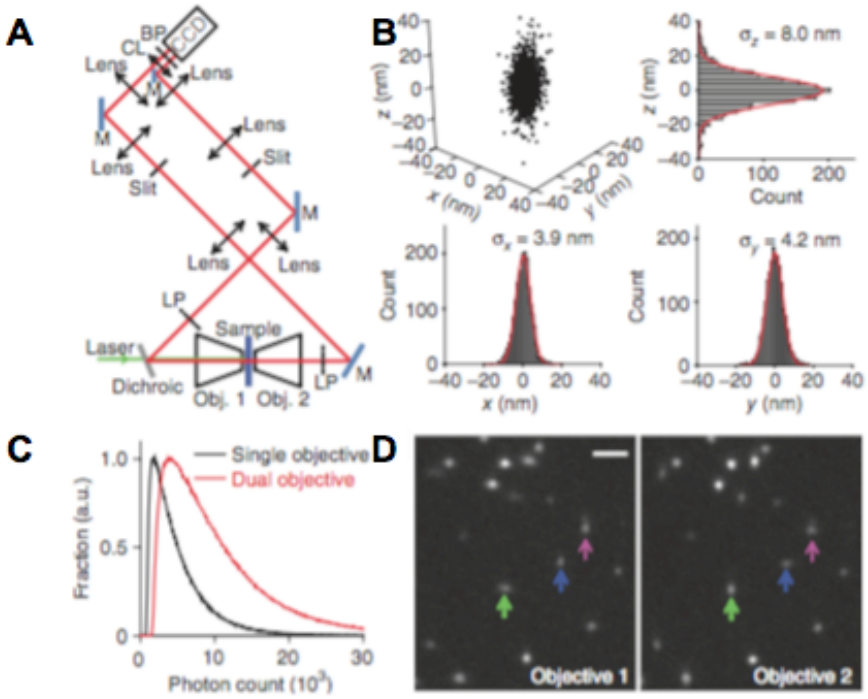

Figure 1.4 Dual-objective microscope setup for improved resolution STORM imaging. A) Microscope setup, where M indicates a mirror, Obj. an objective, LP a long-pass filter, CL a cylindrical lens, and BP a band-pass filter. B) Each molecule is repeatedly activated and imaged, resulting in a cluster. The center of mass is determined and the x, y, and z position can be determined by fitting to a Guassian function. C) Distribution of the number of photons collected, with an average of 5,200 for the single-objective and 10,600 for the dual-objective setups. D) Images of the Alexa Fluor 647 molecules. Comparing objectives 1 and 2, the green and blue arrows indicate the same molecules as the molecules are elongated in opposite directions (one x, the other y). Conversely, the pink arrows indicate two different, but closely positioned, molecules, indicated by elongation in the same directions. Scale bar is 2 μm. Modified from Xu Nat. Method 2012.[56]

Correlative Techniques

To bypass the limitations of super-resolution techniques, a number of groups have combined other techniques with super-resolution imaging to investigate the cytoskeleton. Heaslip, et al. studied how actin and microtubules direct insulin granule secretion in pancreatic β-cells by imaging cells with classical epifluorescence, TIRF, and STORM microscopy. By combining these techniques, they were able to get data about the location, size, and speed of growth of the cytoskeletal elements of interest.[70] STED microscopy has been paired with both fluorescence correlation spectroscopy (FCS) and atomic force microscopy (AFM) to study cell membrane-cytoskeleton interactions.[71,72] Mueller, et al. used STED microscopy in conjunction with FCS to show that lipid complex formation involving sphingolipids was dependent upon the cytoskeleton.[71] In another example, by using both AFM and STED, Sharma, et al. were able to correlate the difference in stiffness in cisplatin-resistant and susceptible ovarian cancer cells to differences in F-actin arrangement in the cytoskeleton.[72]

1.3 Conclusion

Despite the fact that super-resolution imaging has only been developed in the last two decades, there has already been a large amount of development in the technique itself and the probes that can be used. These developments have made super-resolution imaging more applicable to cellular imaging, extending it to three-dimensions and multi-color imaging. The use of super-resolution in combination with other techniques also results in interesting discoveries, and further pairing could be beneficial. An ideal pairing would be AFM with STORM to correlate cell membrane stiffness with high-resolution cytoskeleton images. In addition, a technique such as Raman could be paired with PALM to monitor both molecular release and cytoskeletal control during exocytosis events.

The application of super-resolution fluorescence imaging in cytoskeleton studies has been fairly narrow to date. Most studies investigate actin dynamics, most

often in neurons. There is minimal work examining microtubule dynamics, and almost no use investigating intermediate filaments. Even in the area of actin imaging, there are many structures and dynamics to probe beyond neurons and podosomes.[69,73] For example, while much work has been done to elucidate cytoskeletal dynamics in B-cells using TIRF, a number of questions about the identity of and mechanism by which regulating proteins guide those dynamics still remain that would be best answered using super-resolution imaging techniques.[44]

There are still many unknowns to be studied with regards to cytoskeletal dynamics but super-resolution imaging has opened up avenues for investigating these questions. Future development of the technique will only further the field. In fact, recently, label-free super-resolution imaging was reported which will effectively eliminate labeling artifacts.[74] Cytoskeletal dynamics are key to many biological processes, and with super-resolution microscopy, we are well on our way to gaining a better understanding of these processes.

Chapter 2

On-chip Evaluation of Platelet Adhesion and Aggregation upon Exposure to Mesoporous Silica Nanoparticles

Reproduced with permission from the Royal Society of Chemistry:
Kim, D.; Finkenstaedt-Quinn, S.; Hurley, K. R.; Buchman, J. T.; Haynes, C. L. "On-chip evaluation of platelet adhesion and aggregation upon exposure to mesoporous silica nanoparticles." *Analyst,* 2014, *139*, 906-913.

I contributed the platelet preparations, viability, and fluorescence imaging of the collected samples to this work.

2.1 Introduction

Recently, mesoporous silica (MS) nanoparticles have gained significant attention from various scientific communities due to their promising characteristics, including large surface areas, flexible surface chemistry, chemical/physical stability, and biocompatibility.[1-3] These particles are of particular interest as drug delivery agents due to their extraordinarily high surface-to-volume ratio.[4] Multiple studies have investigated the effects of particle size, shape, and surface coating on cell viability,[5-14] generally concluding that MS nanoparticles equipped with a biocompatible coating such as polyethylene glycol (PEG) or polyethylimine (PEI) do not induce cell death.[10-14] However, the study of nanoparticle impacts on blood cells has been largely limited to live/dead viability studies, and the understanding of more complex biological interactions with these MS nanoparticles is still in its infancy. Clinical application of MS nanoparticles would likely involve intravenous injection and blood circulation; thus, understanding the potentially subtle effects of MS nanoparticle exposure on blood components is critical. The current knowledge gap is partly due to technical difficulties in conventional assay platforms; as such, this research is intended to provide a simple platform that yields insight into the mechanistic interactions of nanoparticles with blood components.

In the in vitro and in vivo studies aimed at understanding the interactions of nanoparticles with various blood components, in vivo assays have been almost the only way to take into account the complex and dynamic nature of the biological system. However, in vivo methods are expensive, slow, ethically questionable, and, due to complexity, often don't yield mechanistic insight into how the nanoparticles and cells interact.[15-18] More importantly, many in vivo animal studies have questionable relevance for humans. As such, simple, cheap, fast, and ethically less-questionable in vitro assays that account for the dynamic and complex nature of physiological systems while using human blood

components would be ideal to answer biological questions in simplified, more controlled environments.

Microfluidic platforms have gained significant attention recently as a potential way to keep the advantages of the in vitro assay platform while enhancing in vivo relevance, particularly with respect to blood components such as red blood cells and platelets.[9,17-23] Our lab has recently performed a nanotoxicological study on endothelial cells using a microfluidic platform where we successfully incorporated the dynamic nature and shear stress relevant in the in vivo milieu.[9] In the previous study, we found that the flow characteristics present in the vascular system has a significant impact on the apparent toxicity of mesoporous silica nanoparticles towards endothelial cells; however, our investigation was still limited to viability assessment on an immortal cell line. Herein, we further develop the analytical platform using primary human platelets with on-chip fluorescence imaging to investigate the impact of nanoparticles on the critical platelet functions of adhesion and aggregation (Figure 2.1). Platelets are anuclear cell fragments that regulate hemostasis and thrombosis.[21-28] If either adhesion or aggregation of platelets is deregulated, platelets may induce damaging or lethal events; thus, any blood borne biomedical nanoparticles must have a minimal effect on platelet behaviour.[21-25]

To develop an analytical assay platform for both platelet adhesion and aggregation under physiologically relevant conditions, this work exploits a simple microfluidic channel coated with a confluent layer of endothelial cells. The endothelial cell-coated microfluidic channel mimics a blood vessel wall; introducing a platelet stream over the endothelial cell layer simulates the vascular system. Herein, this platelet stream is subjected to various doses of MS nanoparticles to examine the nanoparticle impact on platelet-endothelial cell interactions. The MS nanoparticles used in this research are fluorescent MS nanoparticles co-modified with PEG and trimethylsilane (FMS@PEG/TMS

throughout the manuscript), a nanostructure which has proven to be colloidally stable in complex biological environments and does not induce cell death.[9] Because the microfluidic platform is optically transparent, the fluorescent MS nanoparticles can easily be imaged along with individual stained platelets and endothelial cells associated with these nanoparticles. The study presented herein provides comprehensive analysis of platelet adhesion and aggregation processes in the presence of MS nanoparticles, yielding fundamental insight into how these nanoparticles will behave upon intravenous injection.

2.2 Methods and Experimental Setup

2.2.1 Fabrication of Microfluidic Platforms

The microfluidic platform was fabricated using standard photolithography techniques. Briefly, the device design was transferred to a chrome mask plate (Nanofilm) and then transferred onto a layer of SU-8 photoresist on a silicon wafer. After development, Sylgard 184 resin:curing agent (10:1) mixture was cast onto the mold and cured on a hot plate overnight. After this curing step, the polydimethylsiloxane (PDMS) layer on the mold was peeled and cut, punched for the inlet and outlet holes, rinsed using methanol, isopropyl alcohol, acetone and water, and then permanently bound to a glass substrate using oxygen plasma treatment. The channel dimensions were 100 μm (height) x 2000 μm (width) x 25000 μm (length).

2.2.2 Endothelial Cell Culture

The Hy926 human endothelial cell line was purchased from ATCC and then cultured in a T-flask. The culture media was Dulbecco's Modified Eagle Medium (DMEM) with high glucose, supplemented with 10% fetal bovine serum (FBS) and 1% penicillin and streptomycin. Two days before experiments, endothelial cells were trypsinyzed and re-suspended into the same culture media (1×10^7 number/mL), and then 20 μL of the cell suspension was plated onto the microfluidic device. Once plated onto a device, cells were fed every 12 hours and

formed a confluent layer in the microfluidic channel within two days. Devices lacking a uniform layer of endothelial cells were discarded.

2.2.3 Platelet Isolation

Human platelets were isolated from freshly-drawn human blood. Human blood samples were obtained from trained professionals at the Memorial Blood Center (IRB protocol E&I ID#07809) where the blood was drawn directly into tubes containing EDTA as an anti-coagulant. Briefly, once blood samples were obtained, the entire contents of the vial (5 mL) was transferred into a 15 mL centrifuge tube and centrifuged at 270xg for 20 minutes with no brake. Then, the top two-thirds of the platelet rich plasma (PRP) layer were transferred into a new centrifuge tube. Hirudin (Sigma-Aldrich, St. Louis, MO) was added at a concentration of 10 U/mL, and then the PRP was allowed to rest at 37 °C for 25 minutes. Following the rest, one-third volume of acid-citrate-dextrose (ACD, 85 mM trisodium citrate dihydrate, 66.6 mM citric acid monohydrate, 111 mM D-glucose) was added, and the PRP was again centrifuged at 800xg for 10 minutes with low brake. The platelet poor plasma (PPP) was removed, and the pellet was resuspended into Tyrodes buffer (137 mM NaCl, 2.6 mM KCl, 1.0 mM $MgCl_2$, 5.6 mM D-glucose, 5.0 mM HEPES, 12.1 mM $NaHCO_3$). The PRP was placed in the incubator for 30 minutes to rest, then centrifuged again at 800xg for 10 minutes with low brake after adding ACD. The formed pellet was again resuspended in Tyrodes buffer and the platelets were kept in the incubator again for 30 minutes to rest prior to 30 minute incubation with 2 μM 5-chloromethylfluorescein diacetate (CMFDA) dye (Invitrogen, Carlsbad, CA) so that platelets adhered onto endothelial cells could be fluorescently monitored. All results reported in this manuscript are derived from many platelets measured from 6 biological replicates (6 donors) unless otherwise specified.

2.2.4 Mesoporous Silica Nanoparticle Synthesis

Fluorescent mesoporous silica (FMS) nanoparticles were synthesized according to our previous work.[14,26] To prepare rhodamine B isothiocyanate (RITC) for incorporation into the silica network, it was first functionalized with 3-aminopropyltriethoxy silane (APTES) by incubating 2.6 mg RITC (Sigma Aldrich, Milwaukee, WI) and 2 µL APTES (Gelest, Morrisville, PA) in 1 mL 99% ethanol (Pharmco-Aaper, Brookfield, CT) with stirring overnight. The next day, 0.29 g cetyltrimethylammonium bromide (CTAB, Sigma Aldrich, Milwaukee, WI) surfactant was dissolved in 150 g of 0.256 M NH_4OH (Mallinckrodt, Phillipsburg, NJ) by stirring at 300 rpm at 50 °C. After 1 h, 2.5 mL of 0.88 M ethanolic tetraethylorthosilicate (TEOS, Sigma Aldrich, Milwaukee, WI) were added, followed quickly by 1 mL of the ethanolic RITC/APTES reaction. The mixture was stirred at 600 rpm and heated at 50°C for 1 h, followed by the addition of 450 µL PEG-silane (500-700 MW, Gelest, Morrisville, PA). After 30 minutes, 68 µL of chlorotrimethyl silane (TMS, Fluka, Buchs, Switzerland) were added. Stirring was stopped after 30 minutes, and the sample was aged at 50 °C for 20 h, allowing excess water to evaporate from the solution (final volume ~50 mL), resulting in sub-50 nm diameter RITC-fluorescent mesoporous silica nanoparticles co-modified with PEG and TMS (FMS@PEG/TMS). All nanoparticle batches were passed through a 0.45 mm filter to exclude large aggregates and placed in an oven at 90 °C for 24 h. This hydrothermal treatment contributes to colloidal stability and biocompatibility as established in our previous work.[14,30] Treated particles were then purified by dialysis and centrifugation and stored in MQ DI water prior to use. All reactions and post-synthetic steps were performed under dark conditions to prevent photobleaching.

2.2.5 Mesoporous Silica Nanoparticle Characterization

Dynamic light scattering measurements were performed on a 90Plus particle analyser (Brookhaven Instruments, Holtsville, NY) with a 35 mW red diode laser at 600 nm. Samples were diluted to 1 mg/mL in water and measured at room

temperature. A FEI Tecnai T12 transmission electron microscope with 120 kV operating potential was used to collect images for particle morphology and sizing. Diameters were calculated from an average of 500 nanoparticles. Nitrogen adsorption/desorption isotherms were acquired on a Micromeritics ASAP 2020 instrument after being degassed at 120 °C for 8 h.

2.2.6 On-chip Adhesion and Aggregation Assays

Once nanoparticles, platelets, and endothelial cell-coated microfluidic devices were ready, the population of platelets was divided and treated as desired. Of the eight experimental conditions considered, the first four conditions involved platelet exposure to no, 20 μg/mL, 200 μg/mL, or 1000 μg/mL FMS@PEG/TMS nanoparticles without intentional platelet activation (labeled as “unactivated” throughout the chapter), and the other four were the exact same nanoparticle conditions except that platelets were intentionally activated with adenosine diphosphate (ADP, ADP-activated throughout the chapter). For ADP-activated conditions, platelets were first exposed to the same four nanoparticle conditions followed immediately by 5 μM ADP. Platelet activation by ADP was used strategically to separate platelet adhesion and aggregation from secretion responses, which take place after activation using other stimuli such as thrombin. ADP is a strong platelet aggregation agonist that results in no direct induction of secretion.[28,29] Following exposure, the platelet suspension was introduced into the microfluidic channel using a syringe pump set at a flow rate of 30 μL/min. Given the dimensions of the microfluidic channel, the shear force generated by this flow rate, ~ 0.1 N/m^2 (~ 150 s^{-1}), will have minimal impact on the cells inside channel.[30-31] The stream of platelets was maintained for 25 minutes, and then the channels were washed with fresh Tyrodes buffer to remove non-adherent platelets from the channel. The platelet suspension coming through the channels was collected at the outlet for further analysis, and the devices placed on the fluorescence microscope for analysis using the Metamorph V.7.7.5 software. In adhesion studies, 3 replicates of 400 μm x 400 μm images (20x magnification)

were obtained from 3 random locations for each of the 6 donors. For the aggregation study, 3 replicates of 200 μm x 200 μm images (40x magnification) were obtained from 5 random locations for each of the 6 donors. Platelet aggregation was further analyzed using qualitative fluorescence imaging at higher magnification as detailed in Section 2.2.8. For the purposes of this study, platelet aggregates were defined as groupings of more than one platelet. Due to day-to-day differences in the absolute number of platelets adhered onto the endothelial cell layer, adhesion levels are reported as the ratio to the control (conditions without nanoparticle exposure in both unactivated and ADP-activated platelets). T-tests with $p = 0.05$ were used for statistical mean ± SEM significance testing.

2.2.7 Viability Assay

First, 20 μL of each platelet condition was collected at the microfluidic outlet and mixed with an equal volume of 0.4% trypan blue aqueous solution. Then, 20 μL of that solution was placed on a hemocytometer for cell counting. Trypan blue can enter dead cells due to their compromised cell membranes, staining them blue. The live and dead cells were counted and percent viability calculated.

2.2.8 Fixed-cell Fluorescence Imaging for Platelet Aggregation Assessment

The remaining platelets collected from the microfluidic device outlet were fixed by the addition of an equal volume of 8% formaldehyde (Sigma Aldrich, Milwaukee, WI) in Tyrodes buffer. Following fixation for 30 minutes at room temperature, the platelets were allowed to settle on poly-L-lysine coated coverslips. Some of the platelet-coated coverslips were then incubated with AlexaFluor 594 phalloidin (Life Technologies, Carlsbad, CA) at room temperature for 20 minutes to fluorescently label platelet actin according to the manufacturer's protocol. Briefly, the AlexaFluor 594 phalloidin vial contents were dissolved in 1.5 mL methanol, and then 5 μL of the stock was dissolved in 400 μL Tyrodes buffer to stain platelets. The platelets were imaged on a Nikon Eclipse TE-2000U using a

100x/1.40 oil immersion objective and various filter cubes to capture the platelet aggregates and association with the nanoparticles. The number of platelets making up each aggregate was analyzed using Metamorph V.7.7.5. The statistical variation between samples was analyzed using a t-test.

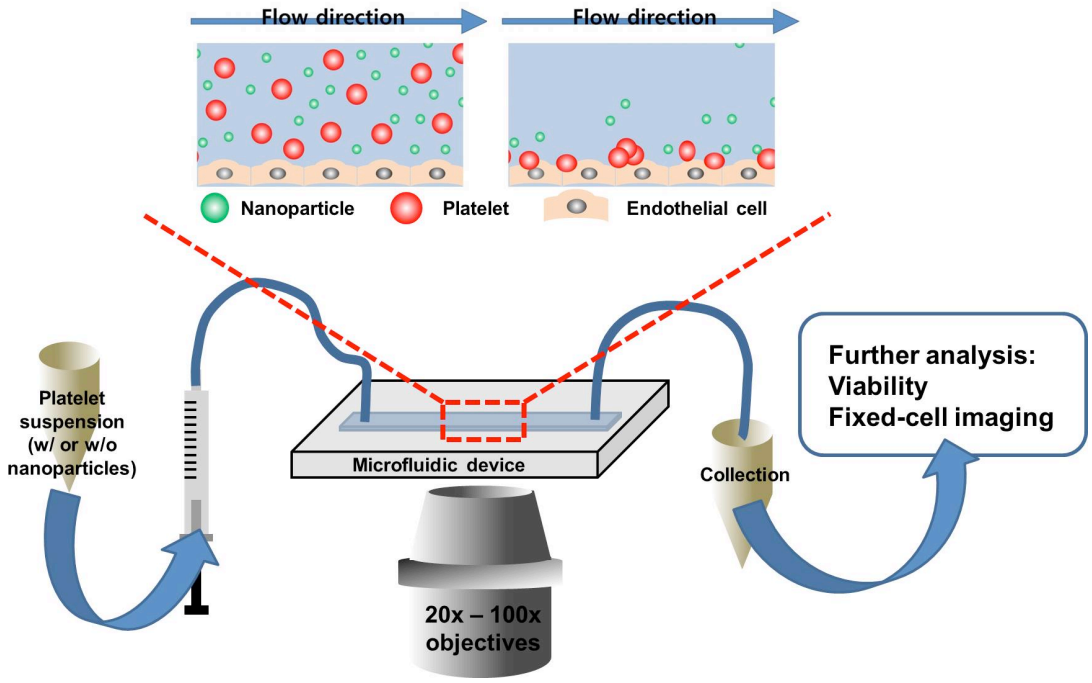

Figure 2.1 On-chip platelet adhesion/aggregation assay platform schematic.

2.3 Results and Discussion

2.3.1 Nanoparticle Synthesis/Characterization

FMS@PEG/TMS nanoparticles were obtained through a procedure based on our previous work. These MS nanoparticles are surface functionalized with both PEG and TMS, a co-modification procedure that has been shown to produce long-term colloidal stability in biological environments such as protein-containing or high ionic strength media.[14,2] TEM imaging of these nanoparticles revealed relatively monodisperse particles with a diameter of 47.9 ± 7.1 nm (Figure 2.2A). DLS hydrodynamic diameter in water was slightly higher, as expected, at 66.8 ± 0.3 nm (Figure 2.2B). Photos of bulk nanoparticle solution under ambient and ultraviolet light (Figure 2.2B inset) show the bright and homogeneous fluorescence achieved with these materials. Nitrogen adsorption/desorption isotherms show that high surface area is obtained despite the functionalization of this material (Figure 2.2C). This high surface area will be critical in future studies where these nanoparticles will be used to deliver drug cargo to platelets or other cell types.

2.3.2 FMS@PEG/TMS and Platelet Viability

Trypan blue staining of platelets collected from the microfluidic device showed no significant loss in platelet viability for any of the conditions (Figure 2.3). This benign nanoparticle interaction was expected for FMS@PEG/TMS nanoparticles as they have been shown to be non-toxic to endothelial cells in the past.[9] The main interest of our investigation, then, was in identifying any deviations in platelet adhesion and aggregation behavior upon exposure to FMS@PEG/TMS nanoparticles.

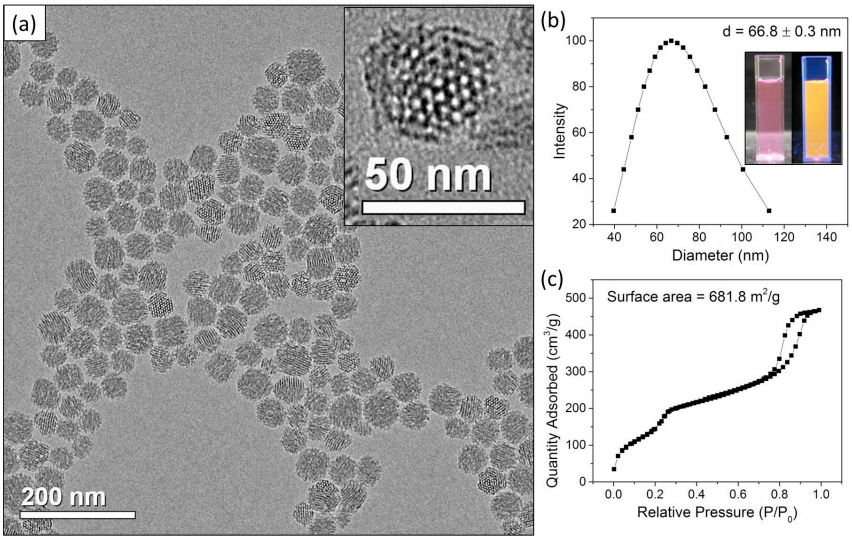

Figure 2.2 RITC-MS@PEG/TMS nanoparticle characterization. A) TEM image B) Hydrodynamic size distribution by dynamic light scattering. C) Nitrogen (N_2) adsorption/desorption data for the fluorescently labeled mesoporous silica nanoparticles co-modified with PEG and TMS (RITC-MS@PEG/TMS).

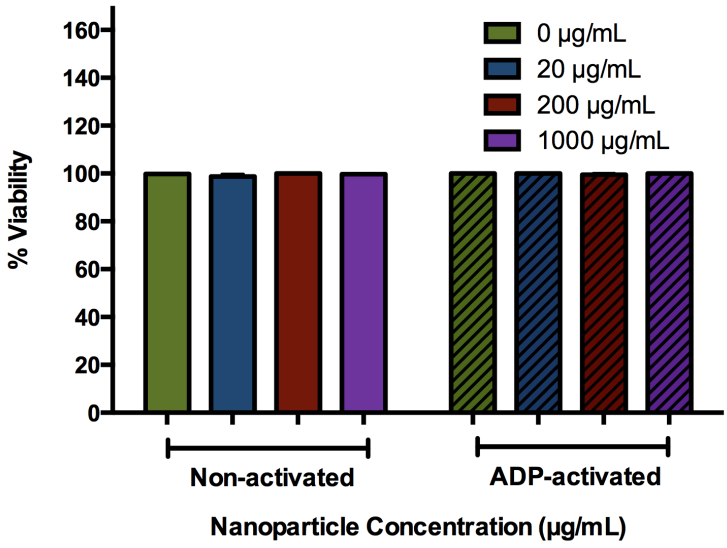

Figure 2.3 Percent viability of platelets by trypan blue assay. Error bars are present on this graph but are difficult to visualize as the SEM is very small in these data. $p > 0.05$ in all cases.

2.3.3 FMS@PEG/TMS and Platelet Adhesion and Aggregation

To investigate the impact of nanoparticle presence on platelet adhesion, varying concentrations of nanoparticles were introduced into the platelet stream on endothelial cells. The chosen concentrations of nanoparticles are 20 μg/mL, 200 μg/mL, and 1000 μg/mL. Assuming 3-5% loading by weight of doxorubicin, a typical cancer therapeutic, a single nanoparticle dose via intravenous injection would be in the range of 3000-4000 mg in a total volume of 10s to 100s of mL. Thus, the doses used in this study are relevant, particularly for platelets near the site of injection. As platelets are sensitive to flow conditions,[36-38] the device operation was kept at a flow rate (30 μL/min in a channel that is 100 μm thick and 2000 μm wide) that minimizes flow-induced activation of platelets. The device used herein had multiple straight channels to perform simple parallel analysis of replicate samples, but it could easily be adapted to include multiple branches to increase the throughput or various channel dimensions to simulate more complex vasculature.

The number of platelets adhering to endothelial cells had a slight variation from day-to-day (or donor-to-donor); as such, the adhesion values reported in this manuscript are presented as the ratio compared to the control cells from that donor. Thus, control cells from both unactivated and ADP-activated cells always show 1 as the adhesion value. Without ADP activation, FMS@PEG/TMS nanoparticle exposure had a significant impact on platelet adhesion to endothelial cells. Both 20 μg/mL and 200 μg/mL nanoparticles resulted in reduced adhesion of platelets to endothelial cells ($p < 0.0001$ for both compared to control, Figure 2.4), and the trend was concentration-dependent. In our experimental system, ~ 3.5×10^6 platelets are introduced to the confluent endothelial cell layer and, assuming an average platelet diameter of 2.5 μm, an average nanoparticle diameter of 48 nm, the shape of each nanoparticle as a hexagonal prism, a pore volume of 0.81 cm^3/g, and a diffusion length of 1 μm for

a nanoparticle, ~ 2000 nanoparticles surround a single platelet during an experiment. Intuitively, the presence of nanoparticles within the platelet suspension may interfere with platelets interacting with one another as well as with the layer of endothelial cells, and this might be a cause of the reduction in adhesion. In previous work, the FMS@PEG/TMS nanoparticles have shown no significant impact on the viability of endothelial cells, so the change in adhesion behaviour can be attributed to nanoparticle effects on the platelets directly.[9]

A similar trend was found in ADP-activated platelets. Compared to the control cells (no nanoparticles) activated by ADP, ADP-activated platelets exposed to both 20 μg/mL and 200 μg/mL FMS@PEG/TMS nanoparticles also showed reduced adhesion to endothelial cells ($p < 0.0001$ for both, Figure 2.4). Thus, it can be concluded that the presence of nanoparticles interferes with the platelet-endothelial cell interaction and reduces physical contact between them. This preliminary conclusion requires further studies into platelet and endothelial cell biology to characterize why this interaction is impeded – possible causes include changes in surface receptor expression, outer bilayer phospholipid composition, or secretion of soluble mediators.

While ADP-activated platelets still had nanoparticle concentration dependence in their adhesion behavior, they display a more complicated trend than their non-activated counterparts. ADP-activated platelets exposed to 200 μg/mL nanoparticles show slightly higher adhesion to endothelial cells when compared to the ADP-activated platelets exposed to 20 μg/mL nanoparticles ($p = 0.025$, Figure 2.4). A previous nanotoxicity study with endothelial cells has shown that activation of cells may result in different trends in cellular responses against nanoparticles compared to their unactivated counterparts.[9] This difference, depending on whether or not platelets are ADP activated, implicates cell-nanoparticle interaction beyond a physical interaction level in platelet adhesion to

endothelial cells; at a certain concentration, the presence of nanoparticles may cause cellular activation that changes adhesion behaviour.

This reasoning is supported by the trend in platelet adhesion exposed to the highest concentration of nanoparticles. Both unactivated and ADP-activated platelets exposed to 1000 μg/mL nanoparticles showed a significant increase in their adhesion to endothelial cells (Figure 2.4). Several data support the hypothesis of a potential signaling cascade triggered by this large dose of nanoparticles. First, fluorescence analysis confirmed nanoparticle association to endothelial cells, and while it was not very clear from on-chip assessment due to the interference from nanoparticles on endothelial cells, our fixed-cell fluorescence imaging (vide infra) confirmed nanoparticle association with platelets (Figure 2.5). Second, our preliminary assessment of platelet adhesion to fibronectin-coated (i.e. without endothelial cells) surfaces has shown that both unactivated and ADP-activated platelets adhered less to fibronectin when they were exposed to 1000 μg/mL than 200 μg/mL (data not shown). Together, these imply an additional signaling cascade between platelets and endothelial cells that is triggered by the high concentration of nanoparticles presented. As adhesion of platelets is a critical step for their in vivo function, future studies could probe platelet secretion of chemical messengers and adhesion studies under the same nanoparticle exposure conditions but with different biological stimuli (e.g. thrombin that induces direct secretion from platelets).

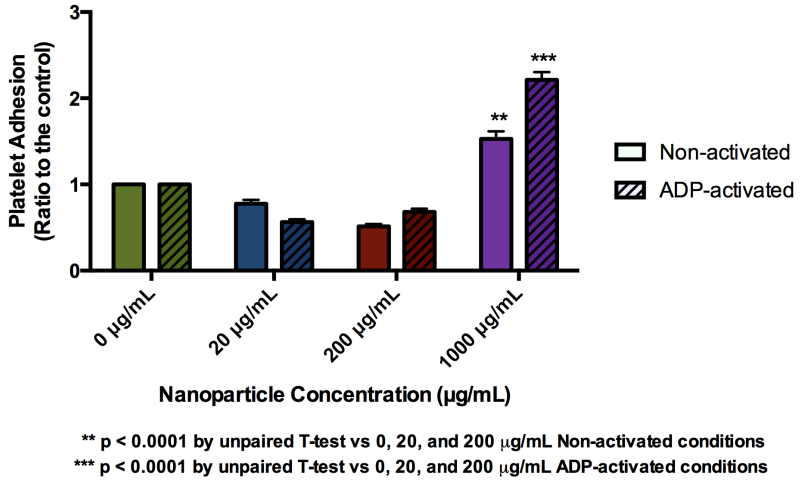

Figure 2.4 Adhesion of non-activated and ADP-activated platelets onto endothelial cells.

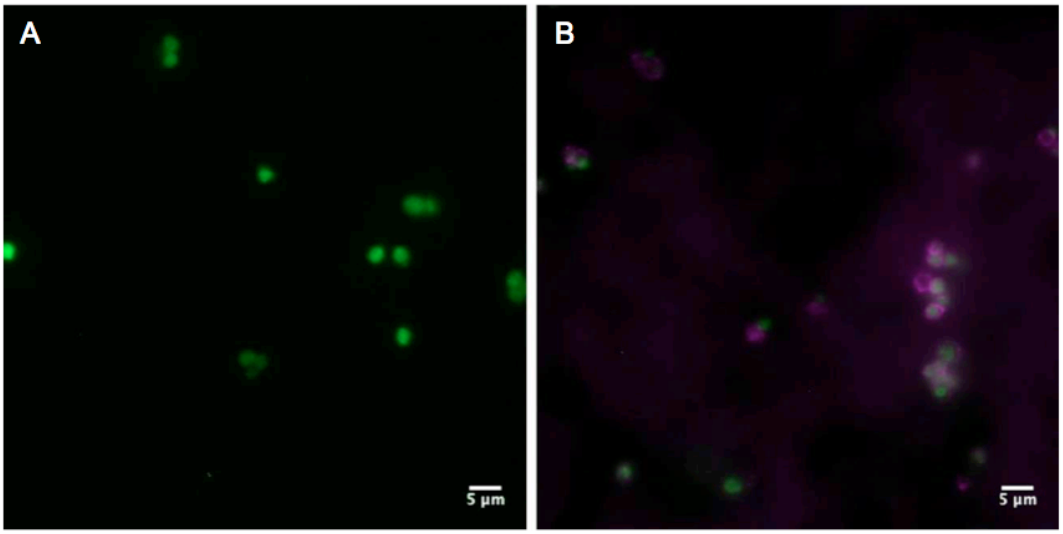

Figure 2.5 Representative images from fixed-cell fluorescence imaging. A) ADP-activated, 0 µg/mL nanoparticle condition showing major population of platelets in single or small aggregates, and B) ADP-activated, 1000 µg/mL nanoparticle condition showing major population of platelets in large aggregates. Images processed for overlaying by ImageJ (green: platelets, purple: nanoparticles).

In addition to adhesion, the presence of nanoparticles also influenced platelet aggregation behaviour (Figure 2.6). Unlike the adhesion assay, the aggregate value obtained in these on-chip experiments is the absolute number of aggregates (normalized to the total area of the collected image). In general, compared to the control cells, the number of platelet aggregates did not significantly change except at the highest nanoparticle dose. Only the 20 μg/mL nanoparticle condition of ADP-activated platelets showed a slightly lower number of aggregates when compared to that in 200 μg/mL condition of ADP-activated platelets ($p = 0.01$). Both unactivated and ADP-activated platelets exposed to 1000 μg/mL nanoparticles show significantly increased aggregation.

These results support the conclusion from the adhesion assay above that the impact of nanoparticles on platelet adherence is mostly physical interference until they reach a certain dose. While on-chip investigation provides an initial assessment of platelet aggregation, the majority of the platelet suspension will pass over the layer of endothelial cells and flow through the device outlet. To assess aggregate formation in non-adherent platelets, we performed conventional fluorescence imaging on fixed platelets delivered to the outlet to complement our on-chip assay results.

The imaging studies of the collected platelet suspensions exhibited similar trends to those found in the on-chip assay (Figure 2.7 and Figure 2.8). First, in both the unactivated and ADP-activated platelets, the majority of the platelets were not part of an aggregate. The isolated state of the majority of platelets is consistent with the fact that activated platelets are likely to adhere to the endothelial cells and form aggregates within the microfluidic device. For unactivated conditions, platelets exposed to 200 and 1000 μg/mL nanoparticle concentrations showed a significantly increased number of aggregates ($p = 0.06$ and $p = 0.03$, respectively). For ADP-activated conditions, only the 1000 μg/mL nanoparticle condition showed a statistically significant increase in aggregation ($p = 0.02$). The

small population of aggregates were analyzed further, focusing specifically on the larger aggregates, namely those with more than 4 platelets. These were counted, and the ratio of the number of aggregates to the total number of platelets in the population was calculated. The unactivated platelet aggregate ratios were the same under all control and nanoparticle exposure conditions. On the other hand, the ADP-activated platelet ratios were similar to those from the unactivated platelets except for the 1000 µg/mL condition. These ADP-activated platelets showed an increased number of large aggregates at this nanoparticle dose ($p = 0.02$ Figure 2.8), which is consistent with the on-chip aggregation results. To be noted, as shown in Figure 2.5, the fluorescence imaging also revealed that the nanoparticles are co-localized with the platelet aggregates. Isolated platelets show weak nanoparticle fluorescence when the platelet and nanoparticle fluorescence signals are overlaid (Figure 2.5A) while the platelet aggregates appear to be highly associated with the fluorescent nanoparticles (Figure 2.5B). All of these results support the conclusion from the on-chip adhesion and aggregation assays, showing high levels of activation and aggregation of platelets at the high nanoparticle dose.

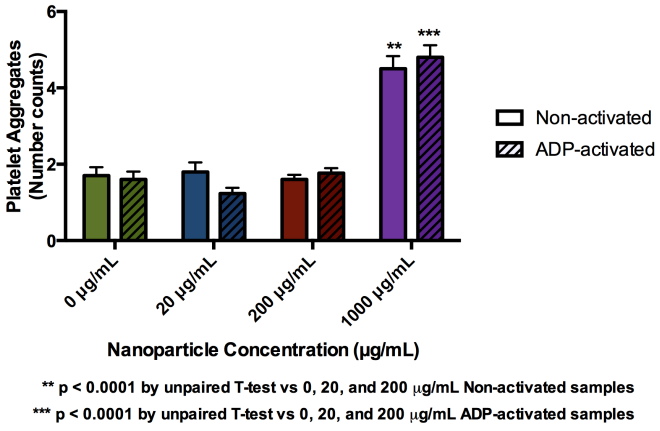

Figure 2.6 Aggregation of non-activated and ADP-activated platelets. The p value indicates significant differences between the 1000 µg/mL treatment with all other treatments within a condition.

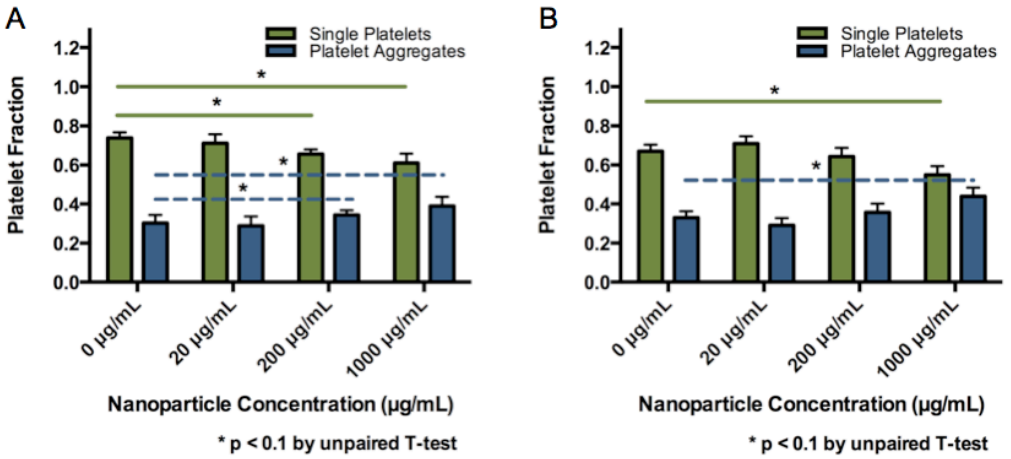

Figure 2.7 Aggregation assay by fixed-cell fluorescence imaging. A) Non-activated platelets. B) ADP-activated platelets.

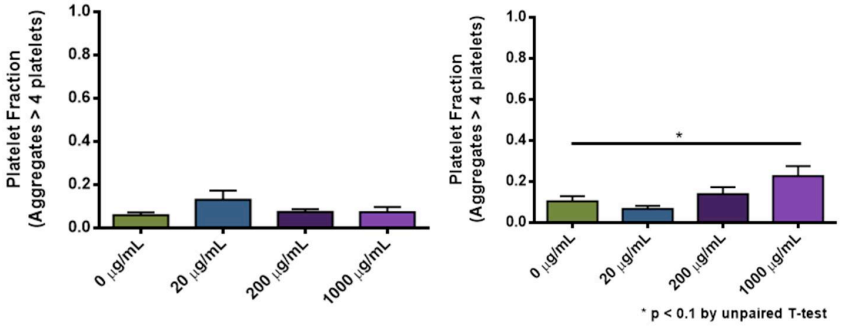

Figure 2.8 Aggregation of more than 4 platelets. A) non-activated platelets and B) ADP-activated platelets obtained from fixed-cell fluorescence imaging.

2.3 Conclusion

This study exploits the use of microfluidics to explore the impact of mesoporous silica nanoparticles on platelets and endothelial cells in a simulated blood vessel system. As the use of nanoparticles as drug delivery agents increases, in particular those with a proposed delivery method of injection into the blood stream, it is important to understand what potential interactions will occur between nanoparticles and the various blood components. It is critical to go beyond considerations of live/dead viability and assess changes in critical cellular functions upon nanoparticle exposure.[39] The simple microfluidic platform used herein incorporated multiple cell types, endothelial cells and platelets, and reveales that introduction of mesoporous silica nanoparticles, especially at high doses, can impact platelet-endothelial cell interactions. Also, in this initial study, we limited our model blood vessel by considering only convective flow conditions and one set of channel dimensions, but it is trivial to expand the scope of studies by changing these parameters to match other physiological environments. For example, flow-induced shear stress varies in our body (e.g. artery vs. vein), and as mentioned earlier in the manuscript, both platelets and endothelial cells have shear stress dependency in their behaviors. Thus, it will be of significant interest in future studies to study the impact of different shear stress levels on such cell-nanoparticle interactions using a similar approach. In addition, this platform can be used with cell types beyond platelets and endothelial cells, and more importantly, assessment of other critical cellular functions, such as secretion or reactive oxygen species generation. Accordingly, this approach will be generally useful in providing good in vitro models for nanotoxicology studies to broaden our understanding of nanoparticle-cell interactions.

Chapter 3

Cytoskeleton Dynamics in Drug-treated Platelets

Adapted from:

Finkenstaedt-Quinn, S. A.; Ge, S.; Haynes, C. L. “Cytoskeleton dynamics in drug-treated platelets.” *Analytical and Bioanalytical Chemistry,* **2015**, *407* (10), 2803-2809.

3.1 Introduction

Platelets play a diverse set of roles in the body. The most well-characterized aspects of platelets are the roles they play in hemostasis and thrombosis, but they have also been implicated in processes such as inflammation and the migration of cancer cells.[1-3]

In vessel injury, endothelial cells expose a variety of adhesion molecules and secrete small molecules. When platelets encounter the site of injury, the exposed adhesion molecules bind to the platelets and impede their travel. The binding of the adhesion molecules and the small molecules secreted by the endothelial cells initiate an activation cascade in the platelets that then leads to clot formation. Specifically, damaged endothelial tissue releases tissue thromboplastin (Factor III), which goes on to activate Factor VII. Additionally, exposed collagen can bind to Factor XII and activate it. Either Factor VII or Factor XII can then initiate the signaling cascade, leading to prothrombin activator (Factor X) formation. Prothrombin activator can then bind to the substrate prothrombin (Factor II), cofactor V, and Ca^{2+} to form prothrombinase. This prothrombinase complex cleaves the prothrombin and releases thrombin. Thrombin serves a few different functions, including activating Factor XI and cleaving fibrinogen, either released from the platelets or found in the blood, to give fibrin. Factor XI is one of the proteins involved in the cascade leading to Factor X activation, and thus thrombin serves to amplify the activation signal. Fibrin functions as the linker between platelets so that they can form clots.[4,5] Two main processes characterize platelet activation: (1) the secretion of small molecules and proteins and (2) a major cytoskeleton-mediated shape change.[6,7] Small molecule secretion functions to propagate the activation signal and initiate the wound healing process by other cells, and there has recently been significant progress in characterizing this secretion process.[8-13] Preliminary work has studied the accompanying shape change, wherein platelets undergo a

major cytoskeletal rearrangement where the cell body swells up and then flattens out to form extensions called lamellipodia and filopodia, but the timeline of shape change has not been quantitatively evaluated.[14]

The two main components that make up the platelet cytoskeleton are the microtubule ring and the actin matrix. Dissimilar to most cells, the microtubules in platelets form a circumferential loop at the outer edge of the platelet while the actin matrix is spread throughout the platelet.[15,16] There are a number of proteins associated with actin and actin dynamics in platelets, a few of which are mentioned here.[17] The actin matrix is attached to the cell membrane primarily through the von Willebrand factor receptor, whereby actin-binding protein bind to a cytoplasmic portion of the receptor. Actin monomer addition is primarily regulated by thymosin β4, which binds monomers to prevent their addition, and profilin, which facilitates monomer addition. Growth of the filaments can also be regulated by CapZ/capping protein which binds to the barbed, fast growth ends to modulate filamentous growth. VASP, a focal adhesion protein, is involved in filamentous bundling and nucleation.[17]

Our goal herein is to develop a way to make a direct connection between platelet secretion and morphological change, allowing both fundamental insight into platelet biology and critical studies about drug or disease effects on blood platelets. With the methods developed, this work demonstrates that as platelets in suspension undergo activation, both the actin matrix and microtubule ring decrease in size. As activation progresses, the actin matrix reaches a stable size whereas the microtubule ring shrinks to a certain extent and then breaks up into small microtubule fragments. It is possible to then compare the results from the imaging data with dynamic secretion measurements and obtain information by correlating the two. The results presented herein, when compared with data previously obtained, verify that the actin matrix acts as a barrier to dense-body

granule secretion and that the microtubule ring is not involved in dense-body granule secretion.[9]

3.2 Materials and Methods

3.2.1 Platelet Isolation

To isolate platelets, approximately 10-15 mL of rabbit blood was drawn from the midear artery of a rabbit after sedation according to IACUC protocol # 1311-31082A. The blood was centrifuged at 500 rcf with a brake speed of 0 for 15 minutes, at which point the supernatant, platelet rich plasma (PRP), was transferred to a clean centrifuge tube. The PRP was mixed with an equal volume of acid citrate dextrose solution (ACD; 85 mM trisodium citrate dihydrate, 66.6 mM citric acid monohydrate, 111 mM D-glucose) to prevent clotting during the platelet isolation. The PRP was then centrifuged at 750 rcf for 9 minutes to pellet the platelets, and the supernatant was removed. Next, the platelet pellet was resuspended in Tyrodes buffer (137 mM NaCl, 2.6 mM KCl, 1 mM $MgCl_2 \bullet 6H_2O$, 5.55 mM D-glucose, 5 mM HEPES, 12.1 mM $NaHCO_3$) and PGI_2 (0.5 μM). To ensure that the platelets had time for recovery, they were not used until 1 hour after isolation. Visual inspection of the platelets upon resuspension was performed to detect any morphological changes in the platelets, indicating activation. The platelet cell count was determined using a hemocytometer, with a typical isolated platelet concentration between 1-2 x 10^8 platelets/mL. The actin and microtubule experiments were performed on different days, and platelet preparations resulted in a lower concentration of platelets for the microtubule conditions.

3.2.2 Immunofluorescence Imaging

Immunofluorescence imaging was performed on fixed platelets. Initially, platelets, at a concentration of 1 x 10^7 platelets/mL, were activated using human thrombin (5 units/mL, Sigma-Aldrich, Milwaukee, WI) at room temperature. Aliquots from the activated PRP were removed at 50 s intervals and activation was quenched

by addition of the PRP to 8% formaldehyde in Tyrodes buffer.[18] Fixation was allowed to proceed for 20 minutes in the same 8% formaldehyde solution, after which the platelets were pelleted by centrifugation for 5 minutes at 2500 rcf. The fixative solution was removed, and the platelets were resuspended in 0.1% Triton X-100 (Sigma Aldrich, Milwaukee, WI) in Tyrodes buffer containing 0.1 mM EGTA (Sigma Aldrich, Milwaukee, WI). After 10 minutes of permeabilization, the platelets were again washed via pelleting, supernatant removal, and resuspension. Next, the platelets were incubated in a 1% BSA (SeraCare Life Sciences Inc., Oceanside, CA) solution in Tyrodes buffer for 30 minutes to block nonspecific antibody binding. After another wash step, the platelets were incubated with either a Cy3-conjugated anti-β-tubulin-antibody (ab11309, Abcam, Cambridge, MA) to label the microtubule ring, with the antibody diluted 1:100 in 1% BSA in Tyrodes, or a FITC-conjugated anti-β-actin-antibody (ab11005, Abcam, Cambridge, MA) to label the actin matrix, with the antibody diluted 1:250 in 1% BSA in Tyrodes buffer. The antibody incubation was performed overnight at 4^{o}C. Finally, the platelets were washed again and allowed to settle onto poly-L-lysine coverslips (1 μg/mL, 0.1% w/v poly-L-lysine in H_2O, Sigma Aldrich, Milwaukee, WI) for imaging.

The fixed and labeled platelets were imaged using a Nikon Eclipse TE2000-U microscope and a Photometrics QuantEM:512SC camera. A 100x/1.40 oil immersion objective was used to obtain sufficient magnification of the platelets to enable clear visualization of the microtubule ring.

3.2.3 Drug Treatment

Drug-treated platelets were incubated with cytochalasin D, latrunculin A, vincristine, or paclitaxel (Sigma Aldrich, Milwaukee, WI) at a concentration of 10 μM for 45 min at room temperature prior to activation. The concentration used was chosen based on previous work examining the platelet cytoskeleton.[9,19] As cytochalasin D, latrunculin A, and paclitaxel are insoluble in water, they were first

dissolved in DMSO. As a control, platelets were also incubated with an equivalent DMSO concentration prior to activation to account for any effects DMSO itself might have on platelets.[20]

3.2.4 Image Analysis

For each condition, approximately 20 82 μm by 82 μm fluorescence images were recorded, with several platelets visible in each image. Shape change progressions are shown in Figures 3.1 and 3.3 for the microtubule ring and actin matrix, respectively. For the microtubule ring-stained platelets, the diameter of each microtubule ring was measured at three locations to account for any non-circular character of the microtubule ring (Figure 3.2A). For the actin-treated platelets, the circumference of the actin matrix was measured. An ellipse was drawn inside the fluorescently labeled actin matrix, touching but not exceeding the edges (Figure 3.4A). For each condition, 25 platelets were measured. By determining the average measured value for each time point, a plot was created showing the change in diameter or circumference over time. Each plot was fit using a one-phase decay curve. Statistical analysis was performed using GraphPad Prism. One-way ANOVA was used to compare the shape change as a function of time. A comparison of fits was also used to determine significance between the various treatments. Any $p < 0.05$ was considered significant.

3.3 Results and Discussion

There are several pharmacological agents with modes of action based on cytoskeletal elements; these drugs present a perfect platform to prove the utility of these platelet imaging analyses. To disrupt microtubule dynamics, platelets were incubated with either vincristine or paclitaxel. At the concentrations used, paclitaxel is known to stabilize microtubules, and vincristine is known to cause destabilization of microtubules.[21] Paclitaxel binds to the inside surface of the β-tubulin subunit in microtubules and causes a conformational change that increases the tubulin subunit's affinity for the adjacent subunits, effectively promoting polymerization.[21] Vincristine binds to both the free tubulin subunits and

ends of microtubules and reduces treadmilling, leading to microtubules of static length.[21] The same procedure was applied to examine the role of the actin matrix in platelet secretion wherein platelets were incubated with either cytochalasin D or latrunculin A, both of which are known to inhibit polymerization of actin filaments. The modes of inhibition vary between cytochalasin D and latrunculin A, where the former binds to the filament and prevents addition of monomers while the latter binds to the monomer to prevent addition to the filament.[22,23]

3.3.1 Microtubule Results

Image Processing

The labeled microtubules exhibited well-defined fluorescence, clearly showing that the labeled structures formed a ring (Figure 3.1). The rings were not completely circular, many being ellipsoidal in shape. To get an accurate measurement of the size change, the diameter of the microtubule ring was measured three times, approximately where the longest, shortest, and an intermediate diameter were chosen (Figure 3.2A). In addition, platelets that appeared to have settled on the coverslip at an angle were not measured, as their dimensions were skewed, appearing thin and long.

No Treatment

Untreated (control) platelets showed a change in microtubule ring diameter from 3.3 ± 0.1 μm to 1.7 ± 0.1 μm during the 240 s time course following activation with thrombin. The primary diameter change occurred over the first 40 s of activation ($p < 0.0001$); while the diameter appears to decrease over the remaining 150 s, the changes are not statistically significant (Figure 3.2B).

DMSO

A control was also performed using DMSO, a necessary reagent to dissolve the paclitaxel. The diameter of the DMSO-treated platelets started and ended at 3.4 ± 0.1 μm and 1.7 ± 0.1 μm, respectively. These diameters were not statistically different from those measured from the non-treated platelets ($p > 0.05$, Figure

3.2B). However, during activation, the DMSO-treated platelets exhibited a more start-stop approach to microtubule shrinkage, where the diameters had statistically significant decreases between 0 and 40 s ($p < 0.0001$) and 90 and 140 s ($p < 0.05$). This was further exemplified by the fact that a one phase exponential fit tested via ANOVA did not fit both data sets ($p < 0.05$).

Vincristine

Treating platelets with vincristine resulted in the destruction of the microtubule ring dynamics (Figure 3.2C). These platelets had microtubule rings that started off with an average diameter of 2.3 ± 0.1 μm and ended at a diameter of 2.5 ± 0.1 μm. The diameter fluctuated throughout the 240 s with a low of 2.2 ± 0.0 μm at 90 s and a high of 2.5 ± 0.1 μm at 240 s.

Paclitaxel

The paclitaxel-treated platelets were statistically compared to the DMSO-treated platelets as the paclitaxel solutions were prepared in DMSO. The paclitaxel-treated platelets started off with a smaller ring diameter, 3.1 ± 0.1 μm, than the DMSO-treated platelets. After activation, the paclitaxel-treated platelets initially exhibited a slower decrease in ring diameter compared to the DMSO-treated platelets ($p < 0.001$). Around 140 s however, the shrinkage dynamics of the microtubule ring in the paclitaxel-treated platelets became greater in magnitude than those of the DMSO-treated platelets, resulting in a final diameter of 1.5 ± 0.0 μm (Figure 3.2D). Similar to the DMSO-treated platelets, the primary shape change occurred between 0 and 40 s ($p < 0.0001$) and 90 and 140 s ($p < 0.05$) of activation.

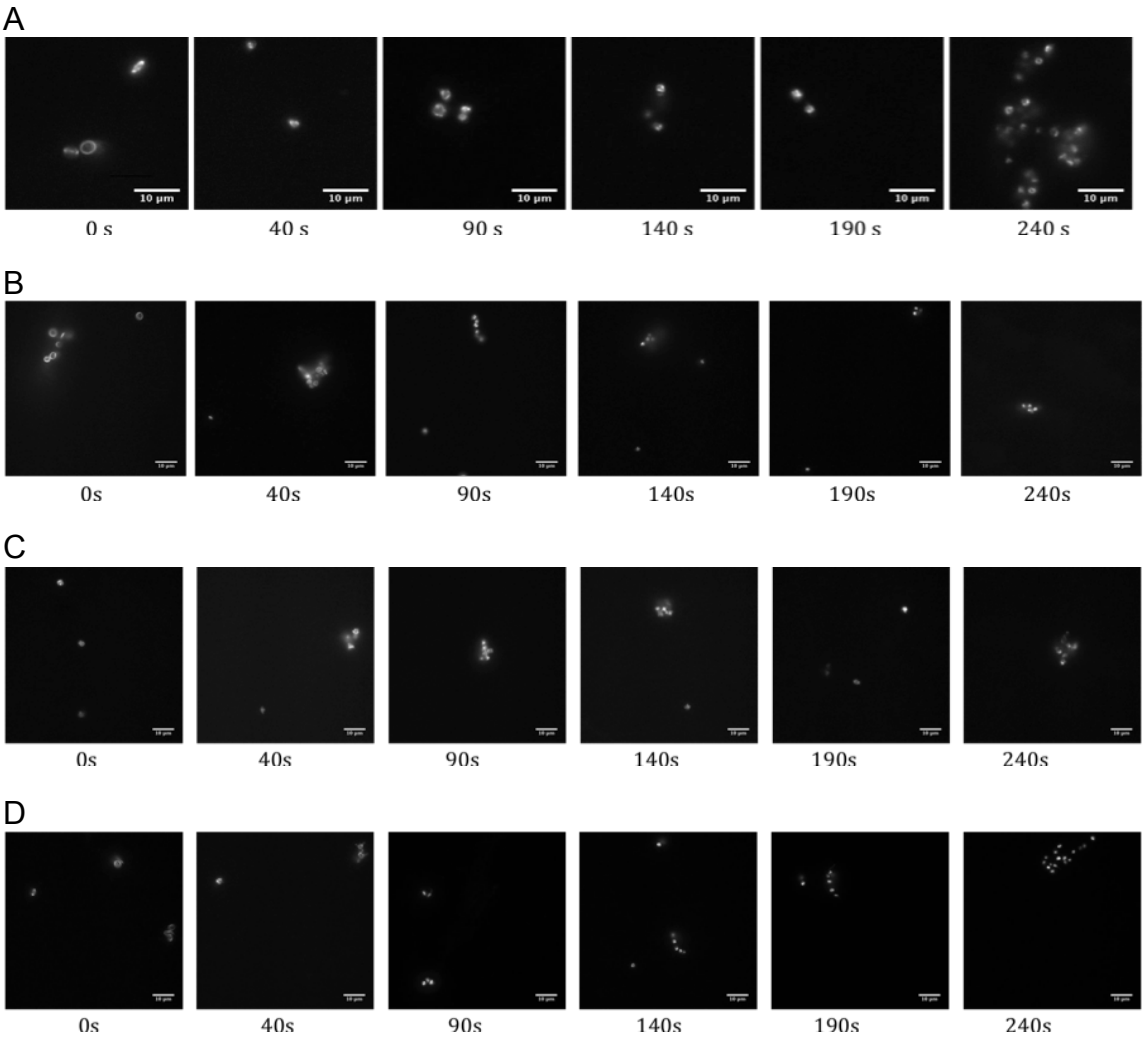

Figure 3.1 Timeline of microtubule ring shrinkage dynamics during activation. A) No treatment – The ring structure of the microtubules can be seen initially but becomes less well-defined as activation progresses. B) DMSO – As in the no treatment condition, the ring structure of the microtubules is visible at early time points but loses definition as activation progresses. C) Vincristine – The vincristine-treated platelets showed a complete destruction of the microtubule ring structure. D) Paclitaxel – In the paclitaxel-treated platelets, the microtubule ring structure is apparent at the early time points, but as activation progresses it becomes harder to distinguish. Scale bar 10 μm.

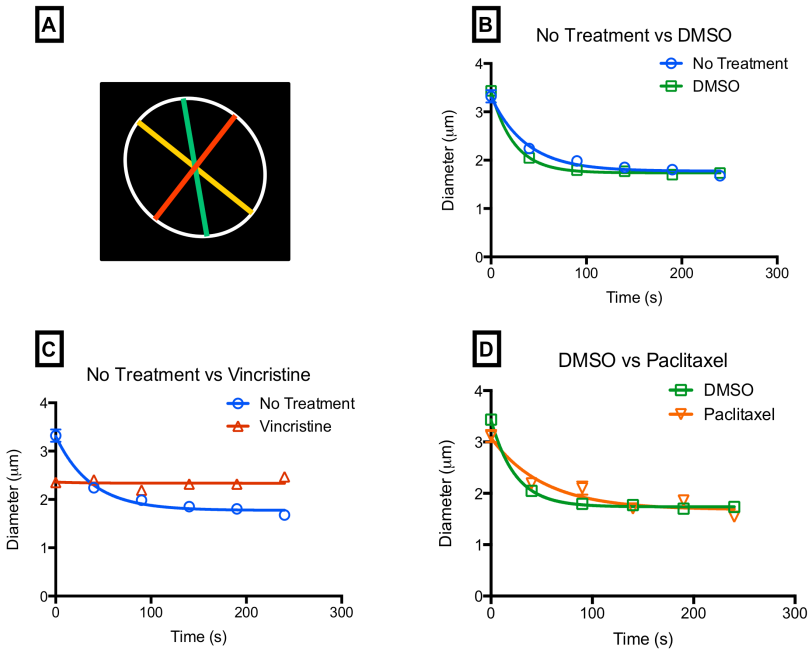

Figure 3.2 Microtubule ring – progressions A) The microtubule ring of each platelet was measured by taking the diameter of the ring at the smallest, largest, and intermediate lengths. B-D) Comparison of the microtubule ring shrinkage curves for non-treated and DMSO-treated platelets, non-treated and vincristine-treated platelets, and DMSO-treated and paclitaxel-treated platelets, respectively. Error bars indicate SEM.

3.3.2 Actin Results

Image Processing

Labeling of the actin matrix is not as straightforward as labeling the microtubule ring because the cytoskeletal element is not as well defined. The actin-based fluorescence images showed diffuse fluorescence that appeared throughout the platelet (Figure 3.3). There were some structures visible in the form of dark spots within the fluorescent area, possibly resulting from granules, but they were uncommon and thus left uncharacterized (Figure 3.5). Like the microtubule rings, the fluorescent structure was not uniformly circular in shape and so it was necessary to determine the best measurement method to characterize the structure. The methods tried include: fitting a circle or ellipse to the exterior or interior of the actin matrix or tracing the edges of each platelet. While tracing the edges initially appeared to be the best method, it became apparent that the time required to accurately trace the edge of each actin matrix was substantial. In addition, the edges were not always clear in the images, making this method somewhat subjective. More of the images exhibited platelets with an elliptical shape than a round shape, and so using the ellipse to approximate the platelet size was found to be most efficient and effective. When comparing measurements made on the exterior or interior of the fluorescent area, the interior measurements visually resulted in a closer fit to the true circumference than the exterior measurements. Thus a best-fit ellipse was used to approximate the actin matrix circumference, though this may result in a slight underestimation of total actin coverage (Figure 3.3A).

No Treatment

The platelets that were not subjected to drug treatment showed a change in actin matrix circumference from 10.9 ± 0.3 μm to 9.1 ± 0.2 μm over the 240 s imaged (Figure 3.4B). The key characteristic found for actin matrix shape change was that the majority of the shrinkage occurs within the first 40 s after platelet activation. While the size did not appear to be completely static during the later

time points, the differences in the circumference were not statistically significant ($p > 0.05$).

DMSO

Similar to the microtubule disruption experiments, a control set of platelets were treated with DMSO as both latrunculin A and cytochalasin D are insoluble in water. The DMSO-treated platelets exhibited a more gradual decrease in circumference compared to the untreated platelets, going from 9.5 ± 0.4 μm to 8.2 ± 0.2 μm during the time monitored (Figure 3.4B). The decrease in size occurred over the first 90 s rather than the first 40 s in the untreated platelets ($p \leq 0.05$). Similarly however to the untreated platelets, later changes were not statistically significant ($p > 0.05$). It is also important to note that, in addition to the change in time course, the DMSO-treated platelets started and ended up with a smaller circumference than the untreated platelets, despite the low DMSO concentrations used, indicating that the DMSO does influence the normal actin dynamics.

Latrunculin A

The latrunculin A-treated platelets started off the same size as the DMSO-treated platelets but did not change size in a statistically significant manner at any point during activation ($p > 0.05$). The circumference varied slightly, within a range in 0.5 μm where they were at their smallest at the 0 s time point and their largest during the 90 s time point, going from 9.6 ± 0.2 μm to 9.9 ± 0.2 μm (Figure 3.4C).

Cytochalasin D

The decrease in size of the cytochalasin D-treated platelets occurred faster than that of the DMSO-treated platelets, where they reached a stable size within the first 40 s of activation. In addition, the cytochalasin D-treated platelet circumferences started off 1.5 μm larger than the DMSO-treated platelets and ended 0.5 μm larger, going from 11.0 ± 0.3 μm to 9.1 ± 0.2 μm, despite the DMSO-treated platelets being larger at the 40 s time point (Figure 3.4D).

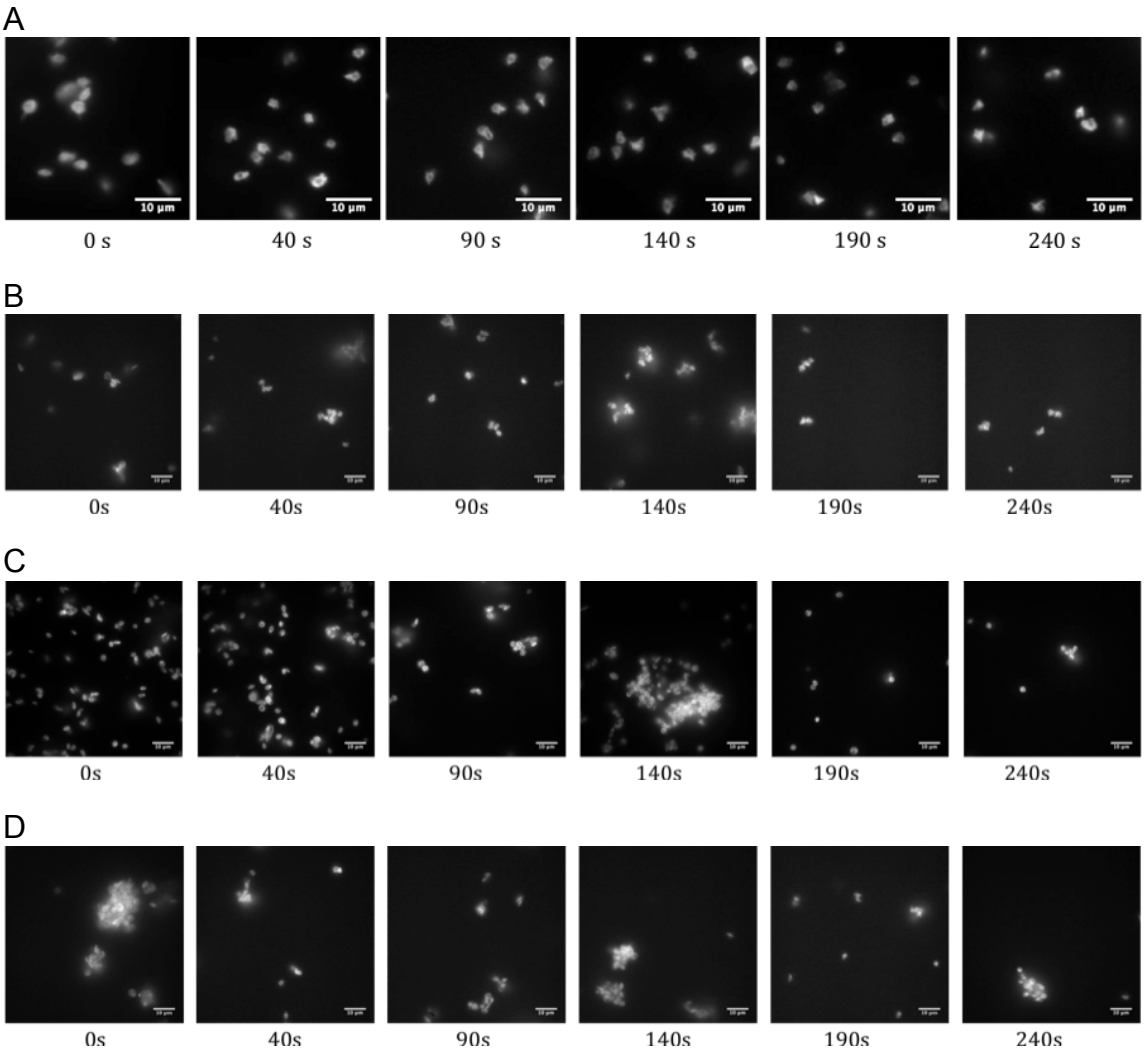

Figure 3.3 Timeline of actin matrix shrinkage dynamics during activation. A) No treatment. B) DMSO – DMSO-treated platelets started and ended with a smaller actin matrix than the no treatment platelets. C) Latrunculin A – The actin matrix of latrunculin A-treated platelets does not appear to go through any circumference changes as activation progresses. D) Cytochalasin D – In cytochalasin D-treated platelets the actin matrix underwent all circumference changes within the first 40 s, after which they reached a stable size. Scale bar 10 µm.

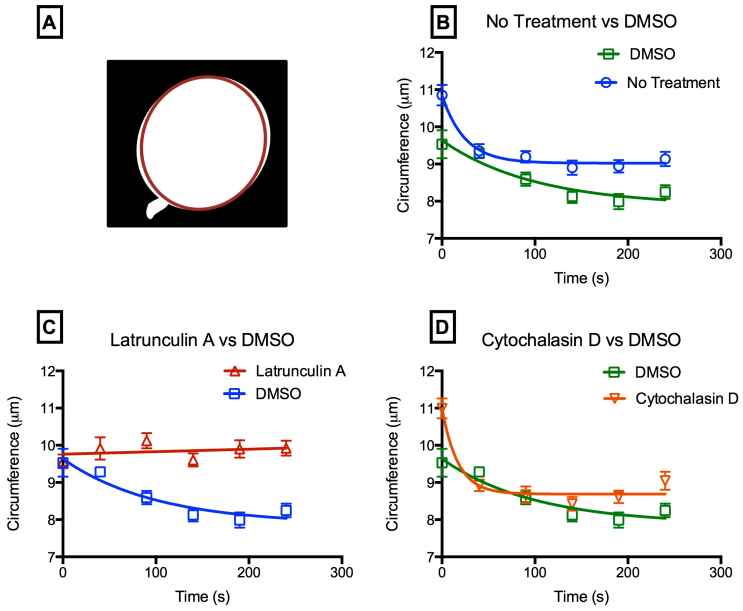

Figure 3.4 Actin matrix – progressions A) The actin matrix of each platelet was measured by using the best fit ellipse to measure the circumference. B-D) Comparison of the actin matrix shrinkage curves for non-treated and DMSO-treated platelets, DMSO- and latrunculin A-, and DMSO- and cytochalasin D-treated platelets, respectively. Error bars indicate SEM.

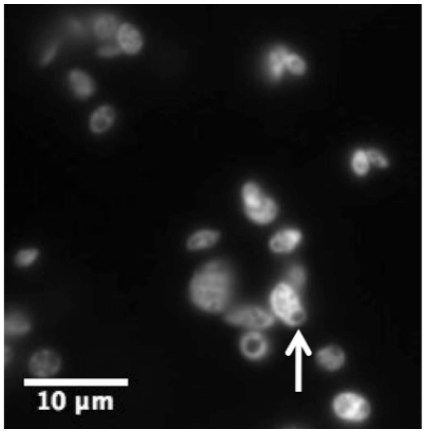

Figure 3.5 Additional structures revealed by actin labeling. Some platelets exhibited one or more dark spots during actin matrix labeling that may be due to chemical messenger-filled granules within the platelet.

Based on the fact that there are some significant changes in platelet cytoskeletal elements upon drug treatment, we considered correlation between these changes and platelet secretion of chemical messenger species. To this end, the microtubule ring and actin matrix dynamics were compared to previously published data showing the release of serotonin from platelets incubated with the same drugs at the same doses and incubation times. Previous results showed that when the platelets were incubated with the microtubule destabilizing drugs, the serotonin secretion from dense-body granules was not affected. However, when the actin matrix was disrupted, serotonin secretion was affected. With this previously published information in concert with the two data sets presented herein, we can see that the microtubule ring is not involved in the dense body granule release process despite the cytoskeletal changes that were observed during activation.[9] Perhaps the microtubule ring is more closely associated with alpha granule release (not assessed here) or shrinks to the inside of the platelet to minimize interactions with the granules during activation.[24] Future work could explore these hypotheses by performing simultaneous imaging of the alpha granules and the cytoskeletal elements.

3.4 Conclusions

Here, the dynamic changes of the cytoskeleton have been quantitatively tracked. Changes in the microtubule ring were tracked during the activation process by measuring the diameter of the ring at various time points. The images show that during activation, the microtubule ring first exhibits a decrease in diameter with retention of its circular or elliptical shape. However as activation proceeds, the microtubule ring begins to break apart into distinct pieces. The dynamics of the actin matrix are more difficult to quantify due to the more diffuse and abstract feature shape; however, changes in the actin matrix were effectively tracked by placing a best fit ellipse into the fluorescent area representing the labeled actin to measure the circumference. Like the microtubule ring, the actin matrix first decreases in size. After the initial decrease in circumference, at about 40 s post-

activation, the actin matrix reaches a steady circumference that remains throughout the rest of the activation process.

Future studies could involve tracking the cytoskeleton dynamics of live rather than fixed cells and a further exploration of the dynamics within the first 40 s of activation, where it became apparent through this work that the majority of cytoskeletal changes are occurring. Also, the application of a super-resolution microscopy technique would make the features within the actin matrix more visible, making it possible to further elucidate the intertwining roles of the platelet cytoskeleton and granule release. TIRF microscopy would be an ideal technique to use as it would allow us to visualize the actin-granule interactions right at the cell surface. Additionally, super-resolution microscopy could be used to investigate the proteins involved in regulating actin during platelet activation.

Chapter 4

Cholesterol Membrane Content Plays a Minor Role in Platelet Aggregation

4.1. Introduction

Platelets play a critical role in the mammalian cardiovascular system, where they are involved in regulating bleeding and the repair and regeneration of connective tissues.[1] When coagulation is poorly controlled, there is a greater chance that thrombosis, the formation of a clot in diseased vessels, can occur.[2] As such, the mechanisms of platelet activation have been a subject of much study and pharmacological targeting. Platelet activation consists of a series of cellular events, including a shape change as detailed in Chapter 3 and the release of chemical messengers and proteinaceous species from granules as detailed in Chapter 5.[1] During shape change, platelets go from a flat, disk shape to more globular bodies with cytoplasmic extensions to promote aggregation.[3] As described in Chapter 3, the dynamics of the platelet cytoskeleton during activation have been studied.

Cholesterol is an important regulator of cell membrane dynamics. It is expected that cholesterol in the platelet membrane has an effect on the activation cascade as cholesterol is known to be a modulator of membrane viscosity, where increasing cholesterol content leads to a stiffer membrane.[4] It plays a large role in microdomain formation, such that reduction of cholesterol in the cell membrane can result in the loss of function for transmembrane proteins.[4] In platelets, many of the proteins integral to the activation cascade are sequestered in the cholesterol-rich microdomains.[5] The clustering of microdomains upon platelet activation has also been observed and is thought to bring together the multimeric proteins involved in the activation cascade, such as the collagen receptor GpVI and FcγRIIa.[5-8]

Herein, and in Chapter 5, we are interested in the biophysical role that cholesterol plays in the platelet membrane. Previous work has shown that in platelets and other cells, increasing cholesterol results in slowed fusion pore

dynamics (see Chapter 5).[9,10] When cholesterol in the membrane is increased, a subsequent increase in secretion time, rate of secretion, and number of narrow pore events results. By substituting epicholesterol for cholesterol in platelets, Ge et al. determined that the effects of cholesterol on granule secretion were biophysical as opposed to biochemical in nature.[9] The proteins involved in both secretion and anchoring the cytoskeleton have been shown to be localized in the cholesterol-rich microdomains of the cell membrane.[11,12] In addition, the phospholipid composition of the plasma membrane is known to effect secretion, aggregation, and shape change in platelets.[13] In an attempt to tie all these related phenomena together in the context of platelet function, this work explores how platelet membrane cholesterol content influences platelet behavior. The study reveals that at decreased membrane cholesterol content, the initial rate of platelet aggregation is slowed and membrane shape change is halted.

4.2 Methods

4.2.1 Platelet Isolation and Membrane Manipulation

Blood was drawn from the mid-ear artery of sedated New Zealand white rabbits following the IACUC protocol #1311-31082A. To isolate platelets, they were first centrifuged at 500xg for 15 minutes at low brake. The top platelet rich layer was transferred to a new centrifuge tube and allowed to rest at room temperature. The platelets were then divided into two aliquots, control and methyl-β-cyclodextrin- (MβCD) treated to assess how cholesterol depletion influences platelet aggregation and shape change. MβCD has been previously used to deplete cholesterol from cell membranes.[9,14,15] A freshly made 20 μM MβCD (Sigma-Aldrich, Milwaukee, WI) solution in Tyrodes buffer (137 mM NaCl, 2.6 mM KCl, 1 mM $MgCl_2 \bullet 6H_2O$, 5.55 mM D-glucose, 5 mM HEPES, 12.1 mM $NaHCO_3$) was made and then added in equal volume to the platelets to achieve a final concentration of 10 μM. An equal volume of Tyrodes buffer was added to the control platelets to avoid dilution effects. The platelets were incubated in the two solutions for 30 minutes at room temperature. Following membrane

manipulation, 1:3 volume of ACD (85 mM trisodium citrate dihydrate, 66.6 mM citric acid monohydrate, 111 mM D-glucose) to platelet suspension was added, and then the suspension was centrifuged at 750xg for 10 minutes at full brake. The supernatant was removed and the platelets resuspended in Tyrodes buffer. The platelets were allowed to rest for at least one hour prior to measurement or visualization. The platelet concentration was determined using a hemocytometer and ranged from 8.1 x 10^7 to 1.5 x 10^8 platelets/mL. For the experiments detailed here, platelets were isolated on three different days to achieve three biological replicates.

4.2.2 Cholesterol Content Determination

Cholesterol content of the control and MβCD-treated platelets was evaluated using the Amplex Red cholesterol assay (Invitrogen Corp., Carlsbad, CA). First, the platelets were lysed. To do this, the platelets were pelleted by centrifugation at 2500xg for 10 minutes. The supernatant was discarded and the pellet resuspended in half the original volume of M-PER Reagent (Thermo Scientific, Rockford, IL). The solution was then sonicated for 10 minutes to break the platelets apart. Next, the solution was again centrifuged at 14000xg for 15 minutes to remove cellular debris. The supernatant was collected and frozen at -80 °C until use. The Amplex Red cholesterol assay was performed following the instructions provided by the manufacturer. Cholesterol oxidase reacts with the cholesterol in the samples to form H_2O_2, which then reacts with the Amplex Red reagent in the presence of horseradish peroxidase to form fluorescent resorufin.[16,17] The formed resorufin was detected by measuring the absorbance of the solution at 571 nm using a microplate reader (Synergy2, Biotek, Winooski, VT). Using known cholesterol concentrations, a standard curve was created, and the cholesterol content of the various samples was determined. To normalize between the different platelet isolation efficiencies, the cholesterol content was calculated per 1 x 10^7 platelets.

4.2.3 Aggregation Assay

A Chrono-Log Whole Blood Lumi aggregometer (Havertown, PA) with Aggro/Link software was used to test the aggregation of the platelets in both conditions. Prior to performing the aggregation assay, the platelets were brought to a concentration of 7.5 x 10^7 platelets/mL. A 400 µL aliquot of platelet suspension was added to a cuvette with a stir bar. The blanks were made using Tyrodes buffer. After setting the baseline and allowing the signal to stabilize, 50 U/mL of thrombin was added to each sample for a final concentration of 5 U/mL. Thrombin-induced activation was allowed to progress for approximately 10 minutes or until the percent transmittance had stabilized. Three analytical replicates were performed each day, resulting in a total of 9 measurements.

4.2.4 Membrane Shape Change

The platelet membrane shape change was monitored via dark-field microscopy. The platelets were activated using a 50 U/mL concentration of thrombin to result in a final concentration of 5 U/mL. At each time point, an aliquot of the platelet suspension was removed from the activating platelets and mixed with 8% formaldehyde to quench activation.[18] Samples were collected at 0 s, 15 s, 30 s, 45 s, 60 s, 75 s, 90 s, and 180 s after activation initiation. To remove the formaldehyde, the suspensions were centrifuged for 5 min at 2500xg to pellet the platelets. The supernatant was discarded and the pellet resuspended in Tyrodes buffer.

The platelets were imaged on a Cytoviva dark-field-equipped Olympus BX43 microscope (Auburn, AL) using a 100X/1.30 oil immersion objective. Samples were prepared by placing 4 µL of fixed platelet suspension on a No. 1 coverslip that was then gently covered with another coverslip. Images were gathered with an exposure time of 137 ms and a gain of 10.8 dB using a Dage MTI XLM 524 camera (Michigan City, IN). Image analysis was performed using ImageJ software (National Institutes of Health). The circumference of the platelet

membrane was determined using a best-fit ellipse, a technique previously optimized and discussed in Chapter 3, Sections 3.2.4 and 3.3.2. For each day, 10 platelets for each condition and time point were analyzed, resulting in 30 measurements for each time point.

4.3.5 Data Analysis

All statistical analysis was performed using GraphPad Prism. Error bars indicate standard error of the mean. Conditions were tested for significance using the unpaired t-test. A p value below 0.05 was considered significant.

4.3 Results and Discussion

To investigate the role that cholesterol plays in platelet aggregation dynamics, we treated platelets with MβCD, a small molecule previously used to manipulate membrane cholesterol levels. MβCD has a high affinity for cholesterol and draws it out of the platelet plasma membrane while minimally disturbing other membrane components.[14,15] Platelets are interesting in their own right, but they can also serve as a model for how cholesterol in the general cell membrane will effect exocytosis and membrane dynamics. Due to platelets' anuclear nature, any response differences upon stimulation can be attributed directly to the cellular manipulations.[9,13,19] Herein, we compared platelet aggregation and size change between control and MβCD-treated, lower level cholesterol, platelets.

4.3.1 Cholesterol Content

The cholesterol content of the control and MβCD-treated platelets was measured using the Amplex Red cholesterol assay. The platelets contained 2.3 ± 0.6 μg cholesterol per 1 x 10^7 platelets and 1.5 ± 0.6 μg cholesterol per 1 x 10^7 platelets for the control and MβCD-treated samples, respectively, which was not significantly different ($p = 0.4388$, Figure 4.1). While this was not significant, to characterize the relative cholesterol content moving forward in this chapter, the ratio of cholesterol in the MβCD-treated platelets to the control platelets for each day was calculated. On average, the MβCD-treated platelets contained 63.8 ±

9.6 % of the cholesterol content of the control platelets. As detailed below, some functional changes were observed, and so further replicates will be performed to clarify whether or not there is a statistically significant difference in membrane cholesterol content between the control and MβCD-treated platelets.

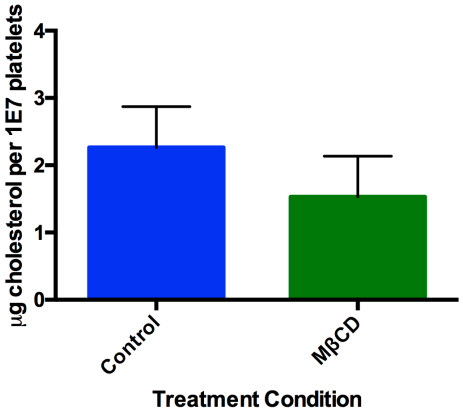

Figure 4.1 Average cholesterol content of control and MβCD-treated platelets. There is no significant difference in the cholesterol content of the control and MβCD-treated platelets though further replicates may reveal otherwise. n = 3

4.3.2 Aggregation

The aggregation behavior of the control and MβCD-treated platelets was monitored via light transmittance. After addition of the thrombin agonist, platelets initially swell up, resulting in a decrease in transmittance. As they continue along the activation cascade, they begin to stick together and form aggregates. This results in an increase in transmittance, which is exacerbated when the platelet aggregates get large enough that they fall out of suspension. Each aggregometer curve was analyzed for the primary aggregation rate, secondary aggregation rate, and overall percent aggregation (Figure 4.2, Table 4.1).[20] The biphasic release pattern is associated with the conversion of ATP to ADP to power the secretion processes and is not thought to be involved in controlling aggregation.[21] The overall percent aggregation and secondary aggregation rate of the platelets did not change upon membrane cholesterol manipulation.

However, the primary aggregation rate decreased in the MβCD-treated samples, dropping from 1.4 ± 0.1 %/s to 0.9 ± 0.1 %/s ($p \leq 0.001$). This indicates that the platelets were not aggregating as quickly, suggesting that the MβCD treatment impacts aggregation. The slowed primary rate of aggregation is most likely due to platelets sticking to one another less efficiently. Whether the decreased rate is related to changes in the membrane biochemical characteristics or to hampered membrane protein dynamics cannot be distinguished with this data alone.

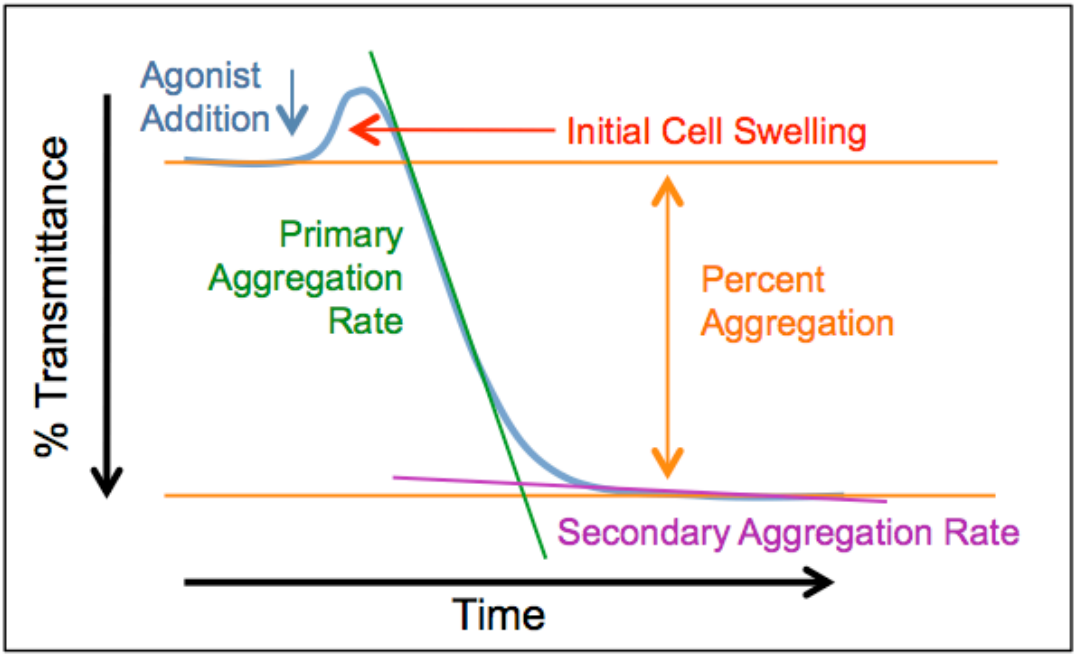

Figure 4.2 Schematic platelet aggregation curve. Model depiction of an aggregation curve and the characteristics analyzed in each curve.

Table 4.1 Platelet aggregation characteristics. The primary aggregation rate, secondary aggregation rate, and total percent aggregation were measured for the control and MβCD-treated platelets in 9 replicates.

	Primary Aggregation Rate (%/sec) ($p \leq 0.001$)	Secondary Aggregation Rate (%/sec)	Percent Aggregation
Control	1.4 ± 0.1	0.1 ± 0.0	74.6 ± 3.0
MβCD	0.9 ± 0.1	0.1 ± 0.0	69.4 ± 4.6

4.3.3 Shape Change Analysis

As platelets are known to go through shape change upon activation, the size of activated platelets was also analyzed after membrane cholesterol level manipulation. To achieve a more dynamic picture of the change of platelet size upon activation, platelets were fixed at eight time points in the activation time line. As the primary cytoskeleton shape change dynamics have been previously shown to be complete after 90 s (Chapter 3, Section 3.3), activating platelets were fixed every 15 s from 0 s to 90 s with an additional time point of 180 s. The platelets were imaged using a dark field microscope setup and analyzed for changes in platelet size. Dark-field microscopy was chosen because it is a label-free method to achieve high contrast images of small entities, like platelets. A representative dark-field image can be seen in Figure 4.3A. The analysis technique used to achieve quantitative information from these images is discussed in Chapter 3, Sections 3.2.4 and 3.3.2. Briefly, a best-fit ellipse was drawn over the platelet to get an approximate cell membrane circumference (indicated by the red ellipse in Figure 4.3 B). To screen quickly, just the 0 s and 180 s time point conditions were imaged and analyzed initially. There was a significant difference in size between the control and MβCD-treated platelets 180 s post-activation (Figure 4.3C, $p \leq 0.05$). The control platelets had an average circumference of 6.6 ± 0.2 μm and the MβCD-treated platelets had an average circumference of 7.4 ± 0.2 μm. Comparison to the 0 s circumferences showed that, despite a lack of statistical significance between the 0 s and 180 s time points, the control platelets underwent an apparent decrease in circumference while the MβCD-treated platelets maintained their original circumference size, with initial circumferences being 7.1 ± 0.2 μm and 7.4 ± 0.1 μm for control and MβCD-treated platelets, respectively. These data imply that not only is the ‘stickyness’ of the platelets, as measured in the aggregation data, impacted by the MβCD treatment but that the cellular components that control platelet shape change are also disrupted upon MβCD treatment. Ge, et al. showed that platelet

secretion is slowed with decreased cholesterol membrane content, yet there is faster pore opening (complimentary results shown in Chapter 5).[9] Together, these results indicate a loss in control of the dynamics involved in platelet activation. In other cells, decreased cholesterol in the cell membrane has been shown to result in an decreased stiffness associated with membrane-cytoskeleton interactions, which pairs well with the loss of shape change upon MβCD treatment.[22,23]

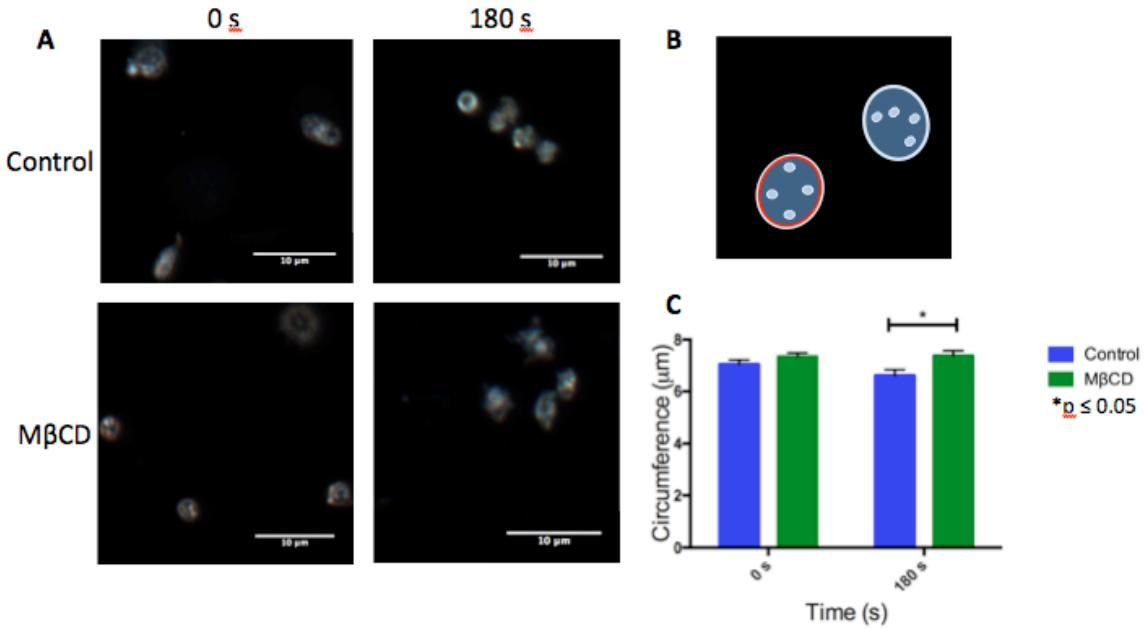

Figure 4.3 Circumference change of the platelet membrane upon activation. A) Representative dark-field images of control and MβCD treated platelets at 0 s and 180 s. B) Schematic showing circumference measurement. C) The circumference changes for both control and MβCD-treated platelets at 0 s and 180 s after activation. n = 30, * indicates $p \leq 0.05$

4.4 Conclusion

This study shows that the primary rate of platelet aggregation is dependent upon MβCD treatment. In addition, after the time traditionally attributed to platelet shape during the activation process, the MβCD-treated platelets exhibited a larger circumference compared to the control platelets, indicating that they did not undergo any decrease in size. These two results correspond well with cholesterol's biophysical role in controlling membrane viscosity as well as microdomain formation. While this study was unable to determine whether one or both of these elements contribute to the reduced rate upon cholesterol depletion, future work could investigate this. It is important to note that these studies were performed in suspensions without blood plasma proteins. The proteins von Willebrand factor and collagen are key players in the aggregation process and their presence would likely result in platelet functional changes.[24,25] In addition, because these experiments were performed in suspension, the platelets may not undergo typical spreading behavior. Thus, future work will also explore the role of cholesterol depletion on platelets in contact with surfaces and blood plasma proteins.

Chapter 5

Variations in Fusion Pore Formation in Cholesterol-Treated Platelets

Adapted from:

Finkenstaedt-Quinn, S. A.; Gruba, S. M.; Haynes, C. L. “Variations in Fusion Pore Formation in Cholesterol-Treated Platelets.” *Biophysical Journal*, in press.

Sarah Gruba and I worked equally on peak analysis, data discussion, manuscript writing, tables, and figures. In addition, I performed the graphing, analysis of cholesterol loaded data, and initial figure design.

5.1 Introduction

To maintain proper physiological function, cell-cell communication occurs through the highly regulated exocytotic process wherein granules dock on the cell membrane, utilizing soluble NSF attachment protein receptor (SNARE) proteins to assist in regulating attachment. These proteins are localized to cholesterol-rich microdomains throughout the cell membrane.[1] The amount of cholesterol in these domains not only plays a role in the proper clustering of SNARE proteins, but also helps stabilize the negative curvature needed for formation and stabilization of the fusion pore between the docked and primed granule and the cell membrane. Cholesterol levels and membrane viscosity are directly correlated, and increasing viscosity is known to result in delayed movement of lipids between the leaflets, which has been hypothesized to increase fusion pore formation and closing times.[2,3] Chemical messenger molecules can be released through this dynamic fusion pore structure into the extracellular space. Literature precedent has shown that cholesterol has a role in controlling exocytosis, but the extent to which it dictates the opening and closing of the fusion pore structure requires more exploration, ideally with a method that can quantitatively assess this dynamic structure.[2,3]

In recent years, it has become clear that the process of granule fusion is more intricate than originally thought. Traditionally, exocytosis was considered to be an all-or-nothing process, but in the last decade the definition has changed to include kiss-and-run events where a granule temporarily fuses with the cell membrane before detaching. More recently, it has become apparent that most granule release events are in fact extended kiss-and-run events which do not result in full chemical messenger content release.[4-7] Schematic portrayals of these various exocytosis events can be seen in Figure 5.1 A-C. Further countering the traditional view of exocytosis, individual granules have also been observed combining with one another, either before or during release, resulting in a process termed compound exocytosis.[8,9] However, in platelets, our chosen

exocytosis model due to its lack of nucleus and therefore decreased ability to up- or down-regulate proteins, granules can also fuse to the open canalicular system (OCS). The OCS is a tubular system located throughout the platelet, which is hypothesized to assist in the release of granular content into the extracellular environment.[10] At the OCS-cytosol interface, it is possible for two granules to attach near one another and release their contents into the OCS where the contents can combine and release simultaneously into the extracellular environment. This phenomenon could lead to chemical messenger release measurements characteristic of compound exocytosis. Unfortunately, current measurement technology does not allow us to distinguish between these two forms. Therefore we will describe all events with large amounts of serotonin release, typically larger than the average amount released in two separate granules, and fast pore opening as bulk fusion (Figure 5.1D).

Even with this limitation, carbon-fiber microelectrode amperometry (CFMA) is an ideal technique for studying the dynamic variations in granule release events. In platelets, the only electroactive compound at 700 mV vs. Ag/AgCl is serotonin, which has been confirmed by cyclic voltammetry.[11,12] Statistical analysis has demonstrated that due to the size of the cell relative to the electrode and the distance between the electrode and platelet, nearly 100% of all released serotonin is detected.[11] Electrode fouling is also checked by monitoring the noise of the connection, as indicated by the root mean square of the current function (I_{RMS}), and replacing the electrode if I_{RMS} increases or the signal goes down. Therefore monitoring the oxidation of serotonin, found in the dense-body granules of platelets, gives us a means to study changes in the pore dynamics when microelectrodes are placed in immediate contact with individual platelets. As each granule fusion pore opens, an increase in current is detected as secreted serotonin is oxidized, resulting in a current spike. In some cases, an individual current spike will be flanked either before or after the current maximum by a smaller current feature known as a “foot” event; these foot events

correspond to the relatively small number of serotonin molecules released when a fusion pore is not fully dilated. Due to the small number of granules in platelets and length of time between granule release events, it is possible to distinguish the start and end of each granule event, including feet events, without overlap from other granule release events. This event resolution allows analysis of the variations in each spike profile, revealing mechanistic biophysical information about fusion pore behavior for each granular release event. Since cells do not typically release their entire content and there is a limited quantity of dense-body granules, it is possible that several of the recorded spikes in each cell amperometric trace are from the same granule. This work examines the modes of pore formation and closure and how membrane cholesterol levels impact these modes. Results indicate that as the cholesterol membrane content increases, there is a corresponding increase in the number of release events with distinguishing characteristics. In particular, an increase in the number of non-traditional events (NTEs) was observed. It was also noted that at greater levels of cholesterol, the NTEs have a slower fusion pore opening, increased release of serotonin molecules during each release event, and a longer duration in which the fusion pore remained open.

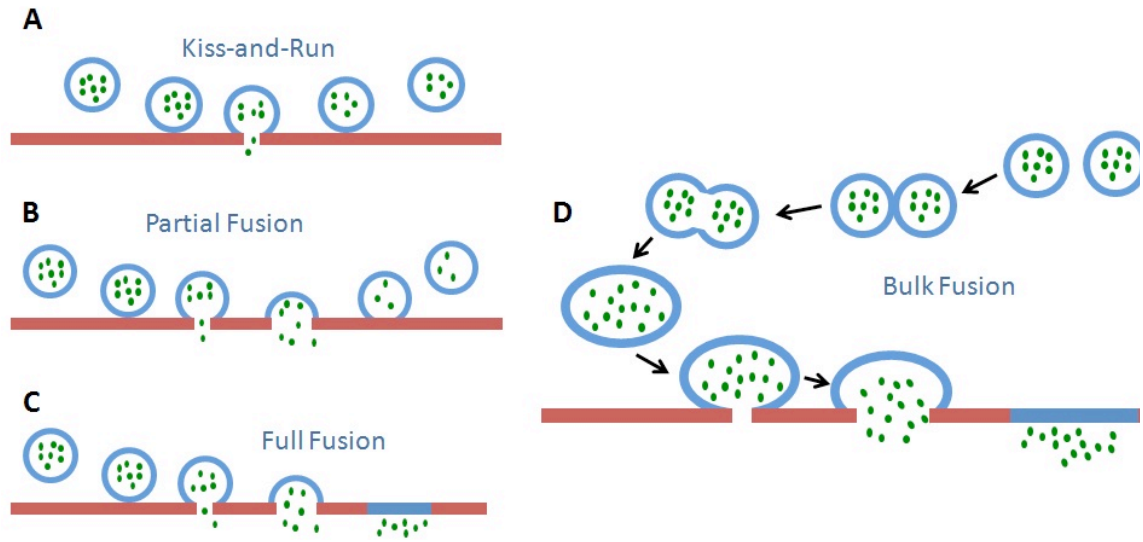

Figure 5.1 Various proposed modes of exocytosis, from least to most chemical messenger release. A) Kiss-and-Run: In kiss-and-run events, the granule fuses briefly with the plasma membrane, releasing only a small portion of its contents without significant dilation of the fusion pore. B) Partial Fusion: In partial fusion events, the granule initially fuses with the plasma membrane, releases some of its contents, and then closes and returns to the platelet cytoplasm. C) Full Fusion: In full fusion events, the granule fully fuses with the plasma membrane and releases all of its contents. D) Bulk Fusion: In bulk fusion, multiple granules are hypothesized to fuse with one another prior to fusing with the plasma membrane; this is commonly referred to as compound fusion. However, platelet granules can adhere to the OCS and release their contents into the extracellular environment together, which is indistinguishable from compound fusion using CFMA. Therefore, we termed all of these events as bulk fusion.

5.2 Materials and Methods

5.2.1 Cell Manipulation and Amperometry

Amperometric traces from individual rabbit platelets were recorded previously by Shencheng Ge using CFMA.[2] Briefly, platelet cholesterol levels were manipulated by exposing platelets either to methyl-b-cyclodextrin (MβCD) (Sigma Aldrich, St. Louis, MO) to achieve cholesterol depletion or MβCD complexed with cholesterol (Sigma Aldrich, St. Louis, MO) to achieve cholesterol enrichment. Platelets with varying levels of cholesterol were stimulated using 10 μM ionomycin and 2 mM Ca^{2+} in Tyrode's buffer. The released serotonin was oxidized by an in-house fabricated carbon-fiber microelectrode at 700 mV vs a Ag/AgCl reference electrode held by an Axopatch 200B potentiostat (Molecular Devices, Sunnyvale, CA), and the resulting current was measured as a function of time. Each collected current vs time trace was filtered at 5 KHz by a four-pole Bessel filter ahead of further analysis.

5.2.2 Peak Categorization

Each amperometric trace (N= 75, 72, and 50 for MβCD-depleted, control, and cholesterol-loaded platelets, respectively) was then digitally filtered at 1000 Hz and analyzed using Mini Analysis software (Snyptosoft Inc., Fort Lee, NJ) for pre- and post-spike feet. The peaks were analyzed visually by using a gain of 15 and a block of 20 unless the current spike was too large for the frame, in which case the gain was decreased so that the entire peak was visible within the frame. After examining each trace, the various features were divided into categories based on the general shape of the release event, resulting in pre- and post-feet and NTEs (Figures 5.3A, 5.7A, and 5.8A). Each peak was analyzed manually using the “group analysis and curve fitting” option to determine the duration and area of both the foot alone and the peak and foot features combined. Schematic representation of these features can be seen in Figure 5.2A. For NTEs, the total event area and duration were measured. The percent frequency of each feature

(pre-foot, post-foot, or NTE) was determined by dividing the total number of events with that feature by the total number of release events in each trace. Within each feature type, the percent frequency was accounted for with respect to the total number of events with that feature (for example, within each trace, a pre-foot type was compared to the total number of granule release events with pre-foot features). Significance ($p < 0.05$) was determined between conditions by one-way ANOVA with all error given as the standard error of the mean.

5.2.3 Non-Traditional Events

Non-traditional events are current spikes that do not display the typical quick current rise due to serotonin release followed by a gradual current decay as serotonin diffuses away. These NTEs were subdivided into six different categories (full fusion, partial fusion, bulk fusion, kiss-and-run, recurring kiss-and-run, and jagged top) based on the area (charge, Q) under each peak, which is proportional, through Faraday's Law, to the amount of serotonin released, and how quickly the fusion pore opened relative to its maximum release ($slope_{10/90}$, the slope between 10% and 90% of maximal current intensity) (Table 5.1). Jagged top features were distinguished by continuous up and down fluctuations of serotonin release at maximum opening, and recurring kiss-and-run displayed several kiss-and-run events within a second of each other.

The cut-off criteria categorizing events with a 10/90 slope under 6 pA/ms was chosen empirically based on the manual analysis of many spikes that represented traditional and non-traditional release events. Non-traditional release events were further categorized based upon the amount of serotonin released. To set an upper limit on the release that could be attributed to kiss-and-run, we averaged the peaks in the control platelets considered to be kiss-and-run and found the highest value within one standard deviation of the mean, then made this our maximum release value. Previous data obtained by HPLC indicated that a 5 minute ionomycin stimulation on rabbit platelets resulted in the average

release of 52% of the total serotonin content.[13] The average area (250 fC per granule in control platelets) was thus assumed to be 52% content release. Full fusion was set as a minimum of 80% content release, or 385 fC/event. Release events where granule fusion resulted in at least 200% content release, or greater than 970 fC, and contained a 10/90 slope of 6 pA/ms or greater were categorized as bulk fusion events. For NTEs, the event area and event duration of the entire peak was analyzed. Example traces of NTEs can be found in Figure 5.8A with additional details in Table 5.1.

Name	10/90 Slope	Area (fC)	Percent Release	Release Mode
Kiss and Run	< 6	<100	0 – 20%	Small release
Partial Fusion	< 6	100 < area < 385	20 – 80%	Partial release
Full Fusion	< 6	385 < area	80 – 200%	Full release
Bulk Fusion	> 6	960 < area	> 200%	OCS or combining granule release

Table 5.1 Non-traditional events were characterized by their 10/90 slope and area. As NTEs are often characterized by slower pore opening, the 10/90 slope was determined to be a good indicator of NTEs. To distinguish between the different types of NTEs the extent of release, or area under the current spike, was used. Commonly, events releasing twice the amount of serotonin or greater than the predicted concentration, had steep 10/90 slopes that were most likely due to more serotonin occupying the larger free space outside the dense-body core. Therefore, bulk fusion events had a 10/90 slope >6. All slopes and areas were calculated using the Mini Analysis software.

5.3 Results and Discussion

5.3.1 Categorization of Foot Events

Based upon previously established methods of release, exocytosis events have been categorized herein into four types 1) kiss-and-run, 2) partial fusion for both normal pore opening rates (10/90 slope > 6 pA/ms) and extended pore opening rates (10/90 slope < 6 pA/ms) (when discussing partial fusion for the remainder of the paper, we are referring to the extended pore opening rates and not the traditional spike formation), 3) full fusion, and 4) bulk fusion (including both granule-granule fusion and bulk OCS fusion). The different models are illustrated schematically in Figure 5.1.[4-9]

After platelets were enriched in cholesterol or depleted of cholesterol by platelet exposure to MβCD (132% and 68%, respectively, compared to control platelet cholesterol levels),[2] the total percentage of events with either a foot or NTE release profile increased with increasing concentrations of cholesterol (52.6 ± 2.4%, 64.7 ± 2.2%, and 76.8 ± 2.8% for depleted, normal, and cholesterol-enriched platelets, respectively, Figure 5.2B). Normal levels of foot events reported with CFMA are traditionally around 10-30%,[2,13,14] which is nominally lower than what we have reported; this discrepancy is likely due to our inclusion of non-traditional type events and post-foot containing events when determining the percentage of events with features-of-interest. When only events with pre-foot characteristics are taken into account, the percentage of events falls in previously described ranges with 15.2 ± 1.8%, 21.9 ± 2.0% and 21.8 ± 2.3% for increasing cholesterol concentrations, respectively (Figure 5.2C). Post-foot events, which have been known to only occur ~2% of the time in PC-12 cells,[6] occur relatively infrequently (4.8 ± 1.0%, 4.2 ± 0.8%, and 6.5 ± 1.2% for increasing cholesterol concentrations) in platelets and do not change significantly as the cholesterol content is changed. Changes in platelet membrane cholesterol have the largest impact on secretion via NTEs, with statistically significant

increases from 33.5 ± 2.5% for cholesterol-depleted platelets to 53.6 ± 3.6% of the events for cholesterol-enriched platelets, with a value of 42.7 ± 2.5% in control platelets. This suggests that cholesterol has a large impact on the whole fusion event rather than just the initial opening or closing of the pore. This difference is not attributable to a change in the number of granules undergoing exocytosis as the membrane cholesterol levels change. By counting the number of peaks in each trace, on average, each platelet released 12.7 ± 0.7, 12.6 ± 0.9, and 13.1 ± 0.9 granules per cholesterol-depleted, control, and cholesterol-enriched platelet, respectively ($p > 0.05$).

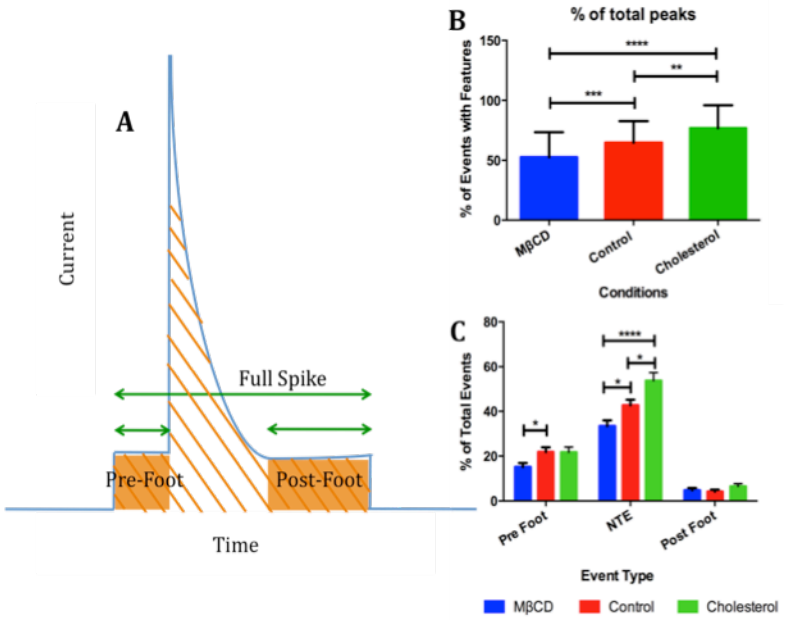

Figure 5.2 Classes of peaks. A) Diagram indicating the parameters used to categorize and quantify various peaks. B) The frequency of events with features upon the different cholesterol treatments. C) Relative frequency of classes of peaks with the different cholesterol treatments. *$p \leq 0.05$, **$p \leq 0.01$, ***$p \leq 0.001$, ****$p \leq 0.0001$

5.3.2 Pre-Spike Foot Events

The occurrence of pre-spike foot events only changes significantly as seen in a decrease for cholesterol-depleted platelets ($p \leq 0.05$). When the pre-foot events are broken down into sub-types, the majority of the pre-feet were present in two forms: those where the initial release took some sort of ramp (an initial slow gradual opening) or those where the initial release took the form of a plateau (an initial opening which is held steady over an extended period of time) (Figures 5.4 and 5.5, respectively). These two general characteristics have been reported before in several papers.[6,14,15] The most commonly reported and most discussed pre-spike foot type is the ramp. Amatore and colleagues reported that in chromaffin cells, of their pre-spike feet events, 70% were ramps, 20% were ramps with plateaus, and 10% were unclassified. They then found a positive correlation between the ramps' maximum current and the maximum current given by the spike.[14] Our data show that the ramp-type pre-spike foot was the most frequently occurring of the pre-spike foot types, at 35.7 ± 5.3%, 34.6 ± 4.7%, and 23.0 ± 3.8% for cholesterol depleted-, control-, and cholesterol-enriched platelets, respectively. For the depleted and control conditions, the percent occurrence of the ramp was significantly enhanced ($p \leq 0.0001$) compared to the other pre-spike foot types. The ramp frequency in cholesterol-enriched platelets was only significantly different from four out of the nine other pre-spike feet types (p ranging from 0.05 to 0.0001). This, along with previous work in other groups, leads us to believe that this ramp characteristic is representative of the traditional entryway for granular fusion. The ramp-like variants, such as jagged rise, could potentially correspond to the opening and closing of the fusion pore during formation, suggesting that the cell is not able to easily transition to the type of curvature needed in the membrane as the fusion pore opens. This inability to rapidly change the membrane curvature paired with increased membrane stiffness is also implicated in the significant increase in the occurrence of long plateau foot events between the cholesterol-depleted and enriched conditions (p

≤ 0.01). In addition, the increase in the duration of the short plateau foot relative to the whole event as cholesterol content increases suggests that increasing membrane rigidity results in a barrier to the pore opening to the proper form (Figure 5.6).

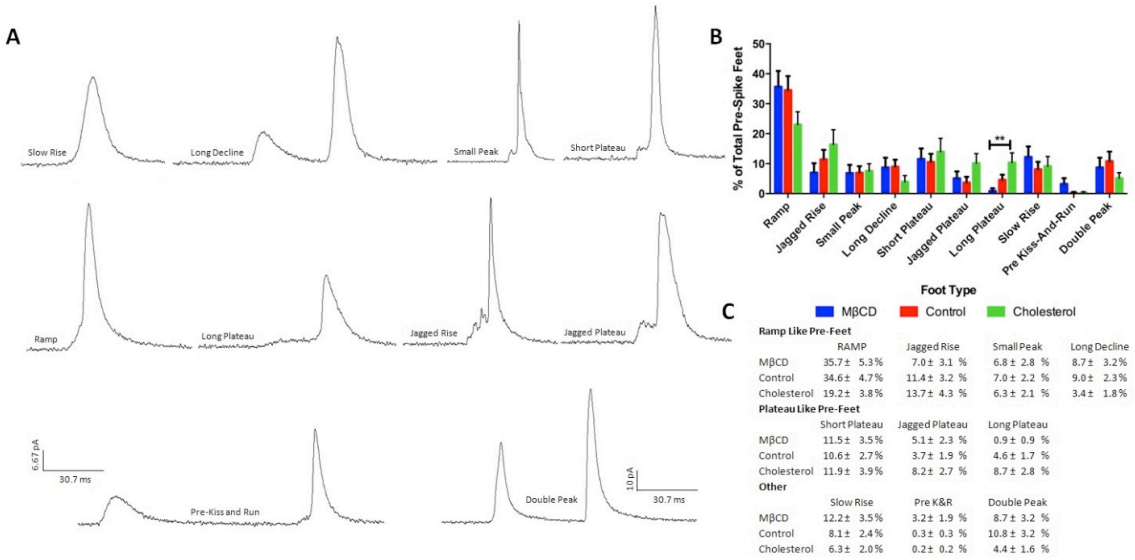

Figure 5.3 Pre-spike foot events. A) Representations of the various pre-spike feet. The representative traces are all on the same current and time scale. B) and C) Percent of total pre-spike feet with varying cholesterol concentrations graphically and in table form, respectively. **p ≤ 0.01

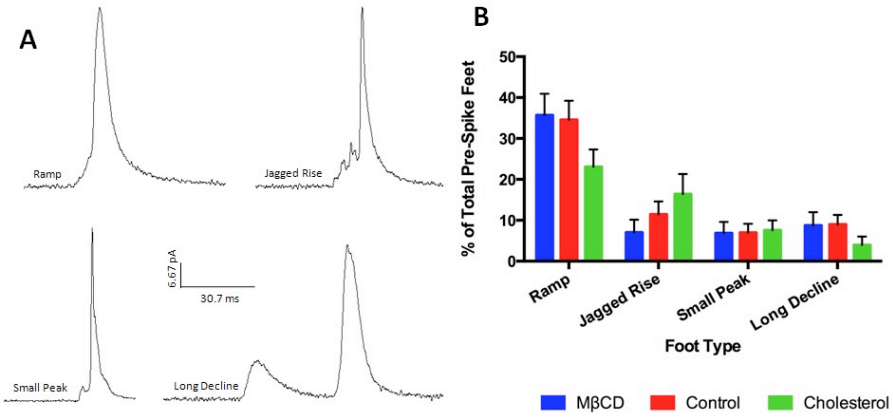

Figure 5.4 Pre-spike foot events with ramp-like character. A) Representative traces of the different types of pre-spike feet that had a ramp-like characteristic. The representative traces are all on the same current and time scale. B) Relative frequency for each type of ramp-like pre-spike foot with the different cholesterol treatments.

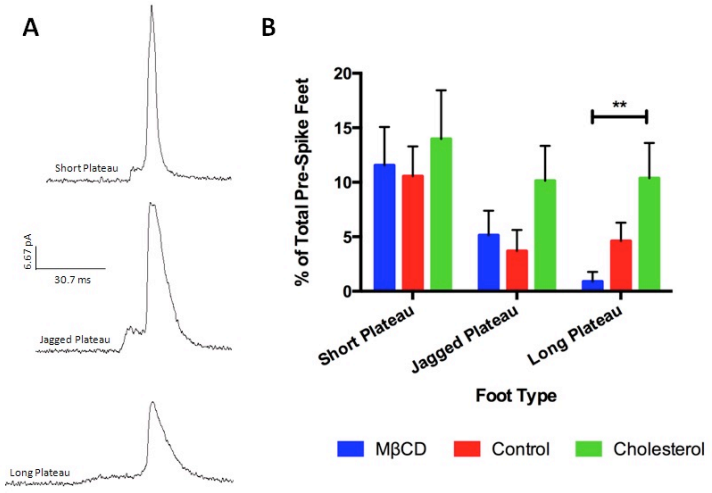

Figure 5.5 Pre-spike foot events with plateau-like character. A) Representative traces of the different types of pre-spike feet that had a plateau-like characteristic. The representative traces are all on the same current and time scale. B) Relative frequency for each type of plateau-like pre-spike foot with the different cholesterol treatments. **p≤0.01

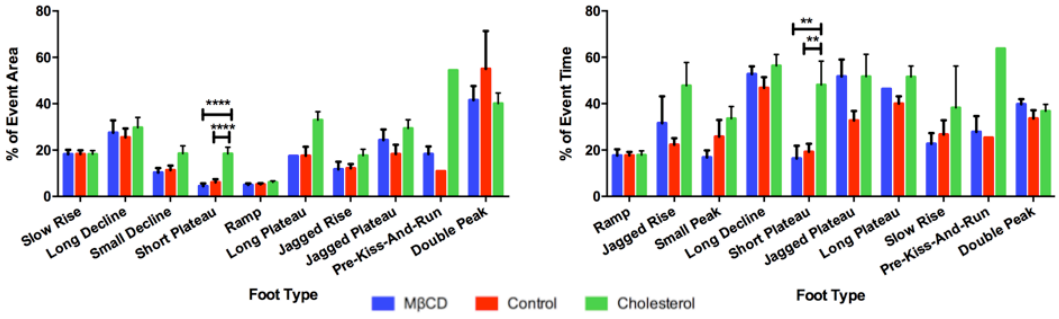

Figure 5.6 Percent of event area and time for pre-spike feet. A) Area the foot feature took up relative to the area of the whole event. B) Time the foot feature took up relative to the time of the whole event. **p ≤ 0.01, ****p ≤ 0.0001

5.3.3 Post-Spike Foot Events

As the post-spike feet were not very prevalent, it was difficult to identify variation in their forms. In total, eight different types of post-spike feet were identified, three of which were categorized as different forms of re-opening: post kiss-and-run, partial re-open, and re-open (Figure 5.7). Of the re-opening type post-spike feet, the partial re-opening type foot showed a significant difference in frequency between the cholesterol-depleted and cholesterol-enriched conditions, with the foot occurring 8.3 ± 4.8% and 46.5 ± 9.4% of the time, respectively. Since the significant increase is only seen in the partial re-open post foot event, where the pore begins to reopen directly after beginning to close, it indicates that the pore initially has difficulty closing, but after closure has been initiated, the cholesterol levels do not impact the process to the extent they do for pre-foot events.

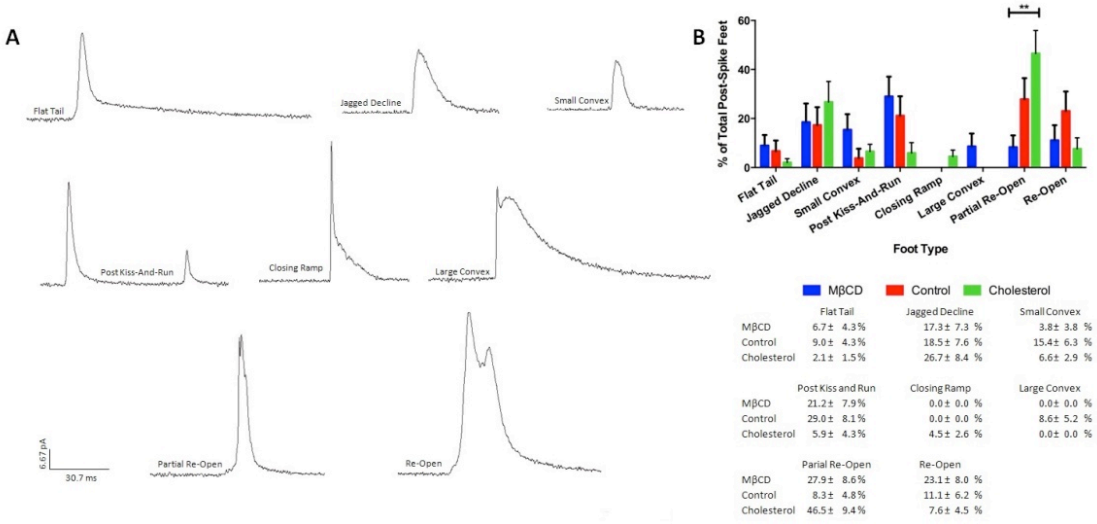

	Flat Tail	Jagged Decline	Small Convex
MβCD	6.7± 4.3%	17.3± 7.3 %	3.8± 3.8 %
Control	9.0± 4.3%	18.5± 7.6 %	15.4± 6.3 %
Cholesterol	2.1± 1.5%	26.7± 8.4 %	6.6± 2.9 %

	Post Kiss and Run	Closing Ramp	Large Convex
MβCD	21.2± 7.9%	0.0± 0.0 %	0.0± 0.0 %
Control	29.0± 8.1%	0.0± 0.0 %	8.6± 5.2 %
Cholesterol	5.9± 4.3%	4.5± 2.6 %	0.0± 0.0 %

	Parial Re-Open	Re-Open
MβCD	27.9± 8.6%	23.1± 8.0 %
Control	8.3± 4.8%	11.1± 6.2 %
Cholesterol	46.5± 9.4%	7.6± 4.5 %

Figure 5.7 Post-spike foot events. A) Representations of the various post spike feet.The representative traces are all on the same current and time scale. B) and C) Percent of total pre-spike feet with varying cholesterol concentrations graphically and in table form, respectively. **p ≤ 0.01

5.3.4 Non-Traditional Events

The most interesting results arising from categorization of the spikes observed upon platelet activation was the prevalence of spikes that were not in the form of traditional release events, meaning that they lacked the typical fast rising current due to pore opening followed by a slow current decrease as serotonin diffuses out of the closing pore. These release events were sorted into six categories by examining a combination of the following characteristics: 10/90 slope, the lack of a foot character, and the area (Figure 5.8, Table 5.1). Table 5.1 gives the 10/90 slope and area characteristics for four out of the six types of NTEs observed. While the NTEs as a category showed significant increases in percent frequency of total events as the cholesterol increases (Figure 5.2C), when the NTEs are broken down into the various exhibited types, no significant changes are observed where one specific category more is affected by the amount of cholesterol (Figure 5.8). However, there are significant changes in the area and duration for the various features as the membrane-cholesterol levels are changed (Figure 5.9). Most surprisingly, these changes in duration and area are seen in events that have set upper and lower limits for the amount of serotonin released, including partial fusion and kiss-and-run events. When comparing the average amount of serotonin released per ms during kiss-and-run events, there is no significant difference between cholesterol conditions (Figure 5.10). This suggests that the cholesterol helps the pore stay open longer, but does not change the size of the pore, assuming that the serotonin diffusion characteristics are unchanged. Therefore, with the small standard deviation associated with each event type's duration and amount of serotonin released and the fact that there is no difference in the rate of serotonin release between conditions, this suggests that all granules going through kiss-and-run will follow a similar pattern of release. In comparison, for partial fusion, there were no significant differences in rate of release, but a downward trend was noted as membrane cholesterol content increased. This suggests that once the pore opens past the kiss-and-run

stage, it may not open as wide at higher cholesterol levels. However, due to the longer length of time it stays open, more serotonin is released which serves to make up for this decreased rate of release. Finally, there is an apparent upward trend in percent occurrence for full fusion events and a corresponding apparent downward trend for partial fusion events as the conditions contribute to higher membrane cholesterol levels. These trends can all be explained by the increased membrane rigidity due to the additional cholesterol. As previously hypothesized, an increase in cholesterol would lead to longer inversion times for the phospholipids needing to change the curvature along the fusion pore, biasing towards full release events.

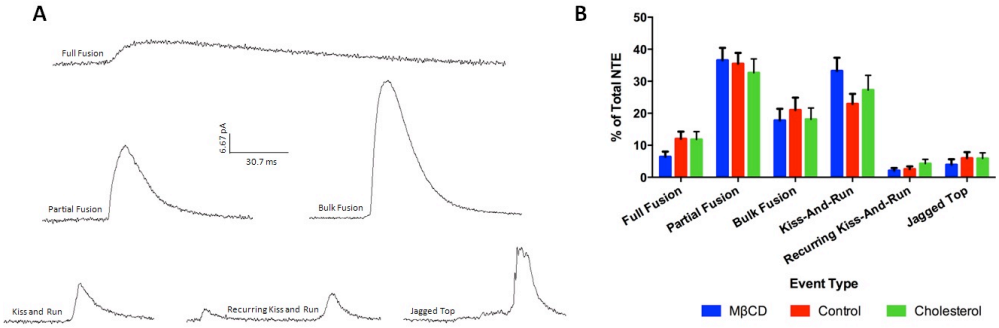

Figure 5.8 Non-traditional events A) Representative traces of the different types of NTE peaks. The representative traces are all on the same current and time scale. B) Relative frequency for each type of NTE under the different treatments.

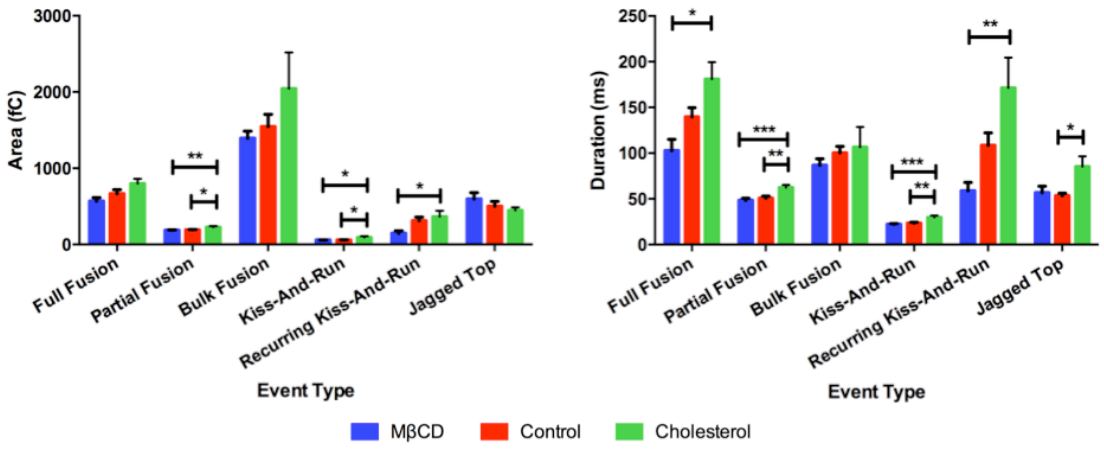

Figure 5.9 Area and duration of non-traditional events A) Average area and b) Average duration of each NTE type under the different cholesterol treatments. *p ≤ 0.05, **p ≤ 0.01, ***p ≤ 0.001

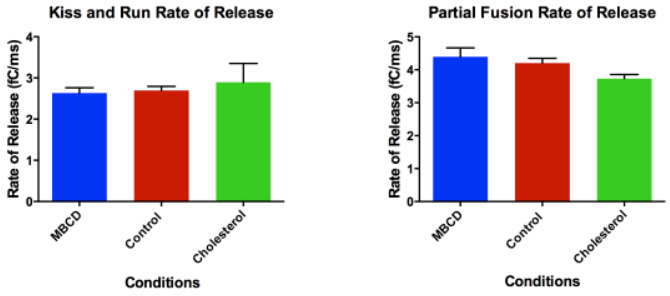

Figure 5.10 Kiss-and-run events. Rate of release for A) kiss-and-run events and B) partial fusion events.

5.4 Conclusion

Close examination of the pre-foot and post-foot spike features from individual platelets with manipulated outer membrane cholesterol levels indicated a few styles of pore opening and closing. Pre-foot features tended to fall into two sub-categories: ramp-like and plateau-like, with the ramp occurring most frequently. There was a slight decrease in the occurrence of pre-foot features in cholesterol-depleted platelets, indicating that the pore opens more quickly at low cholesterol levels, bypassing the slower foot-inducing features. The post-foot features occurred fairly infrequently and had primarily re-opening characteristics. The most prevalent category of non-traditional secretion events showed an increase in frequency as the cholesterol content of the membrane increased. These events are characterized by an increase in the amount of serotonin released, increased duration of the pore opening, and a slowing in the opening of the pore. From these analyses, we conclude that as the cholesterol concentration in platelets is increased, the membrane-granule fusion curvature transitions are slowed due to increased rigidity, leading to a slower pore opening and closing.

Even though the fusion pore dynamics of human platelets have not been studied directly with CFMA, it has been shown that platelets from other species, in particular cow which has comparatively increased levels of cholesterol, demonstrate similar fusion pore dynamics as the rabbit platelets incubated with cholesterol. These included increased T_{rise} and $T_{1/2}$ times compared to rabbit platelets without cholesterol modification which are often associated with NTEs.[2,13] In addition, since platelets are anucleate, the up- and down- regulation of proteins and receptors is limited, suggesting that the only difference between the conditions was the concentration of cholesterol. Therefore we believe these results, though they are measured in an animal system, can be generalized to human platelets and other cell types that undergo exocytosis.

Human platelets have been shown to undergo changes in cholesterol membrane content due to various diseases, drugs, or pre-dispositions.[16,17] In addition, platelets are known to increase cholesterol uptake in vitro when suspended in cholesterol-rich environments.[18] Previous literature indicates that cholesterol plays a role in human platelet sensitivity, microtubule ring formation, and aggregate size due to cholesterol levels.[18,19] Thus, it is likely that the results presented herein can inform understanding of human platelets and the diseases affecting them.

Chapter 6

Engaging Chemistry – Learning by doing

Adapted from:

Meyer, A.; Knutson, C.; Finkenstaedt-Quinn, S. A.; Gruba, S. M.; Meyer, B.; Thompson, J.; Maurer-Jones, M.; Halderman, S.; Tillman, A.; DeStefano, L.; Haynes, C. L. Activities for Middle School Students to Sleuth a Chemistry "Whodunit" and Investigate the Scientific Method. *J. Chem. Educ.* **2014**, *91*(3), 410-413.

To the above manuscript, I contributed to the writing of the manuscript and experiment developments. The manuscript was also included in the thesis of Audrey Meyer.[1]

Finkenstaedt-Quinn, S. A.; Styles, M.; Juelfs, A.; Haynes, C L. Increasing Climate Change Awareness through Ted-ED Videos and Demonstrations. *In preparation.*

To the above manuscript, I contributed to the experiment development, data analysis, and writing of the manuscript to this work.

Finkenstaedt-Quinn, S. A.; Schoeller, S.; Haynes, C. L. Increasing chemical understanding using literature to stimulate student interest. *In preparation.*

To the above manuscript, I contributed to the experiment development and writing of the manuscript to this work.

6.1 Introduction

Chemistry is often-cited by students around the world as a subject that is hard for them to relate to and become engaged in, partially due to its requiring background mathematical knowledge and abstract concepts.[2-4] In an effort to make chemistry more relatable and accessible to students, I have worked on the development of several teaching modules. These modules are aimed at K-12 students. By presenting basic scientific concepts in an engaging way we hope to (1) cultivate scientifically interested citizens and (2) combat the development of misconceptions early in science education that are hard to unlearn.[5] Two of the modules included herein were implemented as part of an outreach event hosted by the Haynes research group at a local community center. The last module is currently being tested in a local high school.

The events developed for and run at the local community center focused on two key scientific ideas, the scientific method and climate change. These matters were chosen as they are key in the field of chemistry. The scientific method is important for students to understand as they enter science, technology, engineering, and mathematics (STEM) classes and begin learning more in-depth scientific concepts. Climate change is a global issue that an engaged citizenship should understand, while also providing opportunities to learn about interdisciplinary science. In addition, we felt that, as the age of the students participating in these activities spanned such a wide range, broader topics would more likely appeal to the diversity of students.

The module in development for the high school chemistry classroom is a series of laboratory experiments designed to increase student engagement by relating chemistry concepts to literature. Each lab draws connections between the chemical concepts being discussed in the lab and a piece of literature. By

framing the chemistry through stories, we aim to make the science accessible and make a connection between the arts and the sciences.

6.2 Activities for Middle School Students to Sleuth a Chemistry "Whodunit" and Investigate the Scientific Method

6.2.1 Background

In recent years, public interest in forensic science has increased greatly, due in part to television shows such as *CSI* and *Bones*, which feature scientists using analytical tools to solve crimes.[6,7] By leveraging student interest in the applied nature of forensic chemistry, educators also have an opportunity to use a practical, problem-solving approach to introduce students to the scientific method,[8] including formulating hypotheses, selecting an appropriate experiment from those available, performing positive and negative controls, and interpreting both conclusive and inconclusive results.

In this outreach activity, we engaged middle school students to select an assay, consider positive and negative controls, and use information gained from several assays to reach a conclusion and solve a mystery. Three mysteries were presented in consecutive years to students participating in a summer program at the West 7th Community Center in St. Paul, MN. Mysteries included an environmental chemical spill, a jewel heist, and a case of sabotage at a solar cell factory. Results of the student answers to pre- and post- experiment questions are included: in Year 2, student comprehension increased for two of the four questions asked from the pre- to the post-activity assessment, and in Year 3, increases in student comprehension were observed for all four of the questions from the pre- to the post-activity assessment.

6.2.2 Methods

This activity involves preparation beforehand of (1) a video (or other format presentation) detailing the events of the mystery to students, (2) evidence kits,

and (3) solutions for assays. The format of the activity as well as the assays made available to students are described herein, and detailed transcripts of the 3 mystery videos as well as instructions for preparation of the evidence kits and assays can be found in the published paper from which this text is adapted.[9] The students first watched a video wherein an investigator described the mystery and interviewed a cadre of suspects. In addition, in the first and second year, students viewed a short video describing the assays available to them. In the third year, assay use instructions were described by graduate student volunteers at each station as the students needed each assay.

In scenario 1, “Chemical Spill on the Mississippi River,” students watched a video that explained that a portion of the Mississippi River was mysteriously lacking in fish and wildlife and watched investigator interviews with the suspects that might have caused this environmental change. In scenario 2, “Jewel Heist at the Science Museum,” students watched a video that explained that the Crown Jewels on display at the Science Museum had been stolen during a break-in, and they were shown interviews with suspects. In scenario 3, “Sabotage at a Solar Cell Factory,” students watched a video depicting a crime of sabotage at the Solar Haynes Industries solar cell factory, including police investigator interviews with potential suspects. For each scenario, students were presented with 4 suspects and 5-6 assays with which to test their evidence. It is possible to change the guilty suspect in any given scenario by altering the evidence apparently collected from each suspect.

Student participants were split into groups of four and assigned to a graduate or undergraduate student ‘guide’ who helped keep the students on-task during the activity (Figure 6.1). Each group was given a box containing (1) approximately six pieces of evidence that they were told had been collected from the suspects or at the crime scene, (2) a list of stations where they could test their evidence, and (3) a set of worksheets to record their results. Additionally, graduate or

undergraduate students were available at each of the assay stations to explain the chemistry concepts of the assay, how to perform the assay, and positive and negative controls where applicable. For all three scenarios, evidence kit contents and assays available to the students are listed in Table 6.1. In addition to the use of several well-known tests widely used in outreach activities (DNA extraction, starch detection with iodine, filter paper chromatography with felt-tip pens), a series of less well-known tests that demonstrate chemical concepts were incorporated. Examples include an acid/base detection of metal salts in scenario 1 and a nanoparticle-based test for pesticide detection in scenario 2. The students were given no instructions regarding which assay to use on which piece of evidence. For each assay, students recorded the evidence tested and the results of the assay as well as the results of the positive and negative controls. Students were also asked to interpret their results in the context of the mystery and determine the guilty party.

All mystery scenarios were tested with students ages 10-14 in a one-day event for socioeconomically disadvantaged students (average of 74% of students identify as racial minorities and 87% of students were from homes below 200% of the Federal Poverty Guidelines) participating in a W. 7th Community Center summer program.[10] Although the mysteries were developed for use in an outreach event, all activities were translated and optimized by a certified Minnesota high school teacher for use in middle or high school classrooms.

In the second and third years of the activity, students were asked multiple-choice pre- and post- questions about important scientific vocabulary related to the scientific method. The questions asked were: (1) What is an observation, (2) What is a hypothesis, (3) What is a positive control, and (4) What is a negative control. They used personal response devices, which have received generally positive student reviews,[11,12] to answer the questions, and student answers were analyzed to evaluate student learning during the course of the activity. Some

students participated in the summer program for multiple years, leading to a small degree of overlap between students each year.

Table 6.1 Overview of the evidence kit contents and available assays for the three mystery activities.

Activity	*Contents of Evidence Kit*[a]	*Assays Available to Students*
Chemical Spill	• Contaminated river water sample • Handwritten notes found in contaminated area • Pens belonging to suspects • Map with fingerprints and fingerprint samples from suspects • Soil sample from contaminated area • Homogenized fish sample from contaminated area	• Acid/base detection of metal ions in solution • Ink chromatography • Flame test • Iodine fingerprint developing or ninhydrin fingerprint developing • Luminol test • pH test
Jewel Heist	• Fingerprint samples from each suspect • Debris from crime scene with fingerprint present • Glass from the display case • Glass found in a suspect's car • Powder found at crime scene • Powder samples found on suspects • Paint collected from security camera • Paint from a suspect's hands • Paint sample from a mural (suspect's alibi)	• Acid/base detection of metal ions in solution • Ink chromatography • Iodine fingerprint developing or ninhydrin fingerprint developing • Nanoparticle test for pesticides • Iodine test for starch
Solar Cell Factory Sabotage	• Piece of plastic left at crime scene • Pieces of plastic from the workplaces of suspects • Sample containing DNA from a cup at the crime scene • DNA sequence pre-processed from each suspect • Handwritten note found at the crime scene • Pens belonging to suspects • Metallic dust found at the crime scene • Metallic dust found on shoes of suspects • Fingerprint samples from suspects • Piece of paper with fingerprint found at crime scene • Sample of scent detected at crime scene • Cologne or perfume from suspects	• Plastic density comparison • DNA extraction • Metal ion flame test • Ink chromatography • Iodine fingerprint developing or ninhydrin fingerprint developing • Silver plating test

[a]Positive and negative control samples were provided to students at the assay stations.

6.2.3 Results and Discussion

During the Jewel Heist Mystery activity (in year 2 of this effort), all groups solved the mystery correctly, and the percent of students answering the pre-activity questions and post-activity questions correctly are listed in Table 6.2. Of the four questions asked, the percent of students answering correctly increased from the pre- to the post-activity assessment for Questions (3) and (4) (by 13% and 25%, respectively), did not change for Question (1) (0.0% change), and decreased for Question (2) (-8.3%). The increase in overall student scores from 60% before the activity to 68% after the activity was found to be non-significant using a two-tailed t-test ($p = 0.5$). Based on the results in Table 6.2, it was clear that increased emphasis on the concepts of the scientific method (observations, hypotheses, and controls) was needed to enhance student comprehension of the scientific method during the activity. As the goal of this activity was for students to learn through problem solving rather than direct instruction, preparations for the assay stations for the following year (Solar Cell Factory Sabotage) focused on improving emphases on observations, hypotheses, and controls. In doing so, students were exposed to these principles through the mini-experiments that they performed at each assay station.

During the Solar Cell Factory Sabotage Mystery activity in year 3, students were asked the same questions before and after the activity as for the Jewel Heist Mystery. Overall student scores increased significantly from 52% to 68% ($p = 0.03$). The percent of students answering correctly increased from the pre- to the post-activity assessment for all four questions asked (Table 6.2). The increase in students correctly answering was 3.7% for Question (1), 11% for Question (2), 22% for Question (3), and 26% for Question (4).

Figure 6.1 Students participating in the 'Whodunit' activity

Table 6.2 Comparison of correct student responses to pre- and post-activity assessments

Assessment Questions	Jewel Heist Activity, *N* = 24		Solar Cell Factory Sabotage Activity, *N* = 27	
	Pre-activity, %	Post-activity, %	Pre-activty, %	Post-activity, %
Question 1: What is an observation?	79	79	70	74
Question 2: What is a hypothesis?	67	58	78	89
Question 3: What is a positive control?	50	63	30	53
Question 4: What is a negative control?	46	71	22	48
Overall Percent Correct	60	68	52	68

To assess the statistical significance between pre- and post-activity responses, the student responses to each question for both of the activities were pooled. Using McNemar's test,[13] the pooled responses showed a significant increase in comprehension for Questions 3 ($p = 0.01$) and 4 ($p = 0.01$). Significant differences between the pre- and post-activity responses were not observed for Questions 1 ($p = 0.6$) and 2 ($p = 0.6$). These results indicate that an outreach activity with no direct instruction can lead to significant increases in student comprehension of concepts related to the scientific method and are promising for student learning when implemented in an outreach event.

While the focus of the investigations when implemented as an outreach activity was on engaging students in solving a mystery through problem solving using chemical assays, each investigation contains multiple activities that could be used to highlight a number of different chemical concepts in a classroom, including solubility, acid-base chemistry, chemiluminescence, and atomic emission spectroscopy. Using a format with minimal direct instruction and instead allowing students to determine which chemical tests were appropriate for certain types of samples, student comprehension of concepts related to the scientific method increased when these concepts were emphasized during the explanation of the assay protocols. This pairs well with the inquiry-based learning currently being implemented in undergraduate chemistry laboratories, priming students for future laboratory classes.[14]

6.2.4 Conclusion

In the activity presented here, three separate investigations were developed where students use simple chemical assays to solve a mystery. In each investigation, students were given a kit of evidence, a list of assays, and minimal direct instruction. Although this activity was originally designed as an outreach event, the activities have also been modified and formatted for implementation in a middle school classroom. Students work in groups, make decisions related to a

course of action for solving a problem, formulate hypotheses, perform positive and negative controls, interpret data, and formulate conclusions based on results of multiple chemical assays. Instructors could also modify activities as needed for a greater focus on scientific concepts of interest to the class.

6.3 Developing a Conceptual Understanding of Climate Change

While understanding a broad concept like the scientific method is critical for young students, there is also significant interest in framing chemistry concepts by current events where possible as a mode to increase engagement. In the second chemical education activity pursued as part of this thesis work, we focused on climate change both due to its importance as a worldwide issue and as a context for teaching students core chemistry concepts.

6.3.1 Background

Anthropogenic climate change is a global issue with widespread impacts. The International Panel on Climate Change warns, "*Warming of the climate system is unequivocal, and since the 1950's, many of the observed changes are unprecedented over decades to millennia. The atmosphere and ocean have warmed, the amounts of snow and ice have diminished, sea level has risen, and the concentrations of greenhouse gases have increased"*.[15] In recent decades, these changes have impacted natural and human ecosystems on all continents and across the oceans.[16] Despite the clear scientific consensus, according to Gallup polls, only 57% of Americans believe that human activities are the driving force in the rapid climate change we are observing, and only one-third feels that climate change is cause for great concern.[17,18] Less than half of Americans know that carbon dioxide (CO_2) traps heat from the Earth's surface, and only 1-in-4 know that increased carbon dioxide in the atmosphere causes ocean acidification.[19]

Young students typically have a strong concern for the environment and enjoy learning about it. However, they are typically more concerned about local environmental issues than global issues. With reinforcement, they have been shown to expand their concern to global environmental issues; without it, they lose their initial concern.[20] High school students can commonly pick out basic facts, such as rising CO_2 levels, but cannot apply their knowledge to determine potential problems or solutions as there appears to be no further curriculum covering this area during high school.[21] Even undergraduate chemistry students consistently fail to accurately discuss climate change.[22,23]

Chemistry principles are key to understanding why the climate is changing and what the effects will be. Many factors in climate change link to topics covered in chemistry courses (Figure 6.2), such as surface albedo, combustion of fossil fuels, the greenhouse effect, cloud and aerosol formation, light scattering and absorption, and ocean acidification.[24] For example, understanding the greenhouse effect requires knowledge of light-matter interactions, vibrational absorbance and emission of long wavelength radiation by gases, and scattering of high energy radiation by clouds and aerosols.

Over the past several decades, there has been a large push to integrate environmental issues into chemistry courses.[25-27] Debates within the chemical education community have led to two conclusions: connecting chemical concepts to real world applications and issues will lead to an increase in student engagement in chemistry classes, and environmental effects have been shown to be useful in motivating and enhancing chemistry learning and fostering pro-environmental attitudes.[28-30] Many teaching modules have been developed that can be formally integrated into high school and college level curriculum.[31-33]

Attempts to implement these modules as supplements to the formal integration of environmental chemistry concepts have been limited but successful when done.

Rather than giving a world-view perspective of environmental issues such as climate change, most outreach programs focus on local environmental issues like drinking water quality, and those that do take a global view focus only on one issue such as ocean acidification. In addition, many of these programs require equipment, software, or chemistry expertise available only at college campuses.

With an increase in ease of creating and sharing media, there has been a boom in educational videos featuring experts talking about their area of specialization. These videos are ideal for use in science education. In formal education, videos are often used as a substitute for interactions between students and teachers rather than as a tool to explain key chemistry principles. Short videos are ideal for use as brief introductions to topics and as tools for ideas more easily explained visually. TED has created a series of videos designed for specific use as mini-lessons through its "TED-Ed" program. TED-Ed has over 100,000 short animated video lessons designed for specific use as mini-lessons; these videos span a wide range of topics, including a series on climate change: *Our Changing Climate*.[34] Despite their broad applicability, in the published literature, TED-Ed has been rarely used as a formal teaching tool. Our work utilizes Ted-Ed videos to give students a short introduction to a topic prior to engaging them in demos and hands-on activities related to that topic, and all topics tie together to give a larger perspective on climate change. Overall, this outreach program was designed to provide a comprehensive overview of climate change by focusing on understanding light-matter interactions and how the burning of fossil fuels impacts the environment. It is suited for a low technology, low expertise setting with broad applicability in terms of educational level and motivation that can be utilized in the traditional outreach style or supplement current chemistry curriculum in schools.

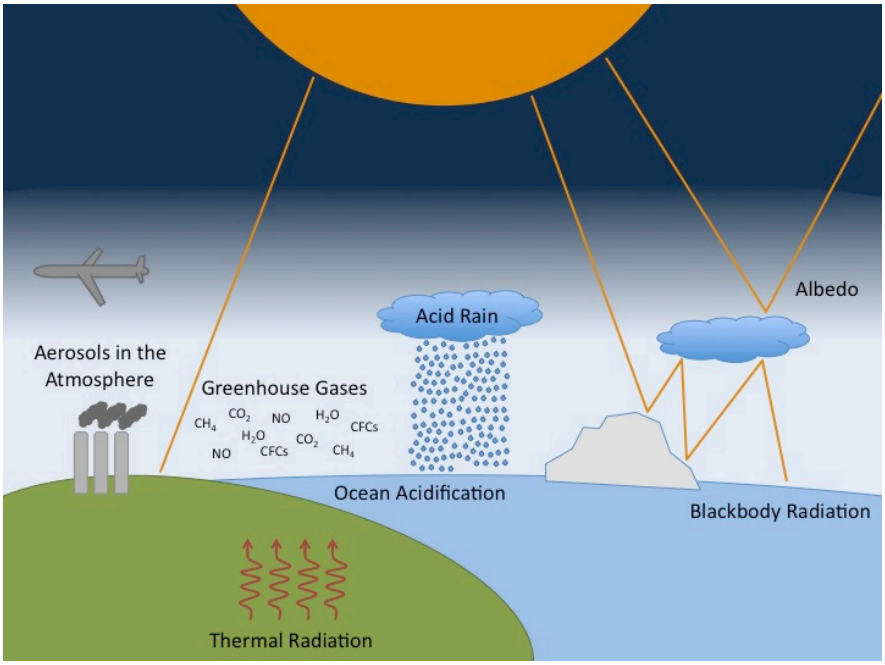

Figure 6.2 Overview of the various chemical processes directing climate change, covering both fossil fuel emission and light-matter interactions.

Figure 6.3 Students participating in the climate change activity

6.3.2 Methods

These modules were developed and tested as part of two half-day outreach programs at the same local community center described in Section 6.2 for socioeconomically disadvantaged (75% come from low income, minority families, and nearly half speak English as a second language) students pre-K through 10th grade and also as part of a week-long STEM summer program for rising high school juniors and seniors (n = 23). At the community center, students were sorted into two groups by age, the 'Little Kids' included pre-K through 4th grade (n = 33) and the 'Big Kids' included 5th –10th grade (n = 38). Each group was divided into sub-groups based on the number of stations (Table 6.3). Each station addressed a different aspect of climate change. The 'Little Kids' stations were more broad and simple in concept. The STEM students and 'Big Kids' stations were more specialized and technical. In addition, the STEM and 'Big Kids' stations included TED-Ed videos while the 'Little Kids' stations did not. Each station had demonstrations and/or hands-on activities to engage the students and facilitate learning of the topic discussed at the station (Table 6.3). Specific processes were addressed with the older students whereas general topics were used to discuss the idea of climate change with the younger students. The STEM students and 'Big Kids' groups were accompanied by graduate or undergraduate student guides who helped to facilitate the discussion.

The activity stations were designed to cover a number of topics that demonstrate the complexity of climate change and the chemistry involved in these topics (Table 6.3). These topics correspond well with the Minnesota state high school science standards. The standards addressed are those relating to the interface between scientific progress, society, and the environment. This includes standards ranging from the interplay of various naturally occurring systems to understanding the impacts that society and technological advances have on our ecosystems.[35]

Two specific areas of chemistry were highlighted in the stations due to their strong ties with climate change: chemical reactivity and light-matter interactions (indicated in Table 6.3 by † and ‡, respectively). We chose to cover chemical reactivity, with a particular focus on the products of fossil fuel combustion, due to the multifaceted roles of released carbon dioxide and aerosols. The stations cover how fossil fuels are linked to global warming, sea level rise, and ocean acidification, with a primary goal of increasing understanding of the impacts of fossil fuel products. The second area covered focuses on the interaction of light and matter and the role these interactions play in exacerbating environmental changes. Relevant phenomena covered include the absorption of infrared (IR) radiation by greenhouse gases, blackbody radiation, and surface albedo.

The students' understanding of climate change was assessed both before and after visiting the activity stations. Assessment was administered using personal response devices (as described in Section 6.2.2 above) for the 'Little Kids' and paper forms for the 'Big Kids' and STEM students. The 'Little Kids' and 'Big Kids' were each asked a series of nine multiple choice questions while the STEM students were asked six multiple choice questions, three "select all that apply" questions, and two short answer questions to better assess their understanding (Table 6.5 details the assessment questions posed to the 'Big Kids', and Tables 6.7 and 6.10 detail the multiple choice/"select all that apply" and short answer assessment questions, respectively, posed to the STEM students). The 'Little Kid' assessment questions are not included in a table as there is only minor discussion of their results; however, the questions can be found in the SI of the paper from which this chapter is adapted.[36]

Student understanding before and after participation in the activity was analyzed for statistical significance using GraphPad Prism. The overall percent change between the pre- and post-tests were tested for significance using an unpaired t-test, with a p-value below 0.05 being considered significant. Error bars in the

presented graphs indicate standard error of the mean. Changes in the percentage of students answering individual questions correctly (data shown in Tables 6.4, 6.6, 6.8, and 6.9 and Figure 6.5) were not tested for significance due to limitations in sample size.

Table 6.3 Overview of outreach program demonstrations and activities

Groups	Stations	Demonstrations/Activities
'Little Kids'	Hydrosphere	Ocean acidification[†] Ocean stratification Oil spill[†]
	Recycling	Sorting Dissolving styrofoam[†] Plastic density
	Energy	Wind turbines Electrolysis of water[†]
	Atmosphere	Cloud in a bottle[†] Blue sky, red sunset[‡]
'Big Kids'/STEM	Greenhouse Gases	*Climate Change: Earth's giant game of Tetris*[‡] *A guide to the energy of the Earth* (recommended) Model atmosphere[‡]
	Ocean Disruptions	*The secret to rising sea levels* Ocean acidification[†] Thermal expansion
	Radiative Properties	*How quantum mechanics explains global warming*[‡] Blackbody radiation[‡] Light interference[‡]
	Clouds/Rain	*Cloudy climate change: how clouds affect earth's temperature*[‡] Cloud in a jar[†] Acid rain[†]
	Surface Albedo	*Why the Arctic is climate change's canary in the coal mine*[‡] Absorbance of energy[‡] Reflection of energy[‡]

TED-Ed video titles are italicized. [†]Activities that focus on chemical reactivity, i.e. combustion, acid/base chemistry, etc. [‡]Activities that focus on light-matter interactions *For STEM students, the Surface Albedo and Radiative Properties stations were combined

6.3.3 Results and Discussion:

Assessment results for the 'Little Kids' group showed significant room for improvement. The participant response rate fluctuated between 25 and 32 throughout the nine questions, and overall results showed no significant changes in correct answers for the 'Little Kids' (Figure 6.4, $p = 0.8292$). The multiple choice assessment questions only showed an increase in the percent of students answering correctly for three out of the six questions (Table 6.4). In addition to not gaining a better understanding of the processes dictating climate change, there appeared a shift towards students thinking that climate change will either occur on a long time scale or will not occur at all (Figure 6.5), clearly not the desired outcome. Casual observation of the 'Little Kids' during the activities revealed that the students were not as engaged as we have seen during other outreach events done with the same demographic students on different topics and with different methods. We attribute this to a decrease in the number of hands-on activities and an increase in demonstrations where the students watched as the volunteers explained the concepts. Additionally, the concepts covered may have been too great in range of information and number for the 'Little Kids'. In future endeavors, we recommend that the focus for young students be on demonstrating the impacts (oil spill, ocean acidification, etc.) and solutions (wind turbines, recycling, etc.) as a means of helping to raise general awareness and cultivate environmentally conscious attitudes rather than focusing on the exact chemistry of the climate processes. Lastly, we feel that making the activities more hands-on and having a greater cohesiveness between the concepts at different stations will likely result in better information transfer and retention for this age group.

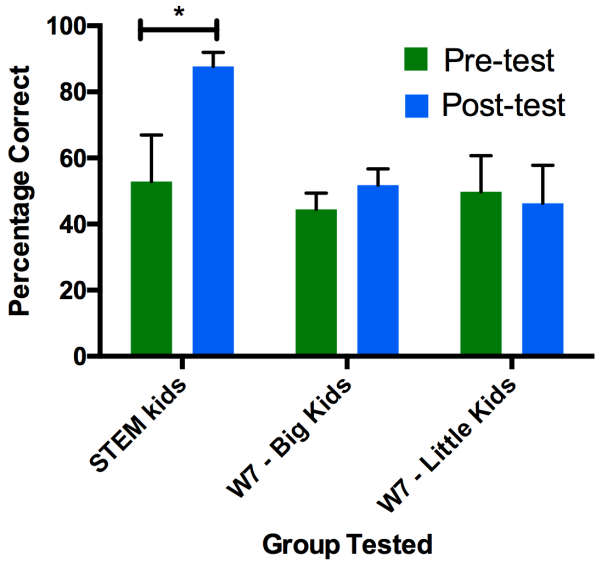

Figure 6.4 Changes in student understanding for the three groups tested. All the multiple choice questions were included in determining the average percentage correct for each group. The number of questions (N) = 6, 9, and 6 for the STEM students, 'Big Kids' and 'Little Kids', respectively. *p ≤ 0.05 and error bars represent SEM.

Table 6.4 'Little Kids' percentage correct of the assessment questions. The number of responses ranged from n = 27 to 33.

Question	4	5	6	7	8	9	Average
Pre-test	65.6	43.8	40.0	67.7	76.7	3.7	49.8 ± 10.9
Post-test	70.0	34.5	28.1	58.1	80.8	7.4	46.3 ± 11.5

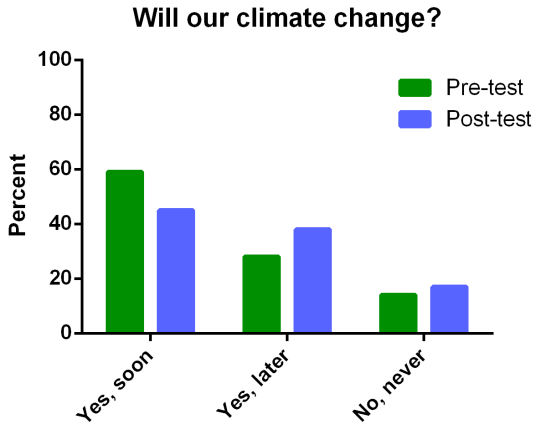

Figure 6.5 'Little Kids' understanding of the time scale of climate change.

Overall there is no statistically significant change in the overall understanding of climate change among the ‘Big Kids’ at the community center outreach event (Figure 6.4, $p = 0.3116$). In the ‘Big Kids’ data, there was an increase in percentage answered correctly for five of the questions, a decrease in percentage answered correctly for three of the questions, and no change for one of the questions (see questions in Table 6.5 and results in Table 6.6). The addition of the TED-Ed videos to the stations did not appear to result in a change in understanding when the results from the ‘Big Kid’ activities (where videos were used) were compared those of the ‘Little Kids’ (where videos were not used).

Questions 1 through 3 and 9 assessed the community center ‘Big Kids’ understanding of how fossil fuels direct climate change. Unfortunately, significant drops were seen in questions 1 and 9 (Table 6.6) for identification of carbon dioxide as the main pollutant in climate change and the complex role of fossil fuels in causing multiple phenomena, respectively. There was however an approximately ten percent change in the percentage of students who identified fossil fuels as the primary pollutant responsible for global warming as seen in question 2 (Table 6.6). This likely resulted from repeated exposure and students’ prior knowledge. Question 3 resulted in no net change, staying at 47.4% percent of the students choosing the correct answer (Table 6.6). A shift in answers toward sea level rise as the only change caused by fossil fuels (question 9) may indicate a bias in the TED-Ed videos over a demo, in this case, as the video talked exclusively about sea level rise while the Ocean Disruptions station required more time to see the result compared to other demos. Overall, there was no significant change in understanding as indicated by the fossil fuel assessment questions (Fig 6.6, $p = 0.7994$).

Student understanding of light-matter interactions was evaluated with questions 4 through 8. Gains of at least ten percent were seen in three of the five questions, however there was also a drop in question 6 of about fifteen percent that may

have resulted from students trying to understand both the albedo and cloud formation demos (Table 6.6). The albedo station indicated that water can absorb a large amount of IR energy (high albedo) and increase its temperature, however, the “cloud in a jar” demo indicated that clouds of water vapor were formed with aerosols which help reflect sunlight and its IR energy. Placing an emphasis on the difference in albedo between water vapor and liquid water along with coordination between the Atmosphere and Surface Albedo stations would serve to reduce confusion. When combined, there was no significant change in understanding of light-matter interactions (Figure 6.6, $p = 0.1359$).

We feel that the use of the TED-Ed videos was good for brief introductions to the topics covered but that the ties between the videos and topics covered should be more explicit. In addition, some of the videos may have been longer than student attention spans (TED-Ed videos ranged in length from 1:15 minutes to 6:40 minutes, averaging of 3:56 minutes). Future uses of these stations should place more focus on the hands-on activities as this is something the students are less likely be able to experience on their own and it may also serve to increase the students’ grasp of the topics covered. In future iterations, students will be asked to watch the free TED-Ed videos ahead of the outreach event and then spend more time at each station working with the hands-on activity associated with those videos.

Table 6.5 Assessment questions for the 'Big Kids'.

Number	Question	Answer Options
1	What is the main pollutant causing global warming?	a. Water (H_2O) b. Nitrogen (N_2) c. Oxygen (O_2) d. Carbon Dioxide (CO_2)
2	What source of energy increases this pollutant?	a. Nuclear b. Corn-based ethanol c. Wind d. Fossil fuels
3	How does burning coal affect the amount of clouds?	a. Increases b. Decreases c. No effect d. I don't know
4	When the Earth gives off energy, ___ absorb(s) it and sends it back to Earth?	a. Greenhouse gases b. Aerosols c. Nitrogen and oxygen, the primary components of air d. I don't know
5	When sunlight shines on ice, the energy ___?	a. Reflected into space b. Absorbed by earth's surface c. I don't know
6	When sunlight shines on clouds, the energy is ___?	a. Reflected into space b. Absorbed by earth's surface c. I don't know
7	When sunlight shines on the ocean, the energy is ___?	a. Reflected into space b. Absorbed by earth's surface c. I don't know
8	When sunlight shines on air, the energy is ___?	a. Reflected into space b. Absorbed by earth's surface c. I don't know
9	Burning fossil fuels will cause which of the following changes?	a. Warming b. Sea level rise c. Ocean acidification d. All of the above

Table 6.6 'Big Kids' percentage correct of the assessment questions. N = 38

Question	1	2	3	4	5	6	7	8	9	Average
Pre-test	71.1	55.3	47.4	42.1	21.1	50.0	26.3	44.7	42.1	44.4 ± 4.9
Post-test	60.5	65.8	47.4	78.9	50.0	34.2	47.4	50.0	31.6	51.8 ± 4.9

Because we didn't see the learning gains expected among the community center outreach participants, we elected to make slight modifications and use similar activities with a different audience, high school juniors and seniors that self-identify as interested in STEM fields. The STEM high school students started off with a better understanding of the concepts of climate change compared to the community center outreach participants. Even with this initial better understanding, the STEM students exhibited statistically significant gains in conceptual understanding after completing the activity stations, with the pre- and post-test averages increasing from 52.9 ± 14.0% to 87.7 ± 4.3% (Figure 6.4, $p = 0.0390$). The questions covering fossil fuels (questions 1 through 4, 7, and 11) showed no significant change in correct answers (Figure 6.6, $p = 0.1729$). Climate science terminology was completely foreign as indicated by question 8 pre-test responses about positive feedback effects, but there was a large increase in students answering correctly by the end of the program (Table 6.8). Students showed little understanding of the light matter interactions, as indicated by questions 5, 6, and 9 (Tables 6.8 and 6.9), before the program. Of those questions, only question 9 showed an increase in the percent of students answering correctly after the activities to above 50%, increasing to 69.6%. The "select all that apply" questions, 5 through 7 do show some possible changes in comprehension (Table 6.9), yet the post-test percentages are surprisingly low compared to the rest for this group of students. It is possible that the nature of these questions, as "select all that apply" questions, explain the lower percentages as they require each student to correctly identify all correct answers rather than one correct answer.

In addition to the multiple choice and "select all that apply" questions, the STEM participants were asked two short answer assessment questions to demonstrate whether or not they could apply their knowledge of climate science to predict problems and evaluate solutions. The answers were assessed for correctness and a demonstration of understanding. Unlike the multiple choice and "select all

that apply" questions, not all the students chose to respond to these questions. The number of student responses, comparing pre- and post-activities, increased from 8 to 13 for question 10 and from 11 to 18 for question 11, suggesting that the student became more familiar with the material during the activity stations. During the pre-test, only 2 students successfully demonstrated understanding of the question and the answer. Post-activities, nearly a quarter of the students were able to demonstrate that they understood the question and correctly answer, a 20-50% increase from pre-test assessment. For example, to answer question 10, one student gave the following answers: pre-test: *"Soot causes more clouds trapping heat.";* post-test: *"The soot can cause the ice to be darker, which takes in more heat. Aerosols can cause more clouds, which trap heat when there is little sunlight. Greenhouse gases cause more infrared light to be sent back to Earth."* The increase in the number of students who answered the short answer questions and the complexity of their answers indicates that the students felt more confident with the concepts surrounding climate change and that they had the ability to apply the basic facts she/he had learned.

Table 6.7 Assessment questions for the STEM kids. Questions 1 through 4, 8, and 9 are multiple choice and questions 5 through 7 are circle all that apply.

Number	Question	Answer Options
1	What is the main pollutant causing global warming?	a. Water (H_2O) b. Nitrogen (N_2) c. Oxygen (O_2) d. Carbon Dioxide (CO_2) e. Methane (CH_4)
2	What source of energy increases this pollutant?	a. Nuclear b. Corn-based ethanol c. Wind d. Fossil fuels e. Solar
3	How does burning coal affect the amount of clouds?	a. Increases b. Decreases c. I don't know
4	On average, how long does carbon dioxide stay in the atmosphere once released by burning fossil fuels?	a. A week b. A month c. A year d. A decade e. A century f. A millenia
5	When the Earth gives off energy, ___ absorb(s) it and sends it back to Earth? (circle all that apply)	a. Carbon dioxide (CO_2) b. Aerosols c. Clouds d. Nitrogen (N_2) e. Oxygen (O_2)
6	When sunlight shines on ___, the energy is mostly reflected into space? (circle all that apply)	a. Ice/snow b. Clouds c. Aerosols d. Ocean e. Air
7	Continued burning of fossil fuels will cause which of the following changes? (circle all that apply)	a. Warming b. Sea level rise c. Ocean acidification d. Acid rain e. Melting of the cryosphere
8	The term positive feedback effect refers to the effect of a change that ____?	a. Benefits our climate b. Warms our climate c. Stabilizes our climate d. Amplifies the initial change
9	What type of energy does the surface of the Earth give off during thermal radiation?	a. Heat b. Infrared light c. Ultra violet light d. Chemical energy

Table 6.8 STEM students' percentage correct of the multiple choice assessment questions (questions 5-7 are "select all that apply" type questions). N = 23

Question	1	2	3	4	8	9	Average
Pre-test	91.3	91.3	65.2	30.4	26.1	13.0	52.9 ± 14.0
Post-test	100.0	87.0	95.7	87.0	87.0	69.6	87.7 ± 4.3

Table 6.9 "Select all that apply" assessment question responses from the STEM students. N = 23

Question	5	6	7
Pre-test	13.0	8.7	30.4
Post-test	30.4	17.4	47.8

Table 6.10 Short answer assessment questions administered to the STEM kids.

Flying planes over the arctic between the US and Russia gives off soot, aerosols, and greenhouse gases. In what ways do each of these pollutants cause warming in the arctic?
Some scientists believe that we might be able to geo-engineer the atmosphere by adding large amounts of sulfuric acid, an aerosol, to the atmosphere to stabilize/reduce warming. a. Why would this cause cooling? Is this a short-term or long-term solution? b. What would be one major disadvantage to cooling by using sulfuric acid?

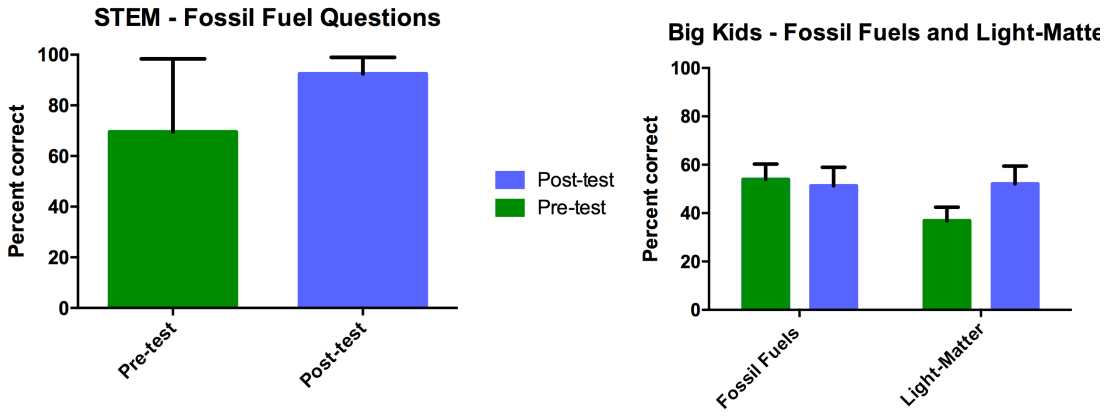

Figure 6.6 Breakdown of the multiple choice questions by fossil fuel or light-matter interaction broad topic categories. There was no significant difference measured. Error bars represent the SEM. The number of questions in each category (n) = 4, 4, and 5 for STEM fossil fuels, 'Big Kids' fossil fuels, and 'Big Kids' light-matter, respectively.

The significant increase in the percentage of STEM students answering the questions correctly with similar gains not seen in the other two student groups has interesting implications. The STEM students are mostly likely to have deeper exposure to and background in chemistry and climate change. It may be that this outreach event is most effective for students who have some background knowledge that can be built upon. Events designed for beginner students can use some of the demos and hands-on activities we have described but should be tailored to a level appropriate for the audience.

6.3.4 Conclusion

The outreach event as we have performed it appears be effective for students who already posses a good science background and ineffective as a mode for introducing and teaching students about climate change when they are relatively young or naïve to the topic. Students with some level of background knowledge were better able to understand the concepts covered and think critically about the topic. While the outreach event, as presented herein, does not appear to be successful for the students at the community center, we think that the subject matter is still important and that the demonstrations and activities just need to be better tailored with the students' science backgrounds taken into consideration or the activities need to be done as part of a larger unit, rather than as a one day outreach event.

The TED-Ed videos paired well with the demos and activities performed and served as an introduction for the concepts for each station. To our knowledge, this is the first published example of pairing TED-Ed videos and STEM outreach activities. Other than the modifications mentioned previously, the addition of an alternative energy module may add to the overall experience of this set of climate change activities. For example, in a five-day science summer camp put together by Canisius College in New York students, two days were devoted to solar and wind power.[37] Including alternative energy would complement the climate change

event overall and educate students on how we might counteract and/or prevent the effects in the future. Overall, we believe that introducing the science of climate change to outreach events is important to cultivate a better understanding of the issue and that its inclusion will result in an overall increase in comprehension and awareness.

6.4 Increasing Chemical Understanding using Literature to Stimulate Student Interest

The last chemical education activity described as part of this work focused on high school juniors and seniors in a formal classroom setting. Therefore, unlike the previous modules, these were primarily developed following the usual laboratory format. To enhance student engagement in fundamental chemistry concepts, activities were developed that tie chemistry concepts with fictional literature. The idea for this activity was inspired by the use of dystopian novels in a freshman seminar course here at the University of Minnesota and by previous use of Kurt Vonnegut's novel *Cat's Cradle* to explain thermodynamics concepts.[38,39]

6.4.1 Methods

A series of novels were chosen that fit into the broad category of science fiction or dystopian literature. While many were considered, ultimately, the novels chosen were *Cat's Cradle* by Kurt Vonnegut, *Fahrenheit 451* by Ray Bradbury, *On the Beach* by Nevil Shute, and the short story *Pate de Foie Gras* by Isaac Asimov.[39,40,41,42] Other books considered included *Forty Signs of Rain* by Kim Stanley Robinson, *Frankenstein* by Mary Shelley, and *Oryx and Crake* by Margaret Atwood.[43,44,45] While initially screening each piece of writing, we marked portions that touched upon an important scientific concept. Looking through the marked excerpts, each book was paired with a unit in the general chemistry high school curriculum. Labs were then developed that linked the excerpt and critical concepts for the unit. Each lab includes a hands-on

laboratory activity as well as pre- and post-lab questions to reinforce the hands-on learning.

These activities are still under development, and so the results presented herein are preliminary. So far, two of the labs have been tested with two high school laboratory sections (N = 53 students, with 31 female and 22 male). A control group of one lab section (N = 32, 15 female and 17 male) performed the labs previously taught as part of the general chemistry classes. The labs were administered over two to three days depending on the length of the lab, and all the work was performed during class time.

Assessment questions were developed to evaluate both student engagement and comprehension. The questions were based on examples found in previous literature.[46-48] Both the experimental and control group students were tested with the assessment questions both prior to and after performing the laboratory, including the pre- and post-lab questions. In addition, the comprehension of the experimental groups was evaluated by examining the post-lab questions. Qualitative results are discussed below and quantitative analysis is still underway.

6.4.2 Preliminary Results

The first lab run with the students was titled ‘Matter, Properties, and Change Calorimetry Lab’ and it was inspired by *Fahrenheit 451* by Ray Bradbury. The lab started off with the students reading a few short passages from the books. Then the students created a soda can calorimeter and were charged with determining the energy released when burning a marshmallow and a page of a book. We gave them pages from a copy of *Fahrenheit 451* to burn, which the students found quite entertaining. Overall the students seemed to enjoy the lab and were engaged during the activity.

The second implementation of the new labs took two different forms. Two activities have been developed around the short story *Pate de Foie Gras* by Isaac Asimov. One was a traditional laboratory experiment where students explored the properties of transition metal complexes and the other was a reading assignment that incorporated critical reading strategies. Due to the lack of time, one laboratory section performed the lab while the other did the reading assignment. The students doing the laboratory activity did not seem to be engaged but the lab itself was rushed and there were only three stations, leading to student crowding.

We chose to develop a reading assignment around *Pate de Foie Gras* in part due to the fact that it was a short story, making it easy for the students to read during one or two class periods. Additionally, Asimov incorporated a large amount of scientific detail in the story, making it ideal for asking both conceptual and calculation-based questions. The details he gave allowed us to pose questions touching upon a number of areas, including the scientific method, dimensional analysis, and transition metal chemistry. While the students did not enjoy this assignment, qualitative analysis of their answers by the high school teacher showed that they were answering questions correctly and well.

The lab based upon *Cat's Cradle* by Kurt Vonnegut will focus on solubility, and *On the Beach* by Nevil Shute will be used to develop a supplemental lab based around nuclear chemistry, a topic often neglected in high school chemistry classrooms. In addition, there may be future collaboration between the Chemistry high school teacher and one of her colleges who teaches English to develop a series of cross-classroom lectures surrounding *On the Beach* by Nevil Shute.

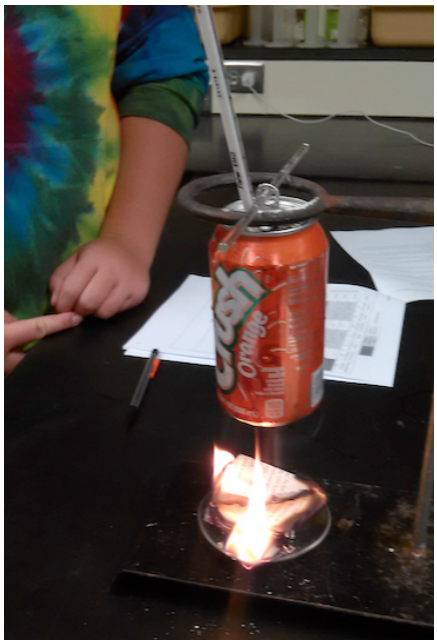

Figure 6.7 *Fahrenheit 451* soda can calorimetry lab

6.5 Conclusion

I have focused on increasing student engagement and understanding in chemistry through both outreach events and in traditional educational settings throughout my time as a graduate student. Outreach events are an important mode for interacting with students who have little experience with chemistry. By creating fun yet informative activities we can teach students scientific concepts they may not be exposed to in school. On the other hand, by creating laboratory experiments that tie in with topics that interest students we hope to increase their engagement and learning. The three modules described above are three different ways that we can increase student interest in chemistry.

References

Chapter 1

1. Chhabra, E. S.; Higgs, H. N. The many faces of actin: matching assembly factors with cellular structures. *Nat. Cell Biol.* **2007**, *9(10)*, 1110-1121.
2. Grigoriev, I.; Akhmanova, A. Microtubule dynamics at the cell cortex probed by TIRF microscopy. In *Method Cell Biol.* Cassimeris, L., Tran, P., Eds.; Elsivier Inc.: Philadelphia, PA, 2010; Vol. 97, pp 91-109.
3. Parry, D. A. D.; Strelkov, S. V.; Burkhard, P.; Aebi, U.; Herrmann, H. Towards a molecular description of intermediate filament structure and assembly. *Exp. Cell Res.* **2007**, *313*, 2204-2216.
4. Block, J.; Schroeder, V.; Pawelzyk, P.; Willenbacher, N.; Köster, S. Physical properties of cytoplasmic intermediate filaments. *Biochim. Biophys. Acta.* **2015**, *1853*, 3053-3064.
5. Pollard, T. D.; Cooper, J. A. Actin, a central player in cell shape and movement. *Science*. **2009**, *326*, 1208-1212.
6. Cooper, G. Structure and organization of actin filaments. In *The cell: a molecular approach (2nd Ed.);* Sinauer Associates: Massachusetts, 2000. http://www.ncbi.nlm.nih.gov/books/NBK9908/ (accessed Jan 10, 2016)
7. Gutierrez, L. M. New insights into the role of the cortical cytoskeleton in exocytosis. In *Int. Rev. Cel. Mol. Bio.;* Jeon, K. W., Ed.; Elsevier Inc.: Philadelphia, PA, 2012; Vol. 295, 109-137.
8. De Forges, H.; Bouissou, A.; Perez, F. Interplay between microtubule dynamics and intracellular organization. *Int. J. Biochem. Cell B.* **2012**, *44*, 266-274.
9. Pekney, M.; Lane, E. B. Intermediate filaments and stress. *Exp. Cell Res.* **2007**, *313*, 2244-2254.
10. Fletcher, D. A.; Mulling, R. D. Cell mechanics and the cytoskeleton. *Nature*. **2010**, *463(20)*, 485-492.
11. Grigoriev, I.; Akhmanova, A. Microtubule dynamics at the cell cortex probed by TIRF microscopy. In *Method Cell Biol.* Cassimeris, L., Tran, P., Eds.; Elsivier Inc.: Philadelphia, PA, 2010; Vol. 97, pp 91-109.
12. Kaverina, I.; Straube, A. Regulation of cell migration by dynamic microtubules. *Sem. Cell Dev Biol*. **2011**, *22*, 968-974.
13. Patel-Hett, S.; Richardson, J. L.; Schulze, H.; Drabek, K.; Isaac, N. A.; Hoffmeister, K.; Shivdasani, R. A.; Bulinski, J. C.; Galjart, N.; Hartwig, J.; Italiano, J. E. Visualization of microtubule growth in living platelets reveals a dynamic marginal band with multiple microtubules. *Blood*. **2008**, *111*, 4605–4616.
14. Mostowy, S.; Cossart, P. Septins: the fourth component of the cytoskeleton. *Nat. Rev. Mol. Cell Biol.* **2012,** *13*, 183-194.
15. Uluc, K.; Kujoth, G. C.; Baskaya, M. K., Operating microscopes: past, present, and future. *Neurosurg. Focus* **2009,** *27* (3), 8.

16. Hell, S. Far-field optical nanoscopy. *Science*. **2007**, *316*, 1153-1158.
17. Betzig, E.; Patterson, G. H.; Sougrat, R.; Lindwasser, O. W.; Olenych, S.; Bonifacino, J. S.; Davidson, W. M.; Lippincott-Schwartz, J.; Hess, H. F. Imaging intracellular fluorescent proteins at nanometer resolution. *Science*. **2006**, *313,* 1642-1645.
18. Rust, M. J.; Bates, M.; Zhuang, X. Sub-diffaction-limit imaging by stochastic optical reconstruction microscopy (STORM). *Nat. Methods.* **2006**, *3(10)*, 793-795.
19. Hell, S. W.; Wichmann, J. Breaking the diffraction resolution limit by stimulated emission: stimulated-emission-depletion fluorescence microscopy. *Opt. Lett.* **1994**, *19(11)*, 780-782.
20. Prasher, D. C.; Eckenrode, V. K.; Ward, W. W.; Prendergast, F. G.; Cormier, M. J. Primary structure of the aequorea Victoria green-fluorescent protein. *Gene*. **1992**, *111(2)*, 229-233.
21. Tsien, R. Y. The green fluorescent protein. *Annu. Rev. Biochem.* **1998**, *67*, 509-544.
22. Schnell, U.; Dijk, F; Sjollema, K. A.; Giepmans, B. N. G. Immunolabeling artifacts and the need for live-cell imaging. Nat. Methods. **2012**, *9(2)*, 152-158.
23. Melan, M. A.; Sluder, G. Redistribution and differential extraction of soluble proteins in permeabilized cultured cells. *J. Cell Sci.* **1992**, *101*, 731-743.
24. Vielkind, U.; Swierenga, S. H. A simple fixation procedure for immunofluorescent detection of different cytoskeletal components within the same cell. *Histochemistry*. **1989**, *91*, 81-88.
25. Smith-Clerc, J.; Hinz, B. Immunofluorescence detection of the cytoskeleton and extracellular matrix in tissue and cultured cells. *Methods Mol. Biol.* **2010**, *611*, 43-57.
26. Giepmans, B. N. G.; Adams, S. R.; Ellisman, M. H.; Tsien, R. Y. The fluorescent toolbox for assessing protein location and function. *Science*. **2006**, *312*, 217-224.
27. Shaner, N. C.; Steinbach, P. A.; Tsien, R. Y. A guide to choosing fluorescent proteins. *Nat. Methods*. **2005**, *2(12),* 905-909.
28. Lymperopoulos, K.; Kiel, A.; Seefeld, A.; Stöhr, K.; Herten, D. P. Fluorescent probes and delivery methods for single-molecule experiments. *Chem. Phys. Chem.* **2010**, *11*, 43-53.
29. Axelrod, D.; Verkman, A. S.; Vetrivel, L.; Haggie, P.; Berland, K.; Spring, K. R.; Davidson, L.; Keller, R., *Methods in Cellular Imaging*. Oxford University Press: 2001; p 434.
30. Li, K; Pu, K. Y.; Cai, L.; Liu, B. Phalloidin-functionalized hyperbranched conjugated polyelectrolyte for filamentous actin imaging in living hela cells. *Chem. Mater.* **2011**, *23*, 2113-2119.
31. Ganguly, A.; Yang, H.; Cabral, F. Detection and quantification of microtubule detachment from centrosomes and spindle poles. In *Method.*

Cell. Biol.; Correia, J. J., Wilson, L., Eds.; Elsevier Inc.: Philadelphia, PA, 2013; Vol. 115, pp 49-62.
32. Stringham, E. G.; Marcus-Gueret, N.; Ramsay, L.; Schmidt, K. L. Live cell imaging of the cytoskeleton. In *Method. Enzymol.;* Conn, P. M., Ed.; Elsevier Inc.: Philadelphia, PA, 2012; Vol. 505, pp 203-217.
33. Thermo Fischer, Detection of actin, intermediate filaments, and tubulin. https://www.thermofisher.com/us/en/home/references/newsletters-and-journals/bioprobes-journal-of-cell-biology-applications/bioprobes-issues-2011/bioprobes-65-july-2011/detection-of-actin-intermediate-filaments-tubulin.html (accessed Jan 12, 2016).
34. Waggoner, A., *Applications of Fluorescence in Biomedical Studies*. Alan R. Liss, Inc: New York, 1986; p 639.
35. Baily, M.; Conway, L.; Gramlich, M. W.; Hawkins, T. L.; Ross, J. L. Modern methods to interrogate microtubule dynamics. *Integr. Biol.* **2013**, *5*, 1324-1333.
36. Taraska, J. W.; Zagotta, W. N. Fluorescence applications in molecular neurobiology. *Neuron*. **2010**, *66*, 170-189.
37. Bakota, L.; Brandt, R. Live-cell imaging in the study of neurodegeneration. In *Int. Rev. Cell. Mol. Biol..;* Elsevier Inc.: Philadelphia, PA, 2009; Vol. 276, pp 49-103.
38. Gauthier-Kemper, A.; Weissmann, C.; Reyher, H.; Brandt, R. Monitoring cytoskeletal dynamics in living neurons using fluorescence photoactivation. In *Method Enzymol.* Conn, P. M., Ed.; Elsevier Inc.: Philadelphia, PA, 2012; Vol. 505, pp 3-21.
39. Koskinen, M.; Bertling, E.; Hotulainen, P. Methods to measure actin treadmilling rate in dendritic spines. In *Method Enzymol.* Conn, P. M., Ed.; Elsevier Inc.: Philadelphia, PA, 2012; Vol. 505, pp 47-58.
40. Hotulainen, P.; Llano, O.; Smirnov, S.; Tanhuanpää, K.; Rivera, C.; Lappalainen, P. Defining mechanisms of actin polymerization and depolymerization during dendritic spine morphogenesis. *J. Cell Biol.* **2009**, *185(2)*, 323-339.
41. Thompson, N. L.; Pero, J. K., *Fluorescence Spectroscopy in Biology*. Springer: Berlin, 2005; Vol. 3, p 305.
42. Toomre, D.; Steyer, J. A.; Keller, P.; Almers, W.; Simons, K., Fusion of constitutive membrane traffic with the cell surface observed by evanescent wave microscopy. *J. Cell Biol.* **2000,** *149* (1), 33-40.
43. Bacallao, R. L.; Yu, W. M.; Dunn, K. W.; Phillips, C. L., Novel light microscopy imaging techniques in nephrology. *Curr. Opin. Nephrol. Hy.* **2003,** *12* (4), 455-461.
44. Batista, F. D.; Treanor, B.; Harwood, N. E. Visualizing a role for the actin cytoskeleton in the regulation of B-cell activation. *Immunol. Rev.* **2010**, *237*, 191-204.
45. Belyy, V.; Yildiz, A. Processive cytoskeletal motors studied with single-molecule fluorescence techniques. *FEBS Lett.* **2014**, *588*, 3520-3525.

46. Zong, W.; Huang, X.; Zhang, C.; Yuan, T.; Zhu, L.; Fan, M.; Chen, L. Shadowless-illuminated variable-angle TIRF (siva-TIRF) microscopy for the observation of spatial-temporal dynamics in live cells. *Biomed. Opt. Lett.* **2014**, *5(5)*, 1530-1540.
47. Tokunaga, M.; Imamoto, N.; Sakata-Sogawa, K. Highly inclined this illumination enables clear single-molecule imaging in cells. *Nat. Methods*. **2008**, *5*, 159-161.
48. Dempsey, G. T.; Vaughan, J. C.; Chen, K. H. Bates, M.; Zhuang, X. Evaluation of fluorophores for optimal performance in localization-based super-resolution imaging. *Nat. Methods*. **2011**, *8(12)*, 1027-1036.
49. Heilemann, M.; van de Linde, S.; Schüttpelz, M.; Kasper, R.; Seefeldt, B.; Mukherjee, A.; Tinnefeld, P.; Sauer, M. Subdiffraction-resolution fluorescence imaging with conventional fluorescent probes. *Angew. Chem. Int. Ed.* **2008**, *47*, 6172-6176.
50. Thompson, M. A.; Biteen, J. S.; Lord, S. J.; Conley, N. R.; Moerner, W. E. Molecules and methods for super-resolution imaging. In *Methods in Enzymology*; Walter, N. G., Eds; Elsevier Inc.: Philadelphia, PA, 2010; Vol. 475, pp 27-59.
51. Sengupta, P.; Van Engelenburg, S.; Lippencott-Schwartz, J. Visualizing cell structure and function with point-localization superresolution imaging. *Developmental Cell*. **2012**, *23*, 1092-1102.
52. Pavani, S.R.; Thompson, M. A.; Biteen, J. S.; Lord, S. J.; Liu, N.; Twieg, R. J.; Piestun, R.; Moerner, W. E. Three-dimensional, single-molecule fluorescence imaging beyond the diffraction limit by using a double-helix point spread function. *Proc. Natl. Acad. Sci.* **2009**, *106*, 2995-2999.
53. York, A. G.; Ghitani, A.; Vaziri, A.; Davidson, M. W.; Shroff, H. Confined activation and subdiffractive localization enables whole-cell PALM with genetically expressed probes. *Nat. Methods*. **2011**, *8*, 327-333.
54. Lee, H. D.; Sahl, S. J.; Lew, M. D.; Moerner, W. E. The double-helix microscope super-resolves extended biological structures by localizing single blinking molecules in three dimensions with nanoscale precision. *Appl. Phys. Lett.* **2012**, *100*, 153701.
55. Huang, B.; Jones, S. A.; Brandenburg, B.; Zhuang, X. Whole-cell 3D STORM reveals interactions between cellular structures with nanometer-scale resolution. *Nat. Methods*. **2008**, *5*, 1047-1052.
56. Xu, K.; Babcock, H. P.; Zhuang, X. Dual-objective STORM reveals three-dimensional filament organization in the actin cytoskeleton. *Nat. Methods.* **2012**, *9(2)*, 185-188.
57. Shtengel, G.; Galbraith, J. A.; Lippincott-Schwartz, C. G.; Gillette, J.; Manley, J. M.; Sougrat, S.; Waterman, R.; Kanchanawong, P.; Davidson, M.W.; Fetter, R. D.; Hess, H. Interferometric fluorescent super-resolution microscopy resolves 3D cellular ultrastructure. *Proc. Natl. Acad. Sci.* **2009**, *106*, 3125-3130.

58. Rittweger, E.; Han, K. Y.; Irvine, S. E.; Eggeling, C.; Hell, S. W. STED microscopy reveals crystal colour centers with nanometric resolution. *Nat. Photo.* **2009**, *3*, 144-147.
59. Izeddin, I.; Specht, C. G.; Lelek, M.; Darzaq, X.; Triller, A.; Zimmer, C.; Dahan, M. Super-resolution dynamic imaging of dendritic spines using a low-affinity photoconvertible actin probe. *PLoS ONE*. **2011**, ***6,*** e15611.
60. Lukinavičius, G.; Reymond, L.; D'Este, E.; Masharina, A.; Göttfert, F.; Ta, H.; Güther, A.; Fournier, M.; Rizzo, S.; Waldmann, H.; Blaukopf, C.; Sommer, C.; Gerlich, D. W.; Arndt, H.; Hell, S. W.; Johnsson, K. Fluorogenic probes for live-cell imaging of the cytoskeleton. *Nat. Methods*. **2014**, *11(7)*, 731-733.
61. Gunewardene, M. S.; Subach, F. V.; Gould, T. J. Penoncello, G. P.; Gudhei, M. V.; Verkhusha, V. V.; Hess, S. T. Supperresolution imaging of multiple fluorescent proteins with highly overlapping emission spectra in living cells. *Biophys. J.* **2011**, *101*, 1522-1528.
62. Uttamapinant, C.; Howe, J. D.; Lang, K; Beránek, V.; Davis, L.; Mahesh, M.; Barry, N. P.; Chin, J. W. Genetic code expansion enables live-cell and super-resolution imaging of site-specifically labeled cellular proteins. *J. Am. Chem. Soc.* **2015**, *137,* 4602-4605.
63. Liu, Y.; Ding, Y.; Alonas, E.; Zhao, W.; Santangelo, P. J.; Jin, D.; Piper, J. A.; Teng, J.; Ren, Q.; Xi, P. Achieving λ/10 resolution CW STED nanoscopy with a Ti:sapphire oscillator. *PLoS ONE*. **2012**, *7(6)*, e40003.
64. Nanguneri, S.; Flottmann, B.; Herrmannsdörfer, F.; Kuner, T.; Heilemann, M. Single-molecule super-resolution imaging by tryptophan-quenching-induced photoswitching of phalloidin-fluorophore conjugates. *Microscopy Research and Technique*. **2014**, *77*, 510-516.
65. Frost, N. A.; Shroff, H.; Kong, H.; Betzig, E.; Blanpied, T. A. Single-molecule discrimination of discrete perisynaptic and distributed sites of actin filament assembly within dendritic spines. *Neuron*. **2010**, *67*, 86-99.
66. Scarselli, M.; Annibale, P.; Radenovic, A. Cell type-specific β2-adrenergic receptor clusters identified using photoactivated localization microscopy are not lipid raft related, but depend on actin cytoskeleton integrity. *Journal of Biological Chemistry*. **2012**, *287(20)*, 16768-16780.
67. Xu, K.; Zhong, G.; Zhuang, X. Actin, spectrin, and associated proteins form a periodic cytoskeletal structure in axons. *Science.* **2013**, *339*, 452-456.
68. Zhong, G.; He, J.; Zhou, R.; Lorenzo, D.; Babcock, H. P.; Bennett, V.; Zhuang, X. Developmental mechanism of the periodic membrane skeleton in axons. *eLife*. **2014**, *3*, e04581
69. Van der Dries, K.; Schwartz, S. L.; Byars, J.; Meddens, M. B. M.; Boomini-Vittori, M.; Lidke, D. S.; Figdor, C. G.; Cambi, A. Dual-color superresolution microscopy reveals nanoscale organization of mechanosensory podosomes. *Molecular Biology of the Cell.* **2013**, *24*, 2112-2123.

70. Heaslip, A. T.; Nelson, S.R.; Lombardo, A. T.; Beck Previs, S.; Armstrong, J.; Warshaw, D.M. Cytoskeletal dependence of insulin granule movement dynamics in INS-1 beta-cells in response to glucose. *PLoS ONE*. **2014**, *9(10)*, e109082.
71. Mueller, V.; Ringemann, C.; Honigmann, A.; Schwarzmann, G.; Medda, R.; Leutenegger, M.; Polyakova, S.; Belov, V. N.; Hell, S. W.; Eggeling, C. STED nanoscopy reveals molecular details of cholesterol- and cytoskeleton-modulated lipid interactions in living cells. *Biophys. J.* **2011**, *101*, 1651-1660.
72. Sharma, S.; Santiskulvong, C.; Bentolila, L. A.; Rao, J.; Dorigo, O.; Gimzewski, J. K. Correlative nanomechanical profiling with super-resolution F-actin imagng reveals novel insights into mechanics of cisplatin resistance in ovarian cancer cells. *Nanomed-nanotechnol.* **2012**, *8*, 757-766.
73. Meddens, M. B. M.; van den Dries, K.; Cambi, A. Podosomes revealed by advanced bioimaging: what did we learn? *Eur. J. of Cell. Biol.* **2014**, *93*, 380-387.
74. Silva, W. R. Graefe, C. T.; Frontiera, R. R. Toward label-free super-resolution microscopy. *ACS Photo.* **2015**, *ASAP*, DOI: 10.1021/acsphotonics.5b00467

Chapter 2

1. Lin, Y. S.; Hurley, K. R.; Haynes, C. L. Critical considerations in the biomedical use of mesoporous silica nanoparticles. *J. Phys. Chem. Lett.* **2012**, *3*, 364-374.
2. Slowing, I. I.; Vivero-Escoto, J. L.; Wu, C. W.; Lin, V. S. Mesoporous silica nanoparticles as controlled release drug delivery and gene transfection carriers. *Adv. Drug Deliv. Rev.* **2008**, *60*, 1278-1288.
3. Slowing, I.; Trewyn, B. G.; Lin, V. S. Effect of surface functionalization of MCM-41-type mesoporous silica nanoparticles on the endocytosis by human cancer cells. *J. Am. Chem. Soc.* **2006**, *128***,** 14792-14793.
4. Tarn, D.; Ashley, C. E.; Xue, M.; Carnes, E. C.; Zink, J. I.; Brinker, J. C. Mesoporous silica nanoparticle nanocarriers: biofunctionality and biocompatibility. A*cc. Chem. Res.* **2013**, *46***,** 792–801.
5. Yu, T.; Greish, K.; McGill, L. D.; Ray, A.; Ghandehari, H. Influence of geometry, porosity, and surface characteristics of silica nanoparticles on acute toxicity: their vasculature effect and tolerance threshold. *ACS Nano*. **2012**, *6,* 2289-2301.
6. Yildirim, A.; Ozgur, E.; Bayindir, M. Impact of mesoporous silica nanoparticle surface functionality on hemolytic activity, thrombogenicity and non-specific protein adsorption. *J. Mater. Chem. B.* **2013**, *1,* 1909-1920.

7. Huang, X.; Li, L.; Liu, T.; Hao, N.; Liu, H.; Chen, D.; Tang, F. The shape effect of mesoporous silica nanoparticles on biodistribution, clearance, and biocompatibility in vivo. *ACS Nano.* **2011**, *5,* 5390-5399.
8. Fu, C.; Liu, T.; Li, L.; Liu, H.; Chen, D.; Tang, F. The absorption, distribution, excretion and toxicity of mesoporous silica nanoparticles in mice following different exposure routes. *Biomaterials.* **2013**, *34,* 2565-2575.
9. Kim, D.; Lin, Y. S.; Haynes, C. L. On-chip evaluation of shear stress effect on cytotoxicity of mesoporous silica nanoparticles. A*nal. Chem.* **2011**, *83,* 8377-8382.
10. Lin, Y. S.; Haynes, C. L. Impacts of mesoporous silica nanoparticle size, pore ordering, and pore integrity on hemolytic activity. *J. Am. Chem. Soc.* **2010**, *132,* 4834-4842.
11. He, Q.; Zhang, Z.; Gao, F.; Li, Y.; Shi, J. In vivo biodistribution and urinary excretion of mesoporous silica nanoparticles: effects of particle size and PEGylation. S*mall.* **2011**, *7,* 271-280.
12. He, Q.; Zhang, J.; Shi, J.; Zhu, Z.; Zhang, L.; Bu, W.; Guo, L.; Chen, Y. The effect of PEGylation of mesoporous silica nanoparticles on nonspecific binding of serum proteins and cellular responses. B*iomaterials.* **2010**, *31,* 1085-1092.
13. Xia, T.; Kovochich, M.; Liong, M.; Meng, H.; Kabehie, S.; George, S.; Zink, J. I.; Nel, A. E. Polyethyleneimine coating enhances the cellular uptake of mesoporous silica nanoparticles and allows safe delivery of siRNA and DNA constructs. A*CS Nano.* **2009**, *3,* 3273-3286.
14. Lin, Y. S.; Abadeer, N.; Hurley, K. R.; Haynes, C. L. Ultrastable, redispersible, and small highly organomodified mesoporous silica nanotherapeutics. *J. Am. Chem. Soc.* **2011**, *133,* 20444-20457.
15. Sayes, C. M.; Reed, K. L.; Subramoney, S.; Abrams, L.; Warheit, D. B. Can in vitro assays substitute for in vivo studies in assessing the pulmonary hazards of fine and nanoscale materials? *J. Nanopart. Res.* **2009**, *11*, 421-43.
16. Maurer-Jones, M. A.; Lin, Y. S.; Haynes, C. L. Functional assessment of metal oxide nanoparticle toxicity in immune cells. *ACS Nano.* **2010**, *4***,** 3363-3373.
17. Di Carlo, D.; Wu, L. Y.; Lee, L. P. Dynamic single cell culture array. *Lab Chip.* **2006**, *6,* 1445-1449.
18. Khan, O. F.; Sefton, M. V. Endothelial bell behavior within a microfluidic mimic of the flow channels of a modular tissue engineered construct. *Biomed. Microdevices.* **2011**, *13***,** 69-87.
19. Derda, R.; Tang, S. K.; Laromaine, A.; Mosadegh, B.; Hong, E.; Mwangi, M.; Mammoto, A.; Ingber, D. E.; Whitesides, G. M. Multizone paper platform for 3D cell cultures. *PLoS One.* **2011**, *6,* e18940.
20. Giridharan, G. A.; Nguyen, M.-D.; Estrada, R.; Parichehreh, V.; Hamid, T.; Ismahil, M. A.; Prabhu, S. D.; Sethu, P. Microfluidic cardiac cell culture model (μCCCM). *Anal. Chem.* **2010**, *82***,** 7581-7587.

21. Neeves, K. B.; Onasoga, A. A.; Wufsus, A. R. The use of microfluidics in hemostasis: clinical diagnostics and biomimetic models of vascular injury. *Curr. Opin. in Hematol*. **2013**, *20*, 417-423.
22. Tovar-Lopez, F. J.; Rosengarten, G.; Nasabi, M.; Sivan, V.; Khoshmanesh, K.; Jackson, S. P.; Mitchell, A.; Nesbitt, W. S. An investigation on platelet transport during thrombus formation at micro-scale stenosis. *PLoS ONE*. **2013**, *8*, e74123.
23. Colace, T. V.; Tormoen, G. W.; McCarty, O. J. T.; Diamond, S. L. Microfluidics and coagulation biology. *Annu. Rev. Biomed. Eng*. **2013**, *15*, 283-303.
24. Lievens, D.; Zernecke, A.; Seijkens, T.; Soehnlein, O.; Beckers, L.; Munnix, I. C.; Wijnands, E.; Goossens, P.; van Kruchten, R.; Thevissen, L.; Boon, L.; Flavell, R. A.; Noelle, R. J.; Gerdes, N.; Biessen, E. A.; Daemen, M. J.; Heemskerk, J. W.; Weber, C.; Lutgens, E. Platelet CD40L mediates thrombotic and inflammatory processes in atherosclerosis. *Blood.* **2010**, *116,* 4317-4327.
25. Sambrano, G. R.; Weiss, E. J.; Zheng, Y.-W.; Huang, W.; Coughlin, S. R. Role of thrombin signalling in platelets in hemostasis and thrombosis. *Nature.* **2001**, *413,* 74-78.
26. Heemskerk, J. W.; Bevers, E. M.; Lindhout, T. Platelet activation and blood coagulation. *Thromb. Haemost.* **2002**, *88,* 186-193.
27. Zwaal, R. F.; Comfurius, P.; Bevers, E. M. Lipid-protein interaction in blood coagulation. *Biochim. Biophys. Acta.* **1998**, *1376,* 433-453.
28. Chasserot-Golaz, S.; Coorssen, J. R.; Meunier, F. A.; Vitale, N. Lipid dynamics in exocytosis. *Cell Mol. Neurobiol.* **2010**, *30,* 1335-1342.
29. Lin, Y. S.; Haynes, C. L. Synthesis and characterization of biocompatible and size-tunable multifunctional porous silica nanoparticles. *Chem. Mater.* **2009**, *21,* 3979-3986.
30. Lin, Y. S.; Abadeer, N.; Haynes, C. L. Stability of small mesoporous silica nanoparticles in biological media. *Chem. Comm.* **2011**, *47,* 532–534.
31. Jin, J.; Quinton, T. M.; Zhang, J.; Rittenhouse, S. E.; Kunapuli, S. P. Adenosine diphosphate (ADP)-induced thromboxane A(2) generation in human platelets requires coordinated signaling through integrin alpha(IIb)beta(3) and ADP receptors. *Blood.* **2002**, *99,* 193-198.
32. Puri, R. N.; Colman, R. W. ADP-induced platelet activation. *Crit. Rev. Biochem. Mol. Biol.* **1997**, *32*, 437-502.
33. Papaioannou, T. G.; Stefanadis, C. Vascular wall shear stress: basic principles and methods. *Hellenic J. Cardiol.* **2005***, 46,* 9-15.
34. Kent, N. J.; Basabe-Desmonts, L.; Meade, G.; MacCraith, B. D.; Corcoran, B. G.; Kenny, D.; Ricco, A. J. Microfluidic device to study arterial shear-mediated platelet-surface interactions in whole blood: reduced sample volumes and well-characterised protein surfaces. *Biomed. Microdevices.* **2010**, *12,* 987-1000.

35. Kim, D.; Haynes, C. L. On-chip evaluation of neutrophil activation and neutrophil-endothelial cell interaction during neutrophil chemotaxis. *Anal. Chem.* **2012**, *84*, 6070-6078.
36. Nesbitt, W. S.; Westein, E.; Tovar-Lopez, F. J.; Tolouei, E.; Mitchell, A.; Fu, J.; Carberry, J.; Fouras, A.; Jackson, S. P. A shear gradient-dependent platelet aggregation mechanism drives thrombus formation. *Nat. Med.* **2009**, *15,* 665-673.
37. Muthard, R. W.; Diamond, S. L. Side view thrombosis microfluidic device with controllable wall shear rate and transthrombus pressure gradient. *Lab Chip* **2013**, *13***,** 1883-1891.
38. Wagner, D. D.; Burger, P. C. Platelets in inflammation and thrombosis. *Arterioscl. Throm. and Vas.* **2003**, *23***,** 2131-2137.
39. Francois, J.; Lutyiye, J.; Bernard, S.; Olivier, B.; Laloy, J.; Alpan, M.; Lucas, M.; Toussaint, C.; Dogne, M. R. A comparison of six major platelet functional tests to assess the impact of carbon nanomaterials on platelet funcion: A practical guide. *Nanotoxicology.* **2014**, *8(2)*, 220-232.

Chapter 3

1. Golebiewska, E. M.; Poole, A. W. Secrets of platelet exocytosis - what do we really know about platelet secretion mechanisms? *Brit. J. Haemat*. **2014**, *165*, 204–216.
2. Sharma, D.; Brummel-Ziedins, K. E.; Bouchard, B. A.; Holmes, C. E. Platelets in tumor progression: a host factor that offers multiple potential targets in the treatment of cancer. *J. Cell Physiol*. **2014**, *229*, 1005–1015.
3. Mannaioni, P. F.; Di Bello, M. G.; Masini, E. Platelets and inflammation: role of platelet-derived growth factor, adhesion molecules and histamine. *Inflamm. Res*. **1997**, *46*, 4–18.
4. Boon, G. D. An overview of hemostasis. *Toxicol. Pathol.* **1993**, *21(2)*, 170-179.
5. Ogedegbe, H. O. An overview of hemostasis. *Lab. Med.* **2002**, *12(33)*, 948-953.
6. Rendu, F.; Brohard-Bohn, B. The platelet release reaction: granules' constituents, secretion and functions. *Platelets*. **2001**, *12*, 261–273.
7. Blockmans, D.; Deckmyn, H.; Vermylen, J. Platelet activation. *Blood Rev*. **1995**, *9*, 143–156.
8. Ge, S.; White, J. G.; Haynes, C. L. Critical role of membrane cholesterol in exocytosis revealed by single platelet study. *ACS Chem. Biol.* **2010**, *5*, 819–828.
9. Ge, S.; White, J. G.; Haynes, C. L. Cytoskeletal F-actin, not the circumferential coil of microtubules, regulates platelet dense-body granule secretion. *Platelets*. **2012**, *23*, 259–263.
10. Koseoglu, S.; Dilks, J. R.; Peters, C. G.; Fitch-Tewfik, J. L.; Fadel, N. A.; Jasuja, R.; Italiano, J. E.; Haynes, C. L.; Flaumenhaft, R. Dynamin-related protein-1 controls fusion pore dynamics during platelet granule exocytosis.

Arterioscl. Throm. Vas. **2013**, *33*, 481–488.
11. Ge, S.; Woo, E.; White, J. G.; Haynes, C. L. Electrochemical measurements of endogenous serotonin release from human blood platelets. *Anal. Chem*. **2011**, *83*, 2598–2604.
12. Ge, S.; White, J. G.; Haynes, C. L. Quantal release of serotonin from platelets. *Anal. Chem*. **2009**, *81*, 2935–2943.
13. Ge, S.; Wittenberg, N. J.; Haynes, C. L. Quantitative and real-time detection of chemical messenger secretion from platelets. *Biochemistry*. **2008**, *47*, 7020–7024.
14. Severin, S.; Gaits-Iacovoni, F.; Allart, S.; Gratacap, M. P.; Payrastre, B. A confocal-based morphometric analysis shows a functional crosstalk between the actin filament system and microtubules in thrombin-stimulated platelets. *J. Throm. Haemost*. **2013**, *11*, 183-216.
15. Patel-Hett, S.; Richardson, J. L.; Schulze, H.; Drabek, K.; Isaac, N. A.; Hoffmeister, K.; Shivdasani, R. A.; Bulinski, J. C.; Galjart, N.; Hartwig, J.; Italiano, J. E. Visualization of microtubule growth in living platelets reveals a dynamic marginal band with multiple microtubules. *Blood*. **2008**, *111*, 4605–4616.
16. Hartwig, J.; Barkalow, K.; Azim, A.; Italiano, J. E. The elegant platelet: signals controlling actin assembly. *Throm. Haemost*. **1992**, *82*, 392–398.
17. Bearer, E. L.; Prakash, J. M.; Li, Z. Actin dynamics in platelets. *Int. Rev. Cytol.* **2002**, *217*, 137-182.
18. Gear, A. R. L.; Burke, D. Thrombin-induced secretion of serotonin from platelets can occur in seconds. *Blood*. **1982**, *60*, 1231–1234.
19. Cerecedo, D.; Stock, R.; Gonzalez, S.; Reyes, E.; Mondragon, R. Modification of actin, myosin and tubulin distribution during cytoplasmic granule movement associated with platelet adhesion. *Haematologica*. **2002**, *87*, 1165–1176.
20. Asmis, L.; Tanner, F. C.; Sudano, I.; Lüscher, T. F.; Camici, G. G. DMSO inhibits human platelet activation through cyclooxygenase-1 inhibition. A novel agent for drug eluting stents? *Biochem. Bioph. Res. Co*. **2010**, *391*, 1629–1633.
21. Jordan, M. A.; Wilson, L. Microtubules as a target for anticancer drugs. *Nat. Rev. Cancer*. **2004**, *4*, 253–265.
22. Coue, M.; Brenner, S. L.; Spector, I.; Korn E. D. Inhibition of actin polymerization by latrunculin A. *FEBS Lett*. **1987**, *213*, 316–318.
23. Cooper, J. A.; Effects of cytochalasin and phalloidin on actin. *J. Cell Biol*. **1987**, 105, 1473–1478.
24. Cerecedo, D.; Cisneros, B.; Mondragon, R.; Gonzalez, S.; Galván, I. J. Actin filaments and microtubule dual-granule transport in human adhered platelets: the role of α-dystrobrevins. *Brit. J. Haemat*. **2010**, *149*, 124–136.

Chapter 4

1. Reed, G. L., *Platelets*. 2 ed.; Elsevier: 2007; p 1343.
2. Marcus, A. J.; Safier, L. B., Thromboregulation-Multicellular modulation of platelet reactivity in hemostasis and thrombosis. *Faseb J.* **1993,** *7* (6), 516-522.
3. Hartwig, J. H., Mechanisms of actin rearrangements mediating platelet activation. *J. Cell Biol.* **1992,** *118* (6), 1421-1442.
4. Silvius, J. R. Role of cholesterol in lipid raft formtion: lessons from lipid model systems. *Biochim. Biophys. Acta.* **2003**, *1610*, 174-183.
5. Bodin, S.; Tronchere, H.; Payrastre, B. Lipid rafts are critical membrane domains in blood platelet activation process. *Biochim. Biophys. Acta.* **2003**, *1610*, 247.257.
6. Gousset, K.; Wolkers, W. F.; Tsvetkova, N. M.; Oliver, A. E.; Filed, C. L.; Walker, N. J.; Crowe, J. N.; Tablin, F. Evidence for a physiological role for membrane rafts in human platelets. *J. Cell Physiol.* **2002**, *190*, 117-128.
7. Boesze-Battaglia, K.; Clayton, S. T.; Schimmel, R. J. Cholesterol redistribution within human platelet membrane: evidence for a stimulus-dependent event. *Biochemistry.* **1996**, 6664-6673.
8. Locke, D.; Chen, H.; Liu, Y. Liu, C.; Kahn, M. L. Lipid rafts orchestrate signaling by the platelet receptor glycoprotein VI. *J .Biol. Chem.* **2002**, *277*, 18801-18809.
9. Ge, S. C.; White, J. G.; Haynes, C. L. Critical role of membrane cholesterol in exocytosis revealed by single platelet study. *ACS Chem. Biol.* **2010**, *5*, 819-828.
10. Wang, N.; Kwan, C.; Gong, X.; de Chaves, E. P.; Tse, A.; Tse, F. W. Influence of cholesterol on catecholamine release from the fusion pore of large dense core chromaffin granules. *J. Neurosci.* **2010**, *30*, 3904-3911.
11. Salaün, C.; James, D. J.; Chamberlain, L. H. Lipid rafts and regulation of exocytosis. *Traffic*. **2004**, *5(4)*, 255-264.
12. Grzybek, M.; Chorzalska, A.; Bok, E.; Hryniewicz-Jonkowska, A.; Czogalla, A.; Diakowski, W.; Sikorski, A. K. Spectrin-phospholipid interactions. Existence of multiple kinds of binding sites? *Chem. Phys. Lipids.* **2006**, *141*, 133-141.
13. Koseoglu, S.; Meyer, A.F.; Kim, D.; Meyer, B.M.; Wang, Y.; Dalluge, J.; Haynes, C.L. Analytical Characterization of the Role of Phospholipids in Platelet Adhesion and Secretion. *Anal. Chem*. **2015**, *87(1)* 413-421.
14. Kilsdonk, E. P. C.; Yancey, P. G.; Stoudt, G. W.; Bangerter, F. W.; Johnson, W. J.; Phillips, M. C.; Rothblat, G. H. Cellular cholesterol efflux mediated by cyclodextrins. *J. Biol. Chem.* **1995**, *270(29)*, 17250-17256.
15. Rothblat, G. H.; de la Llera-Moya, M.; Atger, V.; Kellner-Weibel, G.; Williams, D. L.; Phillips, M. C. Cell cholesterol efflux: integration of old and new observations provides new insights. *J. Lipid Res.* **1999**, *40*, 781-796.
16. Mohanty, J. G.; Jaffe, J. S.; Schulman, E. S.; Raible, D. G. A highly sensitive fluorescent micro-assay of H_2O_2 release from activated human

leukocytes using a dihydroxyphenoxazine derivative. *J. Immun. Methods.* **1997**, *202*, 133-141.
17. Zhou, M.; Diwu, Z.; Panchuk-Voloshina, N.; Haugland, R. P. A stable nonfluorescent derivative of resorufin for the fluorometric detemination of trace hydrogen peroxide: applications in detecting the activity of phagocyte NADPH oxidase and other oxidases. *Anal. Biochem.* **1997**, *253*, 162-168.
18. Gear, A. R. L.; Burke, D. Thrombin-induced secretion of serotonin from platelets can occur in seconds. *Blood*. **1982**, *60*, 1231–1234.
19. Ge, S.; Wittenberg, N. J.; Haynes, C. L. Quantitative and real-time detection of chemical messenger secretion from platelets. *Biochem.* **2008**, *47*, 7020-7024.
20. Platelet function testing: light transmission aggregometry [LTA]. http://www.practical-haemostasis.com/Platelets/platelet_function_testing_lta.html (Accessed Jan 6, 2016)
21. Holmsen, H.; Day, H. J.; Setkowsky, C. A. Behaviour of adenine nucleotides during the plateet release reaction induced by adenosine diphosphate and adrenaline. *Biochem. J.* **1972**, *129*, 67-82.
22. Sun, M.; Northus, N.; Marga, F.; Huber, T.; Byfield, F.; Levitan, I.; Forgacs, G. The effect of cellular cholesterol on membrane-cytoskeleton adhesion. *J. Cell Sci.* **2007,** *120*, 2223-2231.
23. Khatibzadeh, N.; Spector, A. A.; Brownell, W. E.; Anvari, B. Effects of plasma membrane cholesterol level and cytoskeleton F-actin on cell protrusion mechanics. *PloS ONE.* **2003**, *8(2)*, e57147.
24. Van Lier, M. Lee, F.; Farndale, R. W.; Gorter, G.; Verhoef, S.; Ohno-Iwashita, Y.; Akkerman, J. N.; Heijnen, H. F. G. Adhesive surface determines raft composition in platelets adhered under flow. *J. Thromb. Haemost.* **2005**, *3*, 2514-2525.
25. Van Lier, M.; Verhoef, S.; Cauwenberghs, S.; Heemskerk, J. W.; Akkerman, J. N.; Heijnen, H. F. Role of membrane cholesterol in platelet calcium signaling in response to VWF and collagen under stasis and flow. *Thromb. Haemost.* **2008**, *99(6)*, 1068-1078.

Chapter 5

1. Salaun, C.; James, D. J.; Chamberlain, L. H. Lipid rafts and the regulation of exocytosis. *Traffic.* **2004***, 5*, 255-264.
2. Ge, S. C.; White, J. G.; Haynes, C. L. Critical role of membrane cholesterol in exocytosis revealed by single platelet study. *ACS Chem. Biol.* **2010**, *5*, 819-828.
3. Wang, N.; Kwan, C.; Gong, X.; de Chaves, E. P.; Tse, A.; Tse, F. W. Influence of cholesterol on catecholamine release from the fusion pore of large dense core chromaffin granules. *J. Neurosci.* **2010**, *30*, 3904-3911.

4. Wightman, R. M.; Haynes, C. L. Synaptic vesicles really do kiss and run. *Nat. Neurosci.* **2004**, *7*, 321-322.
5. Omiatek, D. M.; Dong, Y.; Heien, M. L.; Ewing, A. G. Only a fraction of quantal content is released during exocytosis as revealed by electrochemical cytometry of secretory vesicles. *ACS Chem. Neurosci.* **2010**, *1*:234-245.
6. Mellander, L. J.; Trouillon, R.; Svensson, M. I.; Ewing, A. G. Amperometric post spike feet reveal most exocytosis is via extended kiss-and-run fusion. *Scientific Reports*. **2012**, *2*, 907.
7. Mellander, L. J.; Kurczy, M. E.; Najafinobar, N.; Dunevall, J.; Ewing, A. G.; Cans, A. S. Two modes of exocytosis in an artificial cell. *Scientific Reports*. **2014**, *4*, 3847.
8. Cabeza, J. M.; Acosta, J.; Alés, E. Mechanisms of granule membrane recapture following exocytosis in intact mast cells. *J. Biol. Chem.* **2013**, *288*, 20293-20305.
9. Staal, R. G.; Mosharov, E. V.; Sulzer, D. Dopamine neurons release transmitter via a flickering fusion pore. *Nat. Neurosci.* **2004**, *7*, 341-346.
10. White, J. Platelet Structure. In *Platelets*; Michelson, A., Ed.; Academic/Elsevier: Amsterdam, 2007; pp 45-74.
11. Ge, S.; White, J. G.; Haynes, C. L. Quantal release of serotonin from platelets. *Anal. Chem. **2009**, 101*, 2351-2359.
12. Ge, S.; Wittenberg, N. J.; Haynes, C. L. Quantitative and real-time detection of secretion of chemical messengers from individual platelets. *Biochemistry*. **2008**, *47*, 7020-7024.
13. Gruba, S. M.; Koseoglu, S.; Meyer, A. F.; Meyer, B. M.; Maurer-Jones, M. A.; Haynes, C. L. Platelet membrane variations and their effects on delta-granule secretion kinetics and aggregation spreading among different species. *Biochim. Biophys. Acta.* **2015**, *1848*, 1609-1618.
14. Amatore, C.; Arbault, S.; Bonifas, I.; Guille, M. Quantitative investigations of amperometric spike feet suggest different controlling factors of the fusion pore in exocytosis at chromaffin cells. *Biophys. Chem*. **2009**, *143*, 124–131.
15. Cookson, E. A.; Conte, I. L.; Dempster, J.; Hannah, M. J.; Carter, T. Characterisation of Weibel- Palade body fusion by amperometry in endothelial cells reveals fusion pore dynamics and the effect of cholesterol on exocytosis. *J. Cell Sci*. **2013**, *126*, 5490-5499.
16. Hochgraf, E.; Levy, Y.; Aviram, M.; Brook, J. G.; Cogan, U. Lovastatin decreases plasma and platelet cholesterol levels and normalized elevated platelet fluidity and aggregation in hypercholesterolemic patients. *Metabolism*. **1994**, *43*,11-17.
17. Lijnen, P.; Echevaria-Vazquez, D.; Petrov, V. Influence of cholesterol-lowering on plasma membrane lipids and function. *Methods Find. Exp. Clin. Pharmacol.* **1996**, *18*, 123-136.

18. Shattil, S. J.; Anaya-Galindo, R.; Bennett, J.; Colman, R. W.; Cooper, R. A. Platelet hypersensitivity induced by cholesterol incorporation. *J. Clin. Invest*. **1975**, *55*, 636-643.
19. Grgurevich, S.; Krishnan, R.; White, M. M.; Jennings, L. K. Role of in vitro cholesterol depletion in mediating human platelet aggregation. *J. Thromb*. *Haemost*. **2003**, *1*, 576-586.

Chapter 6

1. Meyer, A. Examining the roles of membrane lipids and secreted bioactive lipids on immune system cell function: studies on mast cells and platelets. Ph.D. Thesis, The University of Minnesota, October, 2013.
2. Risch, B. Teaching chemistry around the world. Waxmann, 2010.
3. Mahdi, J. Student attitudes towards chemistry: an examination of choices and preferences. *Am. J. of Educ. Res.* **2014**, *2(6)*, 351-356.
4. Korn, M. Chemistry departments try to attract more students by retooling the major. *The Wall Street Journal*. April 12, 2015.
5. Nakhleh, M. B. Why some students don't learn chemistry: chemical misconceptions. *J. Chem. Educ.* **1992**, *69(3)*, 191-196.
6. Schweitzer, N. J.; Saks, M. J. The *CSI* effect: popular fiction about forensic science affects the public's expectations about real forensic science. *Jurimetrics.* **2007**, *47*, 357-364.
7. Milanick, M. A.; Prewitt, R. L. Fact or fiction? General chemistry helps students determine the legitimacy of television program situations. *J. Chem. Educ*. **2013**, *90*, 904-906.
8. Kazilek, C.J.; Pearson, D. Using the scientific method to solve mysteries. http://askabiologist.asu.edu/teaching-scientific-method. (accessed Jul 2013).
9. Meyer, A.; Knutson, C.; Finkenstaedt-Quinn, S. A.; Gruba, S. M.; Meyer, B.; Thompson, J.; Maurer-Jones, M.; Halderman, S.; Tillman, A.; DeStefano, L.; Haynes, C. L. Activities for middle school students to sleuth a chemistry "whodunit" and investigate the scientific method. *J. Chem. Educ.* **2014**, *91(3),* 410-413.
10. Murphy, J. Personal Communication to C.L. Haynes, 2011-2013. Demographics of W. 7th Community Center.
11. Caldwell, J. E. Clickers in the large classroom: current research and best practice tips. *CBE Life Sci. Educ*. **2007**, *6*, 9-20.
12. MacArthur, J. R.; Jones, L. L. A review of literature reports of clickers available to college chemistry classrooms. *Chem. Educ. Res. Pract*. **2008**, *9*, 187-195.
13. Agresti, A.; Franklin, C. *Statistics: The Art and Science of Learning from Data*; 3rd ed.; Pearson: USA, 2012; pp 504.
14. Domin, D. S. A review of laboratory instruction styles. *J. Chem. Educ.* **1999**, *76(4)*, 543-547.
15. Stocker, T.F.; Qin, D.; Plattner, G. K.; Tignor, M.; Allen, S.K.; Boschung,

J.; Nauels, A.; Xia, Y.; Bex, V.; Midgley, P. M. *IPCC, 2013: Summary for Policymakers. In: Climate Change 2013: The Physical Science Basis.* Contribution of Working Group I to the Fifth Assessment Report of the Intergovernmental Panel on Climate Change: Cambridge, United Kingdom and New York, NY, USA, 2013.

16. Field, C. B.; Barros, V. R.; Dokken, D. J.; Mach, K. J.; Mastrandrea, M. D; Bilir, T. E.; Chatterjee, M.; Ebi, K. L.; Estrada, Y. O.; Genova, R. C.; Girma, B.; Kissel, E. S.; Levy, A. N.; MacCracken, S.; Mastrandrea, P. R.; White, L. L. *IPCC, 2014: Summary for policymakers. In: Climate Change 2014: Impacts, Adaptation, and Vulnerability. Part A: Global and Sectoral Aspects.* Contribution of Working Group II to the fifth assessment report of the intergovernmental panel on climate change: Cambridge, United Kingdom and New York, NY, USA, 2014.
17. Saad, L. A steady 57% in U.S. blame humans for global warming. *Gallup*. **2014**. http://www.gallup.com/poll/167972/steady-blame-humans-global-warming.aspx?g_source=CATEGORY_CLIMATE_CHANGE&g_medium=topic&g_campaign=tiles. (Accessed Nov 30, 2015)
18. Newport, F. Americans show low levels of concern on global warming. *Gallup.* **2014**. http://www.gallup.com/poll/168236/americans-show-low-levels-concern-global-warming.aspx?g_source=CATEGORY_CLIMATE_CHANGE&g_medium=topic&g_campaign=tiles. (Accessed Nov 30, 2015)
19. Leiserowitz, A.; Smith, N.; Marlon, J. R. *Americans' Knowledge Of Climate Change*. Yale Project on Climate Change Communication: New Haven, CT, 2010.
20. Rickinson, M. Learners and learning in environmental education: A critical review of the evidence. *Enviro. Educ. Res*. **2001**, *7(3)*, 207-320.
21. Gambro, J. S.; Switzky, H. N. A national survey of high school students' environmental knowledge. *J. Enviro. Educ.* **1996**, *27(3)*, 28-33.
22. Versprille, A. N.; Towns, M. H. General chemistry students' understanding of climate change and the chemistry related to climate change. *J. Chem. Educ*. **2015**, *92*, 603−609.
23. Kerr, S. C.; Waltz, K. A. "Holes" in student understanding: addressing prevalent misconceptions regarding atmospheric environmental chemistry. *J. Chem. Educ.* **2007**, *84(10),* 1693-1696.
24. Grassian, V. H.; Stone, E. A. Chemistry's contributions to our understanding of atmospheric science and climate. *J. Chem. Educ.* **2015**, *92*, 595−597.
25. Zoller, U.; Pushkin, D. Matching higher-order cognitive skills (HOCS) promotion goals with problem-based laboratory practice in a freshman organic chemistry course. *Chem. Educ. Res. Pract.* **2007**, *8(2)*, 153-171.
26. Marks, R.; Eilks, I. Research-based development of a lesson plan on shower gels and musk fragrances following a socio-critical and problem-oriented approach to chemistry teaching. *Chem. Educ. Res. Pract*. **2010**, *11*, 129–141.

27. Parchmann I.; Gräsel, C.; Baer, A.; Nentwig, P.; Demuth, R.; Ralle, B. "Chemie im Kontext": A symbiotic implementation of a context-based teaching and learning approach. *Int. J. Sci. Educ*. **2006**, *28*, 1041–1062.
28. Genseberger, R.J. A study about curriculum development at the Open Schoolgemeenschap Bijlmer. Ph.D. Thesis, Universität Utrecht, 1997.
29. Mahaffy, P. The future shape of chemistry education. *Chem. Educ. Res. Pract.* **2004**, *5(3),* 229-245.
30. Robelia, B.; McNeill, K.; Wammer, K.; Lawrenz, F. Investigating the impact of adding an environmental focus to a developmental chemistry course. *J. Chem. Educ.* **2010**, *87(2),* 216-220.
31. Mandler, D.; Mamlok-Naaman, R.; Blonder, R.; Yayon, M.; Hofstein, A. High-school chemistry teaching through environmentally oriented curricula. *Chem. Educ. Res. Pract.* **2012**, 13, 80-92.
32. About the Chem Connections project. http://www.wwnorton.com/college/chemistry/chemconnections/modules.html. (accessed Jan 9, 2016)
33. American Chemical Society. *Chemistry in the community: ChemCom (5th ed.)*; W. H. Freeman: New York, 2006.
34. TedEd: Lessons worth sharing, Our changing climate series page. http://ed.ted.com/series/our-changing-climate (Accessed Jan 03, 2016).
35. Minnesota Department of Education K-12 Academic Standards – Science. http://education.state.mn.us/MDE/EdExc/StanCurri/K-12AcademicStandards/Science/index.htm (Accessed Nov 30, 2015).
36. Finkenstaedt-Quinn, S. A.; Styles, M.; Juelfs, A.; Haynes, C L. Increasing climate change awareness through TedED videos and demonstrations. *In preparation.*
37. Sheridan, P. M.; Szczepankiewicz, S. H.; Mekelburg, C. R.; Schwabel, K. M. Canisius College summer science camp: combining science and education experts to increase middle school students' interest in science. *J. Chem. Educ.* **2011**, *88(7)*, 876-880.
38. Liberko, C. A. Using science fiction to teach thermodynamics: Vonnegut, ice-nine, and global warming. *J. Chem. Educ.* **2004**, *81(4)*, 509-512.
39. Vonnegut, K. *Cat's cradle*; Random House Inc.: New York, 1963.
40. Bradbury, R. *Fahrenheit 451*; Simon and Schuster: New York, 1951.
41. Shute, N. *On the beach*; Random House Inc.: New York, 1957.
42. Asimov, I. *Pate de foie gras*; Street and Smith: New York, 1956.
43. Robinson, K. S. *Forty signs of rain*; Random House Inc.: New York, 2004.
44. Shelley, M. *Frankenstein*; Lackington, Hughes, Harding, Mavor, & Jones: London, 1818.
45. Atwood, M. *Oryx and crake*; Random House Inc.: New York, 2003
46. Wellborn, J. G. Engaged and disaffected action: the conceptualization and measurement of motivation in the academic domain. Ph.D. Thesis, University of Rochester, 1991.
47. Fredericks, J. A.; Blumenfeld, P.; Friedel, J.; Paris, A. School engagement. *What do children need to flourish? Conceptualizing and*

measuring indicators of positive development; Moore, K. A., Lippman L., Eds.; Springer Science and Business Media: New York, 2005; pp 305-321.

48. Appleton, J. J.; Christenson, S. L.; Kim, D.; Reschly, A. L. Measuring cognitive and psychological engagement: validation of the student engagement instrument. *Journal of School Psychology*. **2006**, *44,* 427-445.

Curriculum Vita

Solaire A. Finkenstaedt-Quinn

University of Minnesota – Twin Cities
L-13, 139 Smith Hall
207 Pleasant St SE
Minneapolis, MN 55455
(612) 626-5282

1400 S 2nd St
C406
Minneapolis, MN 55454
finke073@umn.edu

OBJECTIVE

Communicate chemistry concepts to all levels of scientific understanding.

EDUCATION

University of Minnesota

PhD in Chemistry *2010-2016*

Thesis: "A Study of the Regulation Mechanisms of Platelet Exocytosis"
Advisor: Christy Haynes

Macalester College

BA in Chemistry with Minors in Biology and Physics *2010*

TEACHING EXPERIENCE

University of Minnesota

Developed curriculum for the High School Chemistry Classroom *2015*

- Worked with a chemistry high school teacher to develop curriculum that pairs literature with chemical concepts to enhance student learning

Mentored Undergraduate Researchers *Summer 2013, Spring - Fall 2014*

- Mentored two visiting students from a PUI and one student from the University of Minnesota
- Trained student in basic lab skills, cell isolation, and microscopy techniques

Mentorship Program for Aspiring Chemistry Teachers *Spring 2014*

- A program run by the Department of Chemistry in which professors mentor students and allow them to run classroom activities
- Under the mentorship of Professor Christy Haynes while she was teaching Honors General Chemistry 2 (CHEM 1072)
- Gave four lectures, helped in the development and running of POGIL activities, developed in-class clicker questions, wrote exam questions, and participated in grading
- I also ran an exam review session for General Chemistry 2 (CHEM 1062)

Teaching in Higher Education GRAD 8101 *Fall 2013*

- A course offered by University of Minnesota's Preparing Future Faculty program covering different teaching pedagogies

Introductory Chemistry (CHEM 1017) – Lab Teaching Assistant *Spring 2012*

- Consisted of giving pre-lab presentations, assisting students during lab, grading weekly lab reports, and tutoring 3 hours/week

Process Analytical Chemistry (CHEM 2121) – POGIL Assistant *Spring 2011*

- Assisted in running three POGIL activities in a sophomore level class covering analytical chemistry principles

Chemical Principles 1 (CHEM 1021) – Lab Teaching Assistant *2010- 2011*

- Consisted of giving pre-lab presentations, assisting students during lab, grading weekly lab reports, and tutoring 3 hours/week

Exam Proctor *Fall 2010-Spring 2012*

- Proctored exams for CHEM 1015, CHEM 1021, and CHEM 1022.

Macalester College

Biochemistry 2 (CHEM 352) – Lab Teaching Assistant *Spring 2010*

- Assisted students with labs
- Performed pre-lab preparations

Quantum Mechanics (CHEM 312) – Grader *Spring 2010*

- Graded weekly homework assignments
- Helped students with questions

RESEARCH EXPERIENCE

University of Minnesota, Department of Chemistry, Christy Haynes

Exploration of Cytoskeletal Elements of Platelets *2010-Present*

- The goal of this project is to better understand the internal mechanisms within platelets leading to granular release
- My role involves performing fluorescence imaging to observe how the platelet cytoskeleton changes during activation

Pesticide Detection Using Silver Nanoparticles *2012-2015*

- The goal of this project is to develop a simple and fast detection scheme using silver nanoparticles for determining the presence of pesticides on produce
- I streamlined the detection process, including speeding up the aggregation processes by the addition of salt

Georgia Institute of Technology, Department of Chemistry, Christine Payne

Nanoparticle Functionalization for Cellular Uptake in MDCK-II Cells *2009*

- I successfully functionalized fluorescent beads with polyarginine and tested their internalization into cells using pyrenebutyrate-mediated delivery
- I characterized the polarizability and tight junctions of MDCK-II cells

Macalester College, Department of Chemistry, Keith Kuwata

Computational Analysis of Anionic Peroxyacetal Fragmentation *2008*

- I modeled the fragmentation patterns of two systems of peroxyacetals involved in the production of active oxygen

PUBLICATIONS

Finkenstaedt-Quinn, S. A.; Qiu, T.; Shin, K.; Haynes, C. L. "Super-Resolution Imaging for Monitoring Cytoskeleton Dynamics." *in preparation.*

Finkenstaedt-Quinn, S. A.; Styles, M.; Juelfs, A.; Haynes, C L. "Increasing Climate Change Awareness through Ted-ED Videos and Demonstrations." *in preparation.*

Finkenstaedt-Quinn, S. A.; Gruba, S. M.; Haynes, C. L. "Variations in Fusion Pore Formation in Cholesterol-Treated Platelets." *Biophysical Journal*, *in press*.

Finkenstaedt-Quinn, S. A.; Ge, S.; Haynes, C. L. "Cytoskeleton dynamics in drug-treated platelets." *Analytical and Bioanalytical Chemistry,* **2015**, *407* (10), 2803-2809.

Meyer, A.; Knutson, C.; **Finkenstaedt-Quinn, S. A.**; Gruba, S. M.; Meyer, B.; Thompson, J.; Maurer-Jones, M.; Halderman, S.; Tillman, A.; DeStefano, L.; Haynes, C. L. "Activities for Middle School Students to Sleuth a Chemistry "Whodunit" and Investigate the Scientific Method." *Journal of Chemical Education,* **2014**, *91* (3), 410-413.

Kim, D.; **Finkenstaedt-Quinn, S.**; Hurley, K. R.; Buchman, J. T.; Haynes, C. L. "On-chip evaluation of platelet adhesion and aggregation upon exposure to mesoporous silica nanoparticles." *Analyst,* **2014**, *139*, 906-913.

Hang, J.; Ghorai, P.; **Finkenstaedt-Quinn, S. A.**; Findik, I.; Sliz, E.; Kuwata, K. T.; Dussault, P. H. "Generation of Singlet Oxygen from Fragmentation of Monoactivated 1,1-Dihydroperoxides." *J. Org. Chem.*, **2012**, *77* (3), 1233-1243.

PRESENTATIONS

Finkenstaedt-Quinn, S. A.; Gruba, S.; Haynes, C. L. *Cholesterol Regulation of Granule Exocytosis in Platelets,* **2015**, Fall 2015 American Chemical Society National Meeting and Exposition.

Finkenstaedt-Quinn, S. A.; Haynes, C. L. *Investigations of Platelet Secretion Mechanisms,* **2014**, Invited Seminar at Augsburg College.

Finkenstaedt-Quinn, S. A.; Haynes, C. L. *Immunofluorescence for Visualization of the Platelet Cytoskeleton,* **2013**, Chemistry Graduate Student Research Seminar.

Finkenstaedt-Quinn, S. A.; Haynes, C. L. *Immunofluorescence for Visualization of the Platelet Cytoskeleton,* **2013**, Graduate Women in Science.

Finkenstaedt-Quinn, S. A.; St. John-Iyer, A.; Paynes, C. *Functionalization of Nanoparticles and Characterization of MDCK-II cells,* **2009**, Macalester Chemistry Seminar Senior Presentations.

Finkenstaedt-Quinn, S. A.; St. John-Iyer, A.; Paynes, C. *Functionalization of Nanoparticles for Fluorescence Microscopy,* **2009**, MDITR/REU Summer Research Symposium.

POSTERS

Finkenstaedt-Quinn, S. A.; Gruba, S. M.; Ge, S.; Kim, D.; Hurley, K. R.; Buchman, J. T.; Meyer, A.; Knutson, C.; Meyer, B.; Thompson, J.; Maurer-Jones, M.; Halderman, S.; Tillman, A.; DeStefano, L.; Styles, M.; Juelfs, A.; Haynes, C. L., et al. *Engaging Chemistry – Learning By Doing*, **2015**, Fall 2015 American Chemical Society National Meeting and Exposition.

Finkenstaedt-Quinn, S. A.; Gruba, S. M.; Ge, S.; Haynes, C. L. *Platelet Dense Body Granule Exocytosis as a Basis for Pore Formation Dynamics,* **2014**, Biophysical Society Conference.

Finkenstaedt-Quinn, S. A.; Haynes, C. L. *Immunofluorescence for Visualization of the Platelet Cytoskeleton,* **2013**, Chemical Biology Interface Training Grant Symposium.

Finkenstaedt-Quinn, S. A.; Haynes, C. L. *Immunofluorescence for Visualization of the Platelet Cytoskeleton,* **2013**, Cell Biology of Platelets and Megakaryocytes-Gordon Research Conference.

Finkenstaedt-Quinn, S. A.; Haynes, C. L. *Immunofluorescence for Visualization of the Platelet Cytoskeleton,* **2013**, Cell Biology of Platelets and Megakaryocytes-Gordon Research Symposium.

Finkenstaedt-Quinn, S. A.; Haynes, C. L. *Immunofluorescence and TIRF for Visualization of the Platelet Cytoskeleton,* **2012**, Pittcon Conference.

Finkenstaedt-Quinn, S. A.; St. John-Iyer, A.; Payne, C. *Functionalization of Nanoparticles for Cellular Uptake,* **2009**, Undergraduate Research Symposium for Biological Sciences and Psychology.

Finkenstaedt-Quinn, S. A.; St. John-Iyer, A.; Payne, C. *Functionalization of Nanoparticles for Cellular Uptake,* **2009**, Macalester College Summer Research Poster Session.

Finkenstaedt-Quinn, S. A.; Kuwata, K. T.; Dussault, P. H. *Computational Analysis of Anionic Peroxyacetal Fragmentation,* **2008**, Macalester College Summer Research Poster Session.

Finkenstaedt-Quinn, S. A.; Kuwata, K. T.; Dussault, P. H. *Computational Analysis of Anionic Peroxyacetal Fragmentation,* **2008**, Midwest Computational Consortium.

AWARDS

MN ACS Travel Award *2015*
Mary Haga Travel Award-Graduate Women in Science *2013*
NSF Fellow – Honorable Mention *2012*
National Science Foundation-Research Experience for Undergraduates *2009*
American Chemical Society-Petroleum Research Fund *2008*

MEMBERSHIPS

American Chemical Society *2008-Present*
WISE-Women in Science and Engineering *2010-Present*
Officer *2014-2015*

Macalester Science Alumni Network *2010-Present*
Student Seminar Committee *2010-Present*
Vice Chair *2012-2013*
Chair *2013-2015*
Biophysical Society *2013-2014*

STEM SERVICE

Graduate Student Symposium Planning Committee *2014-2015*

- Was a key member of the University of Minnesota student group that organized the symposium 'Academic Innovations for Tomorrow's Industries' for the Fall 2015 American Chemical Society National Meeting and Exposition

GED Test Preparation Classes *2014-Present*

- Assist in planning and running a series of small labs, with a focus on scientific concepts, held for adult students studying for their GED test

Women's Faculty Cabinet Retreat Volunteer *2014-Present*

- Helped with the planning and organization of the WFC Retreat

Chemists in the Library *2011-Present*

Run stations as part of a program organized by the Minnesota chapter of the American Chemical Society where kids visiting the public libraries perform hands-on activities that cover a range of chemical principles

Cool Chemistry *2011-Present*

- Designed a DNA extraction station and a polymer station as part of a day long program run by Women In Science and Engineering to introduce young girls to chemistry

Graduate School Workshop *2012-Present*

- Presented and participated in panel discussions about graduate school in the field of chemistry to locally based primarily undergraduate institutions

Chemistry Days *2010-Present*

- Led stations during an annual half-day event run by the Haynes group to expose kids at West 7th Community Center to chemistry
- Designed 'mysteries' to guide students to a better understanding of the scientific method and environmental station

Energy and U *2010-Present*

- Managed children at a demo show designed to teach kids the First Law of Thermodynamics through a series of chemistry demos

MRSEC STEM Days *2015*

- Performed demos and ran a station at an outreach event designed to teach scientifically inclined 11th and 12th graders about the chemical processes involved in climate change

UMN Chemistry Department Exhibit at the Minnesota State Fair *2014, 2015*

- Ran hands-on activities used to introduce students to chemistry

Twin Cities Regional Science Fair Judge *2013, 2014*

- Judged 6th and 7th grade science projects in the areas of chemistry and physics

Upward Bound Presentation-Chemistry in the Real World *2014*

- Presented to 9th grade Upward Bound students about my path to chemistry and its real world applications

Biophysical Society Conference Volunteer *2014*

- Helped with room counting and in the career center

Math and Science Family Fun Fair *2011, 2012, 2014*

- Worked at the chemistry exhibit as part of a day-long program featuring different STEM fields

Girl Scouts Home Scientist Badge Day *2012*

- Interacted with 2nd and 3rd grade girls as part of a program meant to expose them to the science all around them

STEM Expo *2012*

- Helped run the chemistry station at an exposition for elementary and middle school students held at The Works in Bloomington

STEM Fair *2012*

- An exposition for K-5 students at the Capitol Hill Gifted & Talented Magnet School meant to expose them to the variety of fields of the physical sciences

STEM Expo *2011*

- An exposition designed to expose high school and middle school students in the Minneapolis public schools to different sciences and science-related jobs

STEM Academy *2011*

- A half-day program run by the Association of Multicultural Scientists for kids from 8-12

RESEARCH INTERESTS

Chemical education, bioanalytical chemistry, biophysical chemistry

SKILLS

Lab: Immunofluorescence imaging, live cell imaging (bright field, fluorescence, dark field), UV-visible spectrometry, noble metal nanoparticle synthesis, cell culture and primary culture isolation

Data Analysis Programs: GraphPad Prism, Microsoft Excel, Microsoft Powerpoint, Microsoft Word

Comprehension Evaluation: POGIL, assessment development, ChimeIn, iClicker

Communication: Technical writing (SOPs, IACUC, IRB, manuscripts), project management, purchasing coordinator (lab supplies, financing liaison)